

Copyright

by

Jesus Alberto Silvas

2017

**The Dissertation Committee for Jesus Alberto Silvas Certifies that this is the  
approved version of the following dissertation:**

**HIJACKING OF CELLULAR PATHWAYS BY NOVEL TICK-  
BORNE PHLEBOVIRUS**

**Committee:**

---

Patricia Aguilar, Mentor, Chair

---

Vsevolod Popov

---

Shinji Makino

---

Tina Wang

---

Hideki Ebihara

---

Dean, Graduate School

**HIJACKING OF CELLULAR PATHWAYS BY NOVEL TICK-  
BORNE PHLEBOVIRUS**

**by**

**Jesus Alberto Silvas, B.S., M.S.**

**Dissertation**

Presented to the Faculty of the Graduate School of

The University of Texas Medical Branch

in Partial Fulfillment

of the Requirements

for the Degree of

**Doctor of Philosophy**

**The University of Texas Medical Branch**

**June 2017**

## **Dedication**

To Savahna and Lily

## **Acknowledgements**

My studies could not have been successfully completed without the help of many individuals. First and foremost, my gratitude goes to my mentor, Dr. Patricia Aguilar, for all the patience, guidance, and effort she put into the many years of my training. I would also like to thank Dr. Vsevolod Popov and members of his lab, Julie Wen and Xia Ding, as some of the most exciting work was performed under their tutelage.

I am very grateful to the members of my committee, Drs. Tian Wang, Shinji Makino, and Hideki Ebihara for all of their support and input during my years of training.

Finally, I would like to thank all the people that at some point provided me with help in order to succeed during my studies.

# **Hijacking of Cellular Pathways by Novel Tick-borne Phlebovirus**

Publication No. \_\_\_\_\_

Jesus Alberto Silvas, Ph.D.

The University of Texas Medical Branch, 2017

Supervisor: Patricia Aguilar

Severe Fever with Thrombocytopenia Syndrome (SFTS) virus is an emerging tick-borne *Phlebovirus* isolated from patients presenting with hemorrhagic manifestations. Case fatality rates of 12-50% have been reported. Limited information regarding SFTS virus pathogenesis is known. Inhibition of interferon (IFN) responses by SFTS virus NSs has been shown to correlate with the relocation of RIG-I signaling proteins into early endosomal-derived cytoplasmic structures positive for SFTS virus NSs. Moreover, ubiquitin, an important post-translational modifier required for initiation of the RIG-I signaling cascade, also localizes to SFTS virus NSs cytoplasmic structures. Recently, through Live Cell Imaging of a stable cell line expressing the SFTS virus NSs-mCherry, we observed secretion of some of the SFTS virus NSs-positive structures into the extracellular space. Concurrently, ultrastructural analysis of secreted structures from SFTS virus infected cells revealed that 50% harbored viral-like particles. These secreted structures were also proven to 1) mediate dissemination of SFTS virus and 2) initiate a successful SFTS virus infection even in the presence of neutralizing antibodies. Additionally, proteomic analysis of cytoplasmic SFTS virus NSs structures from infected

cells detected components of the 26S proteasome within these structures and transient expression of the SFTS virus NSs resulted in decreased levels of ubiquitinated proteins. Furthermore, SFTS virus infection leads to the reduction of RIG-I and TBK-1 expression, which were recovered when the Ubiquitin-Proteasomal Pathway was inhibited using MG-132. Lastly, we observed that mutation of ubiquitination sites of RIG-I and TBK-1 prevented and reduced the interaction with SFTS virus NSs, respectively. Altogether, our study suggests a novel mechanism for dissemination and innate immune evasion not previously described for tick-borne phleboviruses.

# TABLE OF CONTENTS

List of Tables .....	xi
List of Figures .....	xii
List of Illustrations .....	xiv
List of Abbreviations .....	xv
<b>CHAPTER 1.....</b>	<b>17</b>
Introduction <sup>1</sup> .....	17
Introduction to Bunyaviruses .....	17
Public Health Importance .....	17
Virion structure and genomic organization .....	18
Attachment, entry, and replication.....	19
Bunyavirus pathogenesis .....	20
Isolation, identification, and classification of SFTS virus.....	21
Transmission and Ecology.....	22
Epidemiology.....	24
Pathogenesis and Molecular Virology.....	27
Specific Aims.....	29
Specific Aim 1 .....	29
Specific Aim 1a .....	30
Specific Aim 2 .....	30
Specific Aim 2a .....	30
Specific Aim 2b .....	31
Specific Aim 3 .....	31
Specific Aim 3a .....	32
Specific Aim 3b .....	32
<b>CHAPTER 2 .....</b>	<b>33</b>
Endosomal trafficking of SFTS virus NSs.....	33
INTRODUCTION .....	33
MATERIALS AND METHODS.....	36



Cells and Reagents .....	36
Live Cell Imaging .....	37
<b>RESULTS .....</b>	<b>37</b>
SFTS virus NSs intracellular vesicles traffic the endosomal recycling pathway .....	37
SFTS virus NSs intracellular vesicles traffic the endosomal recycling pathway and harbor an acidic environment .....	38
<b>DISCUSSION .....</b>	<b>40</b>
<b>CHAPTER 3.....</b>	<b>45</b>
<b>EXTRACELLULAR VESICLES MEDIATE RECEPTOR INDEPENDENT TRANSMISSION OF NOVEL TICK-BORNE BUNYAVIRUS<sup>2</sup> .....</b>	<b>45</b>
Introduction.....	45
<b>MATERIALS AND METHODS.....</b>	<b>47</b>
Cells, Plasmids, and Viruses .....	47
Transfections and Immunoblotting .....	48
Immunofluorescence.....	49
Live cell imaging .....	50
Isolation and Purification of extracellular vesicles.....	50
Infection of HeLa cells with purified extracellular vesicles. ....	51
Transmission Electron Microscopy (TEM) .....	52
Statistical analysis .....	54
<b>RESULTS .....</b>	<b>54</b>
SFTS virus infection induces the formation of cytoplasmic structures reminiscent of early endosomes.....	54
SFTS virus NSs-positive structures are released into the extracellular space.....	55
Ultrastructural analysis of purified SFTS virus NSs-positive extracellular vesicles.....	60
SFTS virus NSs-positive extracellular vesicles contain SFTS virions. ...	62
Extracellular vesicles produced during SFTS virus infection mediate receptor-independent transmission of SFTS virus.....	66
Discussion.....	68

<b>CHAPTER 4 .....</b>	<b>73</b>
<b>SUBVERSION OF THE UBIQUITIN-PROTEASOMAL PATHWAY BY SFTS VIRUS FOR INHIBITION OF INNATE IMMUNE RESPONSES.....</b>	<b>73</b>
INTRODUCTION .....	73
MATERIALS AND METHODS.....	76
Cells, Plasmids, Reagents .....	76
Transfection, immunoblotting, and immunoprecipitation. ....	77
Immunofluorescence and confocal microscopy.....	78
RESULTS .....	79
SFTS virus NSs localizes with components of the RIG-I signaling cascade. ....	79
SFTS virus infection leads to a decrease in RIG-I NT and TBK-1 expression. ....	79
Proteasome inhibition leads to recovery of RIG-I signaling cascade .....	80
Ubiquitination in part mediates interaction/colocalization between SFTS virus NSs and RIG-I or TBK-1.....	83
88	
DISCUSSION .....	89
<b>SUMMARY .....</b>	<b>92</b>
<b>REFERENCES .....</b>	<b>93</b>

Vita 102

## List of Tables

Table 1. Cellular distribution and mechanism of IFN inhibition/target of bunyavirus	
NSs.....	28

## List of Figures

Figure 1.1 Bunyavirus virion structure and genome organization.....	19
Figure 1.2. Transmission and ecology of SFTS virus.....	26
Figure 2.1. Pathways of endocytosis. Adapted from <a href="https://www.nature.com/article-assets/npg/nrm/journal/v12/n8/images/nrm3151-f1.jpg">https://www.nature.com/article-assets/npg/nrm/journal/v12/n8/images/nrm3151-f1.jpg</a> .....	34
Figure 2.2 Endosomal trafficking of human transferrin and epidermal growth factor receptors.....	35
Figure 2.3. SFTS virus NSs-mCherry positive cytoplasmic structures are associated with the endocytic recycling pathway. ....	39
Figure 2.4. SFTS virus NSs-mCherry positive cytoplasmic structures are associated with the endocytic recycling pathway.....	42
Figure 2.5. SFTS virus NSs-mCherry positive cytoplasmic structures harbor an acidic environment. ....	44
Figure 3.1. SFTS virus NSs induces the formation of endosomal-like structures. ....	56
Figure 3.2. Cytoplasmic vesicles containing SFTS virus NSs-mCherry are secreted into the extracellular space and are endocytosed by neighboring cells. ....	58
Figure 3.3. Isolation and characterization of SFTS virus NSs-positive secreted extracellular vesicles.....	59
Figure 3.4. Characterization of extracellular microvesicles secreted during SFTS virus infection. ....	61

Figure 3.5. Isolated extracellular vesicles are positive for SFTS virus NSs and the exosomal marker CD63. ....	64
Figure 3.6. SFTS virus NSs-positive extracellular vesicles harbor infectious SFTS virus virions. ....	65
Figure 3.7. SFTS virus NSs-positive extracellular vesicles can mediate receptor- independent transmission of SFTS virus. ....	67
Figure 3.8. Virions harbored within SFTS virus NSs-positive extracellular vesicles are capable of establishing a productive infection. ....	69
Figure 4.1. SFTS virus NSs localizes with endogenous TBK-1 and ubiquitin. ....	81
Figure 4.2. SFTS virus infection decreases levels of TBK-1 and RIG-I NT. ....	82
Figure 4.3. SFTS virus infection does not affect RIG-I and TBK-1 mRNA levels. ....	83
Figure 4.4. Inhibition of the Ubiquitin-Proteasomal Pathway restores TBK-1 and RIG-I NT levels. ....	84
Figure 4.5. Ubiquitination in part mediates interaction between SFTS virus NSs and RIG-I or TBK-1. ....	85
Figure 4.6. Ubiquitination in part mediates colocalization between SFTS virus NSs and RIG-I. ....	87
Figure 4.7 Ubiquitination in part mediates colocalization between SFTS virus NSs and TBK-1. ....	88

## **List of Illustrations**

Illustration 1.1 Worldwide distribution of members of the Bunyaviridae.....	18
---	----

## **List of Abbreviations**

ADP	Adenosine triphosphate
Arf	ADP-ribosylation factors
BSA	Bovine Serum Albumin
BUNV	Bunyamwera virus
CCHFV	Crimean Congo Hemorrhagic Fever Virus
CDE	Clathrin-dependent endocytosis
CIE	Clathrin-independent endocytosis
DIC	Disseminated intravascular coagulopathy
EE	Early endosome
EGFR	Epidermal Growth Factor Receptor
GSBS	Graduate School of Biomedical Science
HEK	Human Embryonic Kidney
HFRS	Hemorrhagic Fever with Renal Syndrome
hpi	hours post infection
HPS	Hantavirus Pulmonary Syndrome
Hpt	Hours post transfection
hr(s)	hour(s)
huTfR-1	Human Transferrin Receptor-1
IFN	Interferon
IL	Interleukin
LACV	La Crosse Virus

LC3	Light chain associated microtubule-3
LCI	Live Cell Imaging
LE	Late Endosome
MDA5	Melanoma differentiation-associated protein 5
mRNA	messenger ribonucleic acid
NSs	Small non-structural protein
NP	Nucleocapsid
PAMP	Pathogen-associated molecular patters
PRR	Pattern recognition receptors
RIG-I	Retonoic inducible gene-1
RNA	Ribonucleic acid
RNP	Ribonucleoprotein
RVFV	Rift Valley Fever Virus
SFTS virus	Severe Fever with Thrombocytopenia Syndrome Virus
TLR	Toll-like receptor
TBK-1	Tank-binding kinase-1
TRIM-25	Tripartite motif-containing protein 25
UB	Ubiquitin
UUKV	UUKeneimi virus
UTMB	University of Texas Medical Branch



# CHAPTER 1

## Introduction<sup>1</sup>

### INTRODUCTION TO BUNYAVIRUSES

The *Bunyaviridae* can be divided into arthropod-borne viruses (arboviruses) and those that can be transmitted via aerosolized rodent excreta, of which the latter only includes *Hantaviruses*. Bunyaviruses transmitted by arthropods (mosquitoes, ticks, sandflies, or thrips) are classified as *Phlebo-*, *Nairo-*, *Orthobunya-* and *Tospovirus*. Most bunyaviruses except *Tospoviruses* (which infect plants) are etiological agents of both human and animal diseases, resulting in asymptomatic to fatal outcomes.

Human disease from bunyavirus infection ranges from a mild, self-limiting illness to fatal severe hemorrhagic febrile illness and encephalitis, while in animals, certain bunyavirus infection leads to abortion storms and stillbirths [1-6]. Even though bunyaviruses pose a significant threat to both humans and animal species, the extensive worldwide distribution and diversity amongst this family hinder progress in developing safe and effective therapeutics against bunyaviruses.

### PUBLIC HEALTH IMPORTANCE

Worldwide distribution of bunyaviral vectors and with over 350 recognized isolates, make the *Bunyaviridae* a global threat to human public health, agricultural productivity, and livestock (**Illustration 1.1**). For example, Rift Valley Fever virus (RVFV), one of the most studied and characterized Phleboviruses, is considered to be a major agricultural threat due to its potential to

<sup>1</sup>A portion of this work has been published as: Jesus A. Silvas and Patricia V. Aguilar. (2017). The Emergence of Severe Fever with Thrombocytopenia Syndrome Virus. *Am. J. Trop. Med. Hyg.*, 00(0), pp1-6 doi:10.4269/16-0967. *In press*.

hinder livestock production [2, 7]. Currently, vaccines against RVFV for use in animals have been developed. However, the search for a better vaccine candidate is still underway [3, 8].



**Illustration 1.1 Worldwide distribution of members of the Bunyaviridae.**

Adapted from <https://mygermanshepherd.org/wp-content/uploads/2011/08/Bunyaviridae-infections.jpg>

#### **VIRION STRUCTURE AND GENOMIC ORGANIZATION**

Bunyavirus virions are spherical particles with a lipid bilayer envelope ranging in size from 80 to 120 nm in diameter (**Figure 1.1**). The glycoproteins Gn and Gc are incorporated into the envelope of the viral particle. The negative-sense single stranded tripartite genome is contained within the viral particle. Bunyavirus genome consists of a large (L) segment that encodes the RNA-dependent RNA polymerase, a medium (M) segment that encodes both Gn and Gc glycoproteins with the inclusion of an NSm protein in some bunyavirus families (Orthobunyavirus and Tospovirus), and the smaller (S) segment that encodes for the nucleocapsid (NP) protein, and a small non-structural protein (NSs) using an ambisense coding strategy in phlebo- and tospoviruses.

(Figure 1.1B), while Orthobunyaviruses have a second frame encoding the NSs. In sharp contrast, some Hantaviruses (except Puumala and Tula viruses) and Nairoviruses do not encode the NSs [9, 10].

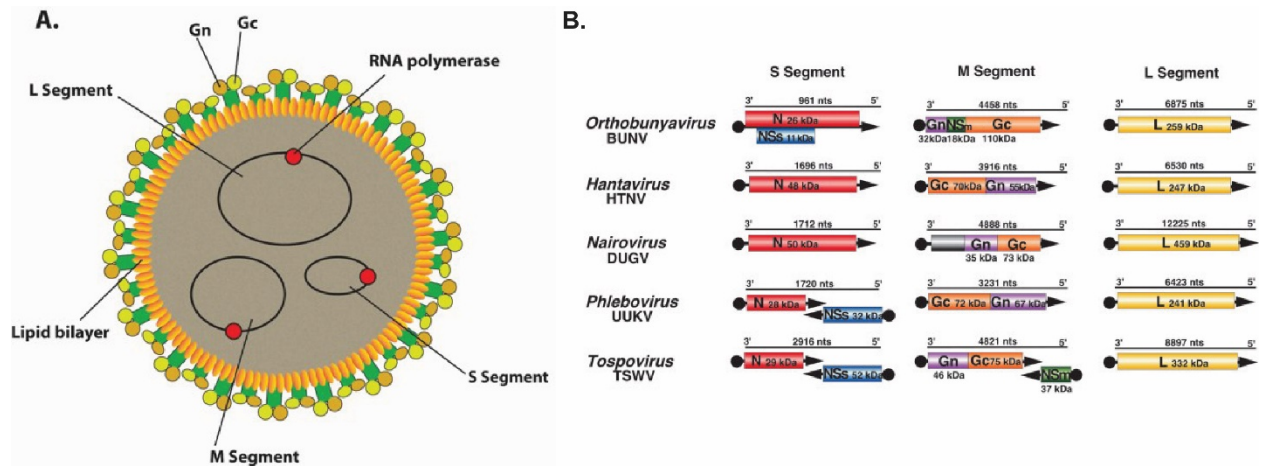


**Figure 1.1 Bunyavirus virion structure and genome organization.**

## ATTACHMENT, ENTRY, AND REPLICATION

Cellular receptors for bunyaviruses include the C-type lectin Dendritic Cell-Specific Intercellular adhesion molecule-3-Grabbing Non-integrin (DC-sign) or Liver-Specific Intercellular adhesion molecule-3-Grabbing Non-integrin (L-SIGN). Additionally, co-factors such as heparan sulfate, nucleolin, or non-muscle myosin heavy chain IIA (NMMHC-IIA) aid in promoting internalization of bunyaviruses into the host cell. Upon receptor-mediated attachment, viral particles enter host cells via endocytosis into the early endosomal compartment. Bunyavirus entry varies from virus-to-virus, with some requiring clathrin-mediated endocytosis and others independent of this pathway. For example, Oropouche virus enters the cell via clathrin-mediated endocytosis [11], in contrast, some studies suggest that Uukuniemi virus does not require clathrin-

mediated endocytosis [12]. Uncoating of the viral particles occurs as the endosomal compartment matures and internal acidification occurs, leading to fusion of both the viral and endosomal membranes. Fusion of the viral and endosomal membranes results in the release of the viral genome into the cell cytoplasm, and primary transcription of the viral complementary mRNA occurs using host cell factors and viral polymerase. Translation of L, M, and S segments mRNA leads to the production of corresponding proteins, with post-translational cleavage of the M segment polyprotein.

### **BUNYAVIRUS PATHOGENESIS**

Pathogenesis due to bunyaviral infection differs from genus to genus. Typically, initial Orthobunyavirus infection occurs in the striated muscle, disseminating into the plasma, then high viremia results in penetration of the blood-brain barrier. Infection with La Crosse Virus (LACV) leads to neuroinvasiveness resulting in cerebral lesions [6, 13-15]. Typical pathology observed in LACV human cases included cerebral edema, glial nodules, focal necrosis, and mild leptomeningitis [13, 14]. In contrast, human infection with phleboviruses such as Rift Valley Fever (RVFV), can remain asymptomatic or present with mild febrile illness [5]. However, 1-3% of RVFV infections in humans can lead to death [5]. RVFV infection of livestock, however, results in more severe outcomes. Livestock typically exhibits leukopenia in first days of infection, followed by alteration of serum levels indicative a hepatic damage in the acute phase, and during the recovery phase leukocytosis. Even though these are the typical manifestation of RVFV disease, they vary significantly. In severe cases, thrombocytopenia and fibrin thrombi suggest disseminated intravascular coagulopathy (DIC) [5].

Nairoviruses such as Crimean-Congo Hemorrhagic Fever Virus (CCHFV) are maintained in their tick hosts. However, infection of vertebrates such as livestock, hare, and large wild herbivores results in subclinical manifestations or present none at all [16-18]. Human infections with CCHFV lead to severe hemorrhagic outcomes. Organs of infected individuals typically exhibit edema, focal hemorrhage, and necrosis. During the first days of infection, thrombocytopenia and increased prothrombin more than likely play a significant role in disease progression, ending in DIC [16].

Unlike the other bunyavirus genera, the Hantaviruses are introduced into the human host through inhalation of infected aerosolized rodent excreta. Hemorrhagic fever with renal syndrome (HFRS) and Hantavirus Pulmonary Syndrome (HPS) are human diseases in which the kidneys or lungs exhibit capillary leakage and fluid loss, respectively [19-21]. The mechanism by which the kidneys undergo extreme pathology remains unclear, however interstitial infiltration of immune system cells such as lymphocytes and macrophages is observed during HFRS. In HPS, pulmonary edema, pleural effusions, and infiltration of mononuclear cells are seen in the lung epithelium [22]. Due to the high abundance of immune system cells infiltrates observed in HPS and HFRS, it has been suggested that disease associated with hantavirus infection is due to the human immune response and not viral-induced cell death [19-24].

#### **ISOLATION, IDENTIFICATION, AND CLASSIFICATION OF SFTS VIRUS**

Surveillance of febrile illness in Chinese provinces led to the identification of Severe Fever with Thrombocytopenia Syndrome (SFTS) virus in 2009. Isolation occurred from patients presenting with fever, thrombocytopenia, leukocytopenia and multi-organ dysfunction. By serological and molecular techniques, SFTS virus was classified as a bunyavirus, genus Phlebovirus [25]. Isolation of the first SFTS virus strain was carried out by inoculating DH82,

L929, Vero cell lines with white cells obtained from a 42-year old patient that presented with febrile illness. Furthermore, 11 more isolates were obtained by 2010, and genetic analysis revealed a 96% homology with the first SFTS virus isolate. Further phylogenetic studies showed that SFTS virus clustered with members of the *Bunyaviridae*, however both RNA-dependent RNA polymerase and glycoproteins were more closely related to Uukuniemi virus. Additionally, SFTS virus NP had 41.4% similarity with RVFV NP while in sharp contrast, the SFTS virus NSs showed a similarity of only 11.2 to 16.0% with amino acids in other phleboviruses [25].

## TRANSMISSION AND ECOLOGY

Ticks were initially suspected as the primary SFTS virus vector because patients recounted being bitten by ticks before illness onset and because ticks were frequently found in areas where the patients reside. Further investigations resulted in the isolation of SFTS virus from the ticks *Haemaphysalis longicornis* and *Rhipicephalus microplus* collected in areas with endemic SFTS virus transmission in China [26-28]. Notably, SFTS virus RNA was detected in *Haemaphysalis longicornis* at different developmental stages (i.e. larvae, nymphs, and adults) and also in eggs oviposited by engorged adult females suggesting that transtadial and transovarial transmission of SFTS virus occurs in ticks [27]. These findings could potentially account for maintenance of the virus in nature. In South Korea, SFTS virus has also been isolated from *Amblyomma testudinarium* and *Ixodes nipponensis* suggesting that they may serve as additional vectors in this country [29]. Nevertheless, laboratory vector competence studies are still needed to confirm their capacity to transmit SFTS virus.

In China, domestic animals are considered potential reservoir hosts for the virus because antibodies against SFTS virus have been detected in goats, cattle, sheep, pigs, dogs, and

chickens [30-32]. In these studies, SFTS virus RNA was detected only in a small fraction of animals (1.7%-5.3%), and none of these animals showed signs of illness. Virus isolates were obtained from some of these viremic animals, and sequencing analyses revealed that they were closely related to isolates obtained from SFTS patients and ticks [30]. Convincing evidence that ticks and possibly goats participate in the SFTS virus transmission cycle was obtained by Jiao *et al.* [26]. Experimental infection of goats with SFTS virus-induced detectable viremia in 3 out of 5 infected animals on day three post infection. Interestingly, viremia lasted only 24 hours, and no viral RNA was detected from nasopharyngeal or anal swabs suggesting that the virus is not shed through respiratory or digestive routes. Control animals that had close contact with the infected animals did not develop antibody responses indicating that close contact transmission of SFTS virus among goats does not occur [26]. Despite this knowledge, evidence demonstrating that the viremia detected in goats experimentally infected with SFTS virus is high enough to infect ticks was not obtained in the study. In another set of experiments conducted by the same authors, goats were naturally infected by exposure to ticks, and seroconversion monitoring and tick collection were performed on a daily basis. All goats were naturally infected by day 34, and viral RNA was detected in the majority of the animals, as well as in *Haemaphysalis longicornis* ticks collected from them. Not surprisingly, virus isolates obtained from both one goat, and its parasitic tick samples demonstrated high sequence homology, supporting the conclusion of natural transmission of SFTS virus [26].

Prevalence in mice and rats, particularly the field mouse *Apodemus agrarius* and the common rat *Rattus norvegicus*, has also been assessed and approximately 3% were found to be SFTS virus antibody positive [32]. The role of rodents in the transmission cycle of SFTS virus remains to be elucidated.

In South Korea, feral cats may also play a role in SFTS virus transmission since 17% of the samples obtained from feral cats had detectable viral RNA present [33]. In Japan, SFTS virus antibodies were also detected in cattle as well as wild boars [34, 35]. Recent studies have suggested a link between the occurrence of SFTS virus and migratory birds. The distribution of *H. longicornis* and the migratory bird routes between mainland China, S. Korea, and Japan suggest that waterfowl are responsible for the dispersal of SFTS virus-infected ticks. Phylogenetic studies performed on isolates from Japan and S. Korea show genetic similarities with SFTS virus strains isolated in mainland China [36, 37]. These findings suggest that additional studies to elucidate the ecology and transmission cycle of SFTS virus in these countries are still needed.

Although tick to human is believed to be the main route of SFTS virus transmission, evidence supporting possible person to person transmission of SFTS virus has also been documented [38-40] (**Figure 1.2**). Given the fact that SFTS virus RNA is found in bodily secretions, this further supports the potential for human to human SFTS virus transmission without the involvement of the tick vector; nevertheless, risk factor analyses did not detect being in close contact with SFTS patient as one of the main risk factors for infection [41]. In contrast, analysis of a family cluster of SFTS virus infections by Yoo et al. suggested the possible transmission of SFTS virus via close contact [42].

## EPIDEMIOLOGY

Although SFTS was first recognized in 2009, the disease first appeared in rural areas of central China in the spring of 2006. Since then, the number of SFTS cases have increased considerably in China from 511 in 2011 to nearly 1,500 cases in 2012 [43]. The initial case



fatality rate reported was up to 30%; however, recent estimates range between 10-12% except for Japan and South Korea where the mortality rate is as high as 50% [44-47]. The disease is mainly seen among farmers engaged in agricultural activities or forest workers, and the majority of the cases (86%) are detected in subjects 50 years of age or older with fatality rates increasing with age [48, 49]. The SFTS case incidence was found to be similar for both females and males [49], although a female to male ratio of 1.58 was reported in an early study in the Xinyang province based on laboratory-confirmed SFTS cases [48]. It has also been noted that approximately 67% of the cases are reported between the months of May and July [48, 49]. The SFTS virus antibody prevalence among healthy subjects residing in endemic areas in China ranges between 0.8-3.8% [32, 50]. Given the limited information available about the duration of antibody responses following exposure to SFTS virus, studies are needed to elucidate if the low prevalence levels are due to low exposure levels, limitation in the sensitivity of antibody detection methods, or short duration of antibody responses following SFTS virus exposure. A recent study in a small cohort of previously SFTS hospitalized patients detected SFTS virus antibodies even four years after hospitalization; nevertheless, the antibody levels had decreased over time among most study subjects [51]. Thus, studies to evaluate the duration of antibody responses in a larger study group following SFTS virus infection are still needed. Due to the increased number of SFTS cases reported in recent years, the presence of SFTS virus within blood donations was assessed from April to October 2012 at multiple blood centers in the Henan province in China. A modest antibody prevalence of 0.54% among the healthy blood donors was reported [52]. Viral RNA was detected in only 2 out of the 17,208

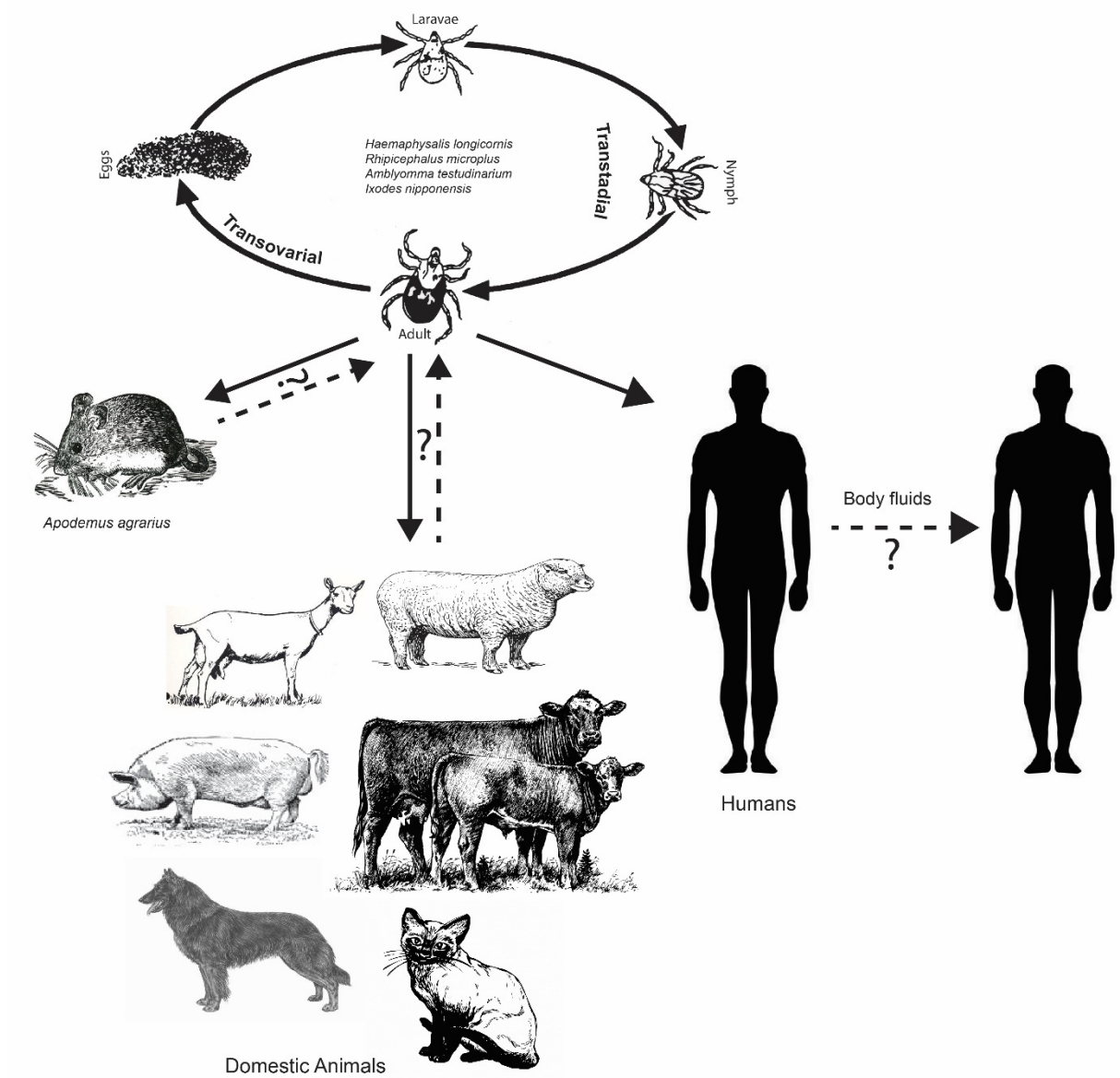


**Figure 1.2. Transmission and ecology of SFTS virus.**

plasma samples tested, and viral load levels were low (less than 20 plaque forming units/mL)[52]. Thus, these findings raise some questions as to whether SFTS virus constitutes a significant threat to blood banks. However, this possibility should not be completely overruled, particularly in endemic areas of SFTS virus circulation.

SFTS cases have also been reported in Japan and South Korea [29, 46, 53]. In South Korea, the first SFTS case was retrospectively identified in a sample collected in August 2012 from a female with a history of insect bites while working on a crop farm and who died from multiple organ failure [54]. Additional cases were later identified by the Korean Center for Disease Control and Prevention in 2013 with a case fatality rate of 47.2 % [46].

#### **PATHOGENESIS AND MOLECULAR VIROLOGY**

Due to its recent emergence, the pathogenesis of SFTS virus has not been fully defined. We do know that inhibition of innate immune responses is a common feature among the mosquito- and sandfly-borne bunyaviruses and this occurs through a variety of mechanisms, including protein degradation and downregulation of host cell transcription [13, 55-58] (**Table 1**). The Phlebovirus nonstructural protein NSs was found to be the major virulence factor involved in the inhibition of IFN responses as well as inhibition of host cell gene transcription [59, 60]. Interestingly, SFTS virus-infected patients have almost no detectable IFN- $\beta$  in their sera suggesting that SFTS virus is also capable of inhibiting IFN responses [45]. Consistent with these observations, studies have demonstrated the ability of the SFTS virus NSs to inhibit IFN responses [61-64]. However, the mechanism by which the tick-borne SFTS virus inhibits IFN responses differs to those described for mosquito and sandfly-borne bunyaviruses. In contrast to protein degradation or inhibition of host cell transcription, the particular ability of SFTS virus NSs to inhibit the innate immune

response correlates with the spatial relocation or sequestration of the main components of the IFN response (i.e. retinoic inducible gene I, Tank-binding kinase 1, and the E3 ubiquitin ligase TRIM25) into the SFTS virus NSs positive-cytoplasmic structures [61, 65, 66].

	Phlebovirus	NSs distribution	Mechanism of IFN inhibition/Target
Mosquito	Rift Valley Fever Virus	Nuclear/ Cytoplasmic	Proteosomal degradation of PKR, TFIIH p62; inhibition of host cell transcription; sequestration of TFIIH p44 and XPB
	Punta Toro Virus	Cytoplasmic	Inhibition of IFN induction
Tickborne	Severe Fever with Thrombocytopenia Syndrome Virus	Endosomal	Sequestration of RIG-I, TBK-1/IKKe, TRIM25, STAT 1/2, IRF3 into endosomal structures

**Table 1. Cellular distribution and mechanism of IFN inhibition/target of bunyavirus NSs.**

Abnormal production of pro-inflammatory cytokines has been recently detected in patients with a severe form of the disease and higher serum viral load correlated with elevated cytokine levels [67]. Key immune mediators such as IL-1 $\beta$ , IL-8, MIP-1 $\alpha$ , and MIP-1 $\beta$  were elevated during the acute phase of the disease in patients who succumbed to infection when compared to those who survived SFTS [67]. SFTS virus has also been shown to bind to platelets. This phenomenon has been suggested as the possible cause of thrombocytopenia observed in patients, because virus bound to platelets are recognized by macrophages and phagocytosed, leading to a decrease in platelet count [68]. Decreased levels of CD3<sup>+</sup> and CD4<sup>+</sup> T lymphocytes have also been reported in SFTS-infected patients, including in those who succumbed to the disease [47, 69].

The SFTS virus NSs has been observed to localize to cytoplasmic structures positive for the early endosomal marker Rab5 and the autophagy marker LC3 [61]; however localization was

to cytoplasmic structures was still observed in mouse cells deficient in conventional autophagy, suggesting these NSs-positive structures are not derived from the autophagy pathway [61]. Further confocal analysis of the SFTS NSs-cytoplasmic structures revealed that they did not localize with markers associated with the endoplasmic reticulum or the Golgi Apparatus. Additionally, through indirect immunofluorescence of SFTS virus infected HeLa cells, we and others observed that the NSs-positive structures also localized with the SFTS virus NP, L, and nascent viral RNA—suggesting these structures could be sites of viral replication [66].

The above-mentioned studies suggest that the NSs-positive structures localize to endosomal derived cytoplasmic structures that correlate with the inhibition of innate immune responses and may have a role in viral replication; however, the exact mechanism and function of these structures still needs to be elucidated. Therefore, in this study, I propose to test the central hypothesis that *SFTS virus exploits the endosomal pathway for inhibition of innate immune responses as well as for viral replication*. This central hypothesis will be tested with the following specific aims:

## **SPECIFIC AIMS**

### **Specific Aim 1**

Determine the source of SFTS virus NSs-positive structures.

Hypothesis: *SFTS virus hijacks structures derived from the early endosomal pathway during viral infection.*

Rationale: The endosomal pathway provides the cell with a vast compartmentalization system for the trafficking of proteins. Regulation of the endosomal pathway is mediated by Rab GTPases and ADP-ribosylation factors (Arfs) that are responsible for sequestration of cargo and directing of endosomal vesicles to distinct pathways. We have reported that the NSs of SFTS virus localizes

to cytoplasmic structures positive for the early endosomal marker Rab5 and the autophagy marker LC3 [11]. Additionally, by Mass Spectrometry Analysis of isolated cytoplasmic SFTS virus NSs-positive structures, we were able to identify additional proteins associated with the endosomal pathway such as Arf-1 (known to regulate formation of clathrin-coated pits), Arf-6 (a regulator of membrane recycling endosomes), the human transferrin receptor (huTfR-1), and the epidermal growth factor receptor (EGFR).

### ***SPECIFIC AIM 1A***

Determine whether SFTS virus NSs localizes to cytoplasmic structures derived from the Endosomal Recycling Pathway.

Hypothesis: *SFTS virus NSs hijacks early endosome structures.*

### **Specific Aim 2**

Determine the role of SFTS virus NSs-positive cytoplasmic structures in viral replication.

Hypothesis: *SFTS virus NSs targets Rab5-positive vesicles for generation of viral factories.*

Rationale: It has been widely described that bunyaviruses undergo viral replication and virion assembly within structures derived from the Golgi apparatus and the endoplasmic reticulum (ER) [14-16]. The NSm protein of bunyaviruses, which is not encoded by SFTS virus, has been shown to be a scaffold protein that associates to these structures [14, 15, 26]. We have reported that the structures positive for SFTS virus NSs do not co-localize with protein markers related to the Golgi or ER, but with endosomal markers. Furthermore, we found that these structures harbor newly synthesized viral RNA as well as viral proteins involved in SFTS virus replication. Additionally, we have observed the active transfer of SFTS virus NSs-positive structures from cell to cell.

### ***SPECIFIC AIM 2A***

Determine whether SFTS virus NSs secreted structures are exosomes.

Hypothesis: *SFTS virus NSs hijacks exosomal structures.*

Rationale: Recent studies have shown that viral pathogens use exosomes or exosome-like vesicles for the dissemination of infectious material or viral progeny [70, 71]. Exosomes or exosome-like vesicles can be derived from the endosomal pathway or directly from the plasma membrane [72, 73]. We have observed that the SFTS virus NSs protein relocates to Rab5+ early endosomal structures and using live cell imaging of SFTS virus NSs expressing cells we noted that 20-30% of these structures are secreted into the extracellular space and endocytosed by neighboring cells.

### ***SPECIFIC AIM 2B***

Determine whether SFTS virus NSs-positive structures contain viral material

Hypothesis: *SFTS virus NSs-positive structures carry infectious viral RNA.*

Rationale: Exosomes have been implicated in the active transfer of viral progeny or viral genetic material [70, 74-77].

### **Specific Aim 3**

Determine the mechanism by which components of the RIG-I signaling cascade are targeted into SFTSV NSs-positive structures

Hypothesis: *Components of the RIG-I signaling cascade are directed into SFTS virus NSs-positive structures via the interaction between NSs and ubiquitin for degradation via the Ubiquitin-Proteosomal Pathway.*

Rationale: It has been reported that SFTS virus NSs prevents the induction of interferon- $\beta$  (IFN- $\beta$ ) responses by sequestering components of the RIG-I signaling cascade such as RIG-I, TRIM-25, and TBK-1, into cytoplasmic structures [11, 12]. Additionally, we observed that ubiquitin also localizes to the SFTS virus NSs-positive structures. Ubiquitination is one of the key posttranslational modifications that modulate protein activity. Ubiquitin moieties, K63- and K48-linked, have been well described as determinants in the proteolytic fate of proteins [30]. Ubiquitination at K63 targets the protein to lysosomes, while K48 ubiquitination leads to

degradation via the 26S proteasome. RIG-I and TBK-1 have been shown to be heavily regulated by ubiquitin [31-33]. Furthermore, Mass Spectrometry analysis of isolated SFTS virus NSs structures revealed components of the 26S proteasome; however, RIG-I, TRIM25, and TBK-1 were not detected. Lastly, as previously stated by live cell imaging, we were able to observe that only a portion of SFTS virus NSs-positive structures exited the cell, while others trafficked within. Thus, the objective of this aim is to investigate if protein ubiquitination mediates the sequestration of components of the RIG-I signaling cascade by SFTS virus NSs.

### ***SPECIFIC AIM 3A***

Determine whether RIG-I signaling components are degraded via the Ubiquitin-Proteasome Pathway during SFTSV infection.

Hypothesis: *SFTS virus NSs targets RIG-I for degradation via the Ubiquitin-Proteasome Pathway.*

Rationale: Mass spectrometry analysis of purified intracellular SFTS virus NSs-positive structures identified key components of the 26S proteasome and ubiquitin. Additionally, we have observed that ubiquitin co-localizes within NSs-positive structures and interacts with SFTS virus NSs.

### ***SPECIFIC AIM 3B***

Determine if protein ubiquitination is the mechanism by which components of the RIG-I signaling cascade are targeted into SFTS virus NSs-positive cytoplasmic structures

Hypothesis: *SFTS virus NSs sequesters ubiquitinated RIG-I and its signaling components into cytoplasmic structures.*

Rationale: Ubiquitination of cellular proteins is one of most widely conserved and utilized post-translational modification used in cellular homeostasis, innate immunity, etc. We have observed, that SFTS virus NSs interacts with ubiquitin and targets ubiquitin into cytoplasmic structures.



## CHAPTER 2

### Endosomal trafficking of SFTS virus NSs

#### INTRODUCTION

The endosomal system is comprised of a vast network of compartments that function in the trafficking of cellular cargo into, within, and out of the cell. Endocytosis can be divided into two classical pathways, clathrin-dependent or clathrin-independent [78, 79]. Clathrin-dependent pathways (CDE) require the shuttling of cargo into endosomal vesicles coated with clathrin, while clathrin-independent (CIE) entry can occur in a multitude of pathways such as macropinocytosis and phagocytosis[80, 81] (**Figure 2.1**). Additionally, cargo can enter the cell through caveolae-dependent endocytosis, in which caveolin-1 coated vesicles are required for the shuttling of cargo from the plasma membrane into the cell [81] (**Figure 2.1**). Regardless of entry cargo that enters the cell is shuttled into an early endosomal compartment for sorting. Extensive studies in CDE have identified receptors that have been established as the standard for studies regarding endocytosis and subsequent pathways such as endocytic recycling and endocytic degradation. It has been suggested that endosomal sorting is initiated at the plasma membrane upon binding of the ligand and this determines the population of endosomal compartments the cargo is shuttled into, dynamic (quick maturation) or static (slow maturation) compartments. Dynamic maturation has been mostly implicated in pathways leading to endocytic degradation, while static maturation leads to endocytic recycling [82, 83].

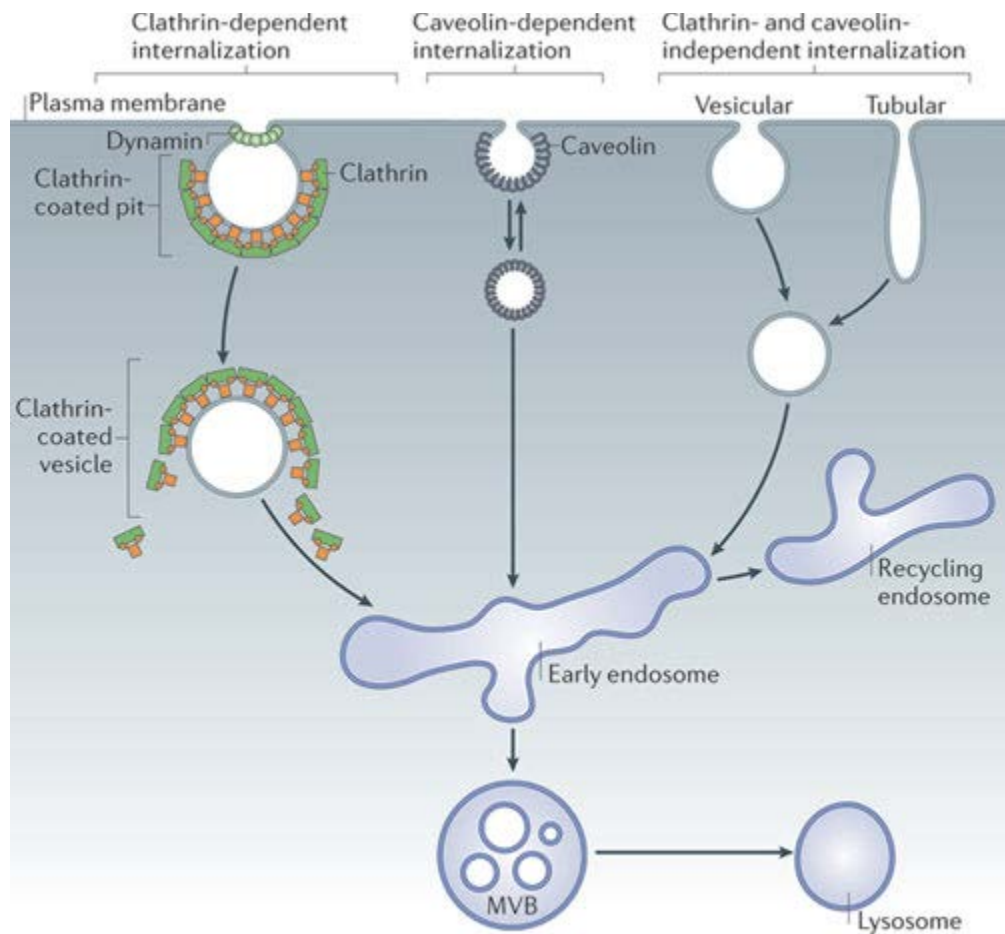


**Figure 2.1. Pathways of endocytosis.** Adapted from <https://www.nature.com/article-assets/npg/nrm/journal/v12/n8/images/nrm3151-f1.jpg>

The human transferrin receptor (huTfR) is one of the receptors that has been used to study endocytic recycling [84-86], while the epidermal growth factor receptor (EGFR) has been utilized for the study of endocytic degradation (**Figure 2.2**) [87-90]. The huTfR travels the recycling pathway via static endosomal compartments, where once its cargo is delivered it gets shuttled back to the plasma membrane. In contrast, the EGFR can travel either the recycling (when bound by transforming growth factor- $\alpha$ ) or degradation (when bound by epidermal growth factor) pathways, dependent on the ligand [83, 88-90].

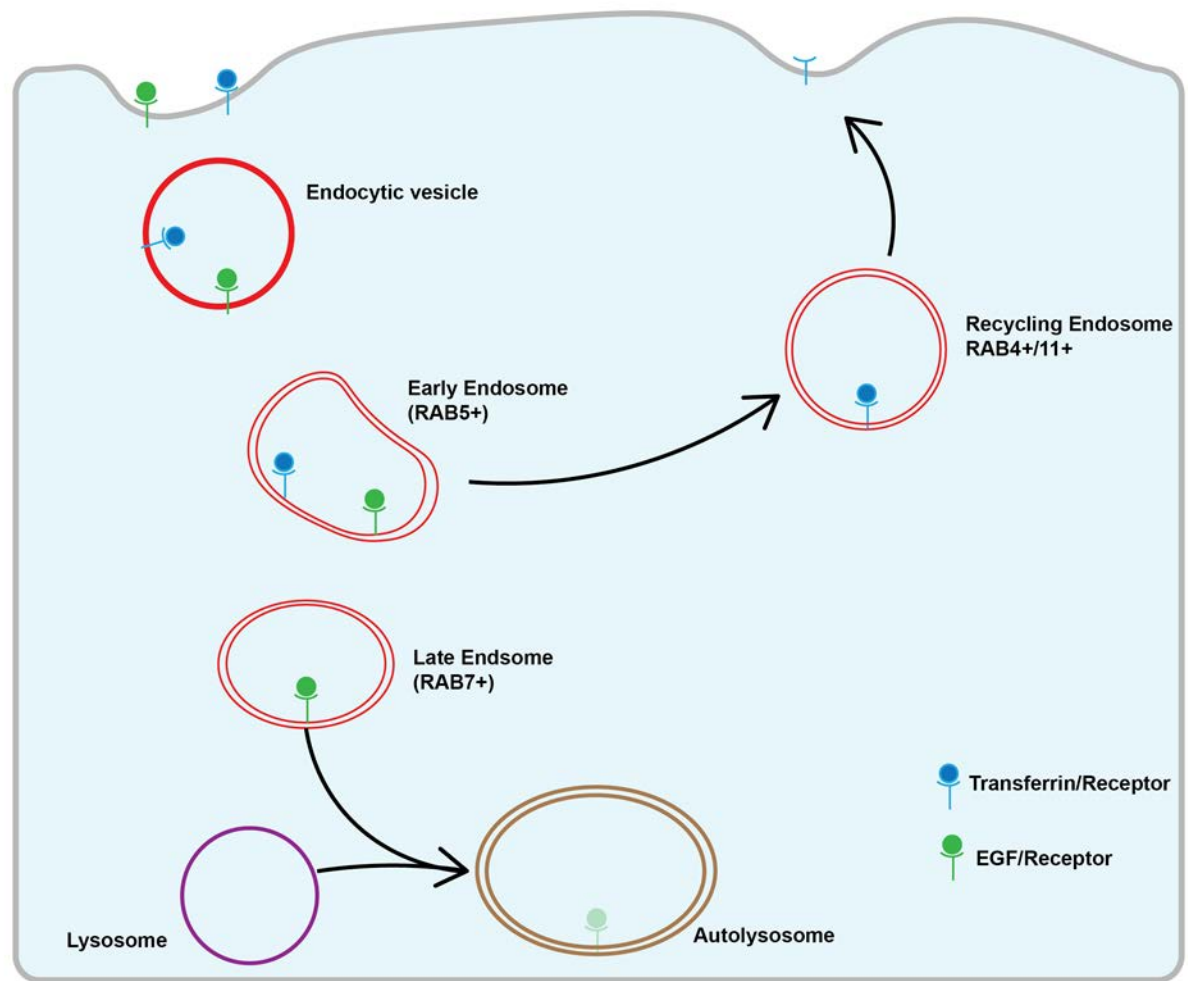


**Figure 2.2 Endosomal trafficking of human transferrin and epidermal growth factor receptors.**

It has been previously reported that the small non-structural protein, NSs, of the emerging tick-borne phlebovirus Severe Fever with Thrombocytopenia Syndrome (SFTS) virus localizes to cytoplasmic structures positive for the early endosomal marker Rab5 and the autophagy marker microtubule-associated protein 1A/1B light chain 3 (LC3) [61, 65, 66, 91]. The association of SFTS NSs with LC3 implicated the autophagy pathway as the source of these structures; however,

this pathway was ruled out when transient expression of NSs in cells deficient in ATG7, critical in the formation of the autophagosome compartment, still led to the localization of NSs into cytoplasmic structures [61]. To this end, using a HeLa cell line stably expressing the SFTS virus NSs fused to mCherry fluorescent protein, we performed live cell imaging (LCI) to visualize the trafficking of EGFR to the endocytic degradation, or huTfR to the endocytic fast recycling pathways and determine their colocalization with the SFTS virus NSs cytoplasmic structures. Interestingly, we observed that the SFTS virus NSs traffics within a diverse population on endocytic compartments involved in both the recycling and degradation pathways. To gain additional insights into the characteristic of these structures, we used pH indicators and determined that the SFTS virus NSs cytoplasmic structures have an acidic pH environment (pH <5). Altogether these data suggest that the SFTS virus NSs traffics multiple endocytic pathways and thus may have multiple roles during SFTS virus infection.

## **MATERIALS AND METHODS**

### **Cells and Reagents**

The SFTS virus NSs plasmid was constructed by PCR using overlapping deoxyoligonucleotides corresponding to the published GenBank Sequence (NC018137.1) and has been described elsewhere [61]. The SFTS virus NSs-mCherry was constructed using standard cloning techniques [61]. The mCherry and the SFTS virus NSs-mCherry genes were then cloned into a third-generation lentivirus vector and used to generate lentiviruses. HeLa cells were transduced with the lentivirus particles, and the mCherry and SFTS virus NSs-mCherry stable cell lines were generated by antibiotic selection and cloning of the mCherry fluorescent cells to select those with a high level of protein expression as determined by confocal microscopy and Western blot analyses.

For visualization of endosomal trafficking, human Epidermal Growth Factor conjugated to AlexaFluor488 (EGF-488), and human Transferrin-conjugated to AlexaFluor488 (huTfn-488) were purchased from Life Technologies. pHrodo Green *E. coli* BioParticles conjugates from Life Technologies were used as pH indicator.

### **Live Cell Imaging**

HeLa cells stably expressing the SFTS virus NSs-mCherry were plated on 35mm glass bottom culture dishes (MatTek Corporation) and incubated overnight at 37°C in 5% CO<sub>2</sub>. Before live cell imaging, cell culture media was removed, cells were washed with DPBS, and live cell imaging solution (Invitrogen) was added. Cells were then treated with endosomal trafficking reagents and visualized for 30 minutes using a Prairie Technologies/Nikon multimodal live cell imaging system.

## **RESULTS**

**SFTS virus NSs intracellular vesicles traffic the endosomal recycling pathway.** It has been previously reported that SFTS virus NSs localizes to cytoplasmic structures positive for the early endosomal marker Rab5 and the autophagy marker microtubule-associated protein 1A/1B light chain 3 (LC3) [61]. The broad use of the endosomal pathway in the trafficking of cellular proteins led us to investigate the pathways which the SFTS virus NSs positive cytoplasmic vesicles associate with. The Rab5 positive early endosome can be related to recycling and degradation pathways. To examine whether the SFTS virus NSs-positive structures were associated with either the recycling or degradation pathways, we performed live cell imaging (LCI) on HeLa cells stably expressing the SFTS virus NSs fused to mCherry fluorescent protein. To visualize the endocytic recycling pathway, we incubated the HeLa SFTS NSs-mCherry cell line with human transferrin

conjugated to AlexaFluor488 (huTrfn-488). Human transferrin once bound to its receptor located on the plasma membrane enters the cell through clathrin-mediated endocytosis and travel the three primary endocytic populations, the early endosome, late endosome and the recycling endosome, which delivers the receptor back to the cell membrane [84, 85, 92]. HeLa SFTS virus NSs-mCherry HeLa cells were incubated with huTrfn-488, and endocytic recycling of the transferrin receptor was visualized for 30 minutes. Interestingly, we noted a mixed population of intracellular SFTS virus NSs-mCherry vesicles that localized with huTrfn-488 (**Figure 2.3**), suggesting that a population of these cytoplasmic vesicles traffic the endosomal recycling pathway.

**SFTS virus NSs intracellular vesicles traffic the endosomal recycling pathway and harbor an acidic environment.** Our previous observation that only a portion of SFTS virus NSs positive cytoplasmic structures localized with the endocytic recycling pathway lead us to characterize these structures further and determine if they were also associated with the endocytic degradation pathway. To investigate this possibility, we used the Epidermal Growth Factor conjugated to AlexaFluor488 (EGF-488) to visualize the trafficking of the Epidermal Growth Factor Receptor (EGFR) as it travels the endocytic degradation pathway. Binding of EGFR by specific ligands such as EGF or transforming growth factor  $\alpha$  leads to receptor degradation or recycling, respectively [90]. EGF bound EGFR is immediately internalized and shuttled into the early endosome and subsequently travels to the late endosome and ultimately to the lysosome for degradation [93]. Robust and continuous ubiquitination of EGF by Cbl ligases maintain EGF bound to EGFR until it becomes degraded via the lysosome [88-90, 94]. Incubation of HeLa SFTS NSs-mCherry cells with EGF-488 lead us to visualize EGFR trafficking of the endocytic degradation pathway in which we observed localization of the NSs-positive structures with this pathway (**Figure 2.4**), suggesting that these structures also travel the endocytic degradation pathway.

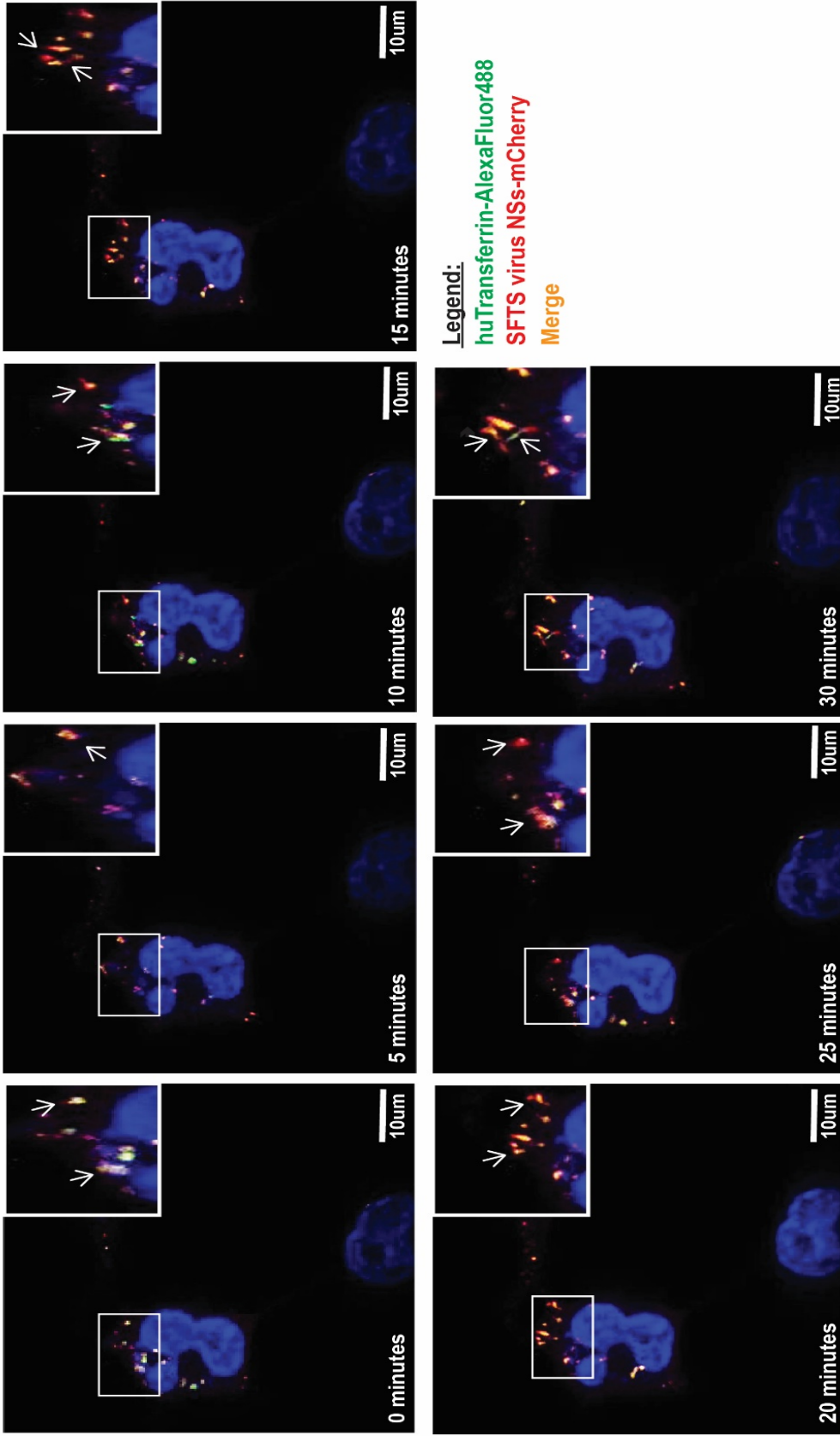


**Figure 2.3. SFTS virus NSs-mCherry positive cytoplasmic structures are associated with the endocytic recycling pathway.**

HeLa SFTS virus NSs-mcherry cell line was incubated in the presence of 10uM huTrfn-488 and visualized for 30 minutes with a Parairie/Technologies/Nikon multimodal live cell imaging system. Representative images were extracted in 5 minute increments.

To further elucidate a potential role during viral infection, we investigated whether the SFTS virus NSs-positive cytoplasmic structures harbored an acidic environment, which would further suggest these structures could be sites of protein degradation. To this end, we incubated HeLa NSs-mCherry cells with pHrodo Green BioParticles which only fluoresce at pH <5. Interestingly, we observed that the SFTS virus NSs-mCherry positive cytoplasmic structures localized with fluorescent pHrodo Green BioParticles, indicating that these structures have a low pH (**Figure 2.5**). Altogether, these data also point towards the use of the endocytic degradation pathway by the SFTSV NSs and harbor an acidic environment.

## DISCUSSION

Internalization of extracellular material in the host cell involves a complex system of interactions between pathways, membranes, and regulatory proteins such as Rab GTPases. Cargo can be internalized via clathrin-dependent (CDE), clathrin-independent endocytosis (CIE), use of caveolin-1 coated pits, or glycolipid rafts [78-81]. Current studies regarding the entry of bunyaviruses into mammalian cells have shown that bunyaviruses enter through RAB5+ early endosomes (EE), however, the use of clathrin-coated pits is not required for all [9, 11, 12, 18, 95]. To date, studies regarding entry of SFTS virus using both live virus or pseudotype Vesicular Stomatitis Virus (VSV) expressing SFTS virus glycoproteins have shown that entry is clathrin dependent and the use of glycolipid-mediated entry has also been suggested [96-98]. These studies have shown that entry into host cells varies greatly and can require the use of multiple pathways. CDE has been extensively studied, and it has been shown that regardless of the ultimate destination of the endocytosed cargo, the Rab5+ EE is the first endosomal compartment that is occupied [99-101]. The EE then continues to mature and travel common pathways such recycling and degradation. Recycling endosomal compartments are characterized as either slow (Rab11+) or fast



(Rab4+/Rab35+) [102, 103]. Slow recycling occurs with cargo that travels from the EE to a Rab7+ late endosome (LE) where it transfers to the Rab11+ endosome and gets shuttled back to the plasma membrane [102]. In contrast to the alternative recycling pathways, the endocytic degradation pathway begins with the Rab5+ EE, where it matures to a Rab7+ and fuses to lysosome for degradation of its cargo [87].

The endocytic recycling pathway has been studied using the human transferrin receptor (huTfR), which has been observed to travel the fast and slow recycling pathways [82, 84]. Likewise, the endocytic degradation pathway has been studied using the epidermal growth factor receptor (EGFR), which can interestingly travel both the recycling and the degradation pathways, dependent on the ligand [90]. Weak binding of EGFR by transforming growth factor- $\alpha$  results in recycling of the receptor, while strong ubiquitination mediated by Cbl ligases between EGFR and EGF leads to receptor degradation [87-90].

The Bunyavirus small-nonstructural protein (NSs) has been attributed as the major virulence factor across the *Bunyaviridae*. Most of the characterization studies performed to identify the function and location of the NSs have been carried out on mosquito- or sandfly-borne bunyaviruses such as Rift Valley Fever (RVFV), La Crosse (LACV), and Bunyamwera (BUNV). For example, the RVFV NSs, a viral protein that accumulates in filamentous structures in the nucleus, where it inhibits host cell transcription [56, 59, 60, 104-106]. Severe Fever with Thrombocytopenia Syndrome (SFTS) virus is a novel tickborne Phlebovirus and a handful of studies have shown that the NSs of this virus also inhibits the host cell immune response, however, the exact mechanism has yet to be described [61, 64, 65, 107]. We and others have described the inhibition of innate immune responses by SFTS virus NSs partially correlates with the removal of signaling components from the signaling cascade into cytoplasmic structures to which the NSs

also localizes to [61, 65, 66, 91]. Even though studies have shown that the cytoplasmic structures positive for SFTS virus NSs contain markers for the early endosomal and autophagy pathways [61], the specific pathway targeted by SFTS virus NSs for the formation of these cytoplasmic structures remains to be determined.

In this study, we sought to characterize the endosomal pathway to which the SFTS virus NSs-positive structures traffic within the cells. Unexpectedly, we observed that the SFTS virus NSs-positive cytoplasmic structures were a dynamic and diverse population, traveling distinct endosomal pathways. We noted that the SFTS virus NSs-positive cytoplasmic structures traveled alongside the huTfR, suggesting that these cytoplasmic structures travel within the recycling pathway. Additionally, we observed co-localization of NSs-positive cytoplasmic structures with EGF bound EGFR, suggesting that these structures also travel the endocytic degradation pathway. This, in turn, correlates with results from mass spectrometry analysis of purified SFTS virus NSs-positive cytoplasmic structures, in which Rab31, involved in shuttling EGF from early to late endosomes [87], was identified. Lastly, we observed that the SFTS virus NSs-positive cytoplasmic structures harbored an environment with a pH <5. The endosomal compartment pH is maintained in a range between 6.5-4.5, decreasing as it matures from EE to LE and finally to lysosome [108]. This data along with co-localization with EGF strongly suggests that a portion of the NSs-positive vesicles might be involved in degradative processes. However, further analysis of the structures of each distinct population would have to be analyzed in order to determine the cargo they contain, as it determines the fate or pathway to be traveled by the structure. Altogether this data suggests that the SFTS virus NSs traffics both the endosomal recycling and degradation pathways, however further studies are needed to elucidate the role that these cytoplasmic structures have during viral infection.

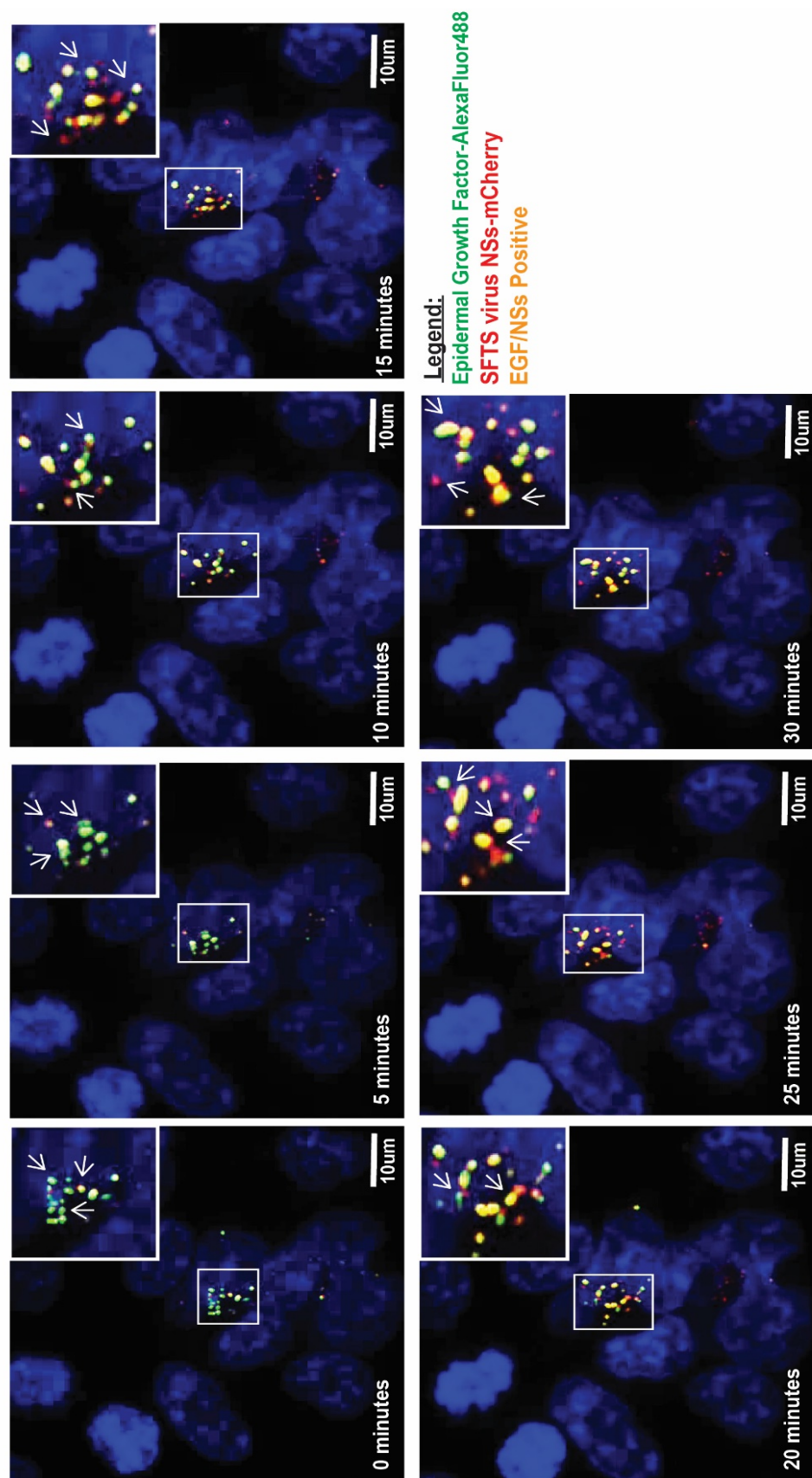


**Figure 2.4. SFTS virus NSs-mCherry positive cytoplasmic structures are associated with the endocytic degradation pathway**

HeLa SFTS virus NSs-mcherry cell line was incubated in the presence of 10uM EGF-488 and visualized for 30 minutes with a Parairie/Technologies/Nikon multimodal live cell imaging system. Representative images were extracted in 5 minute increments.

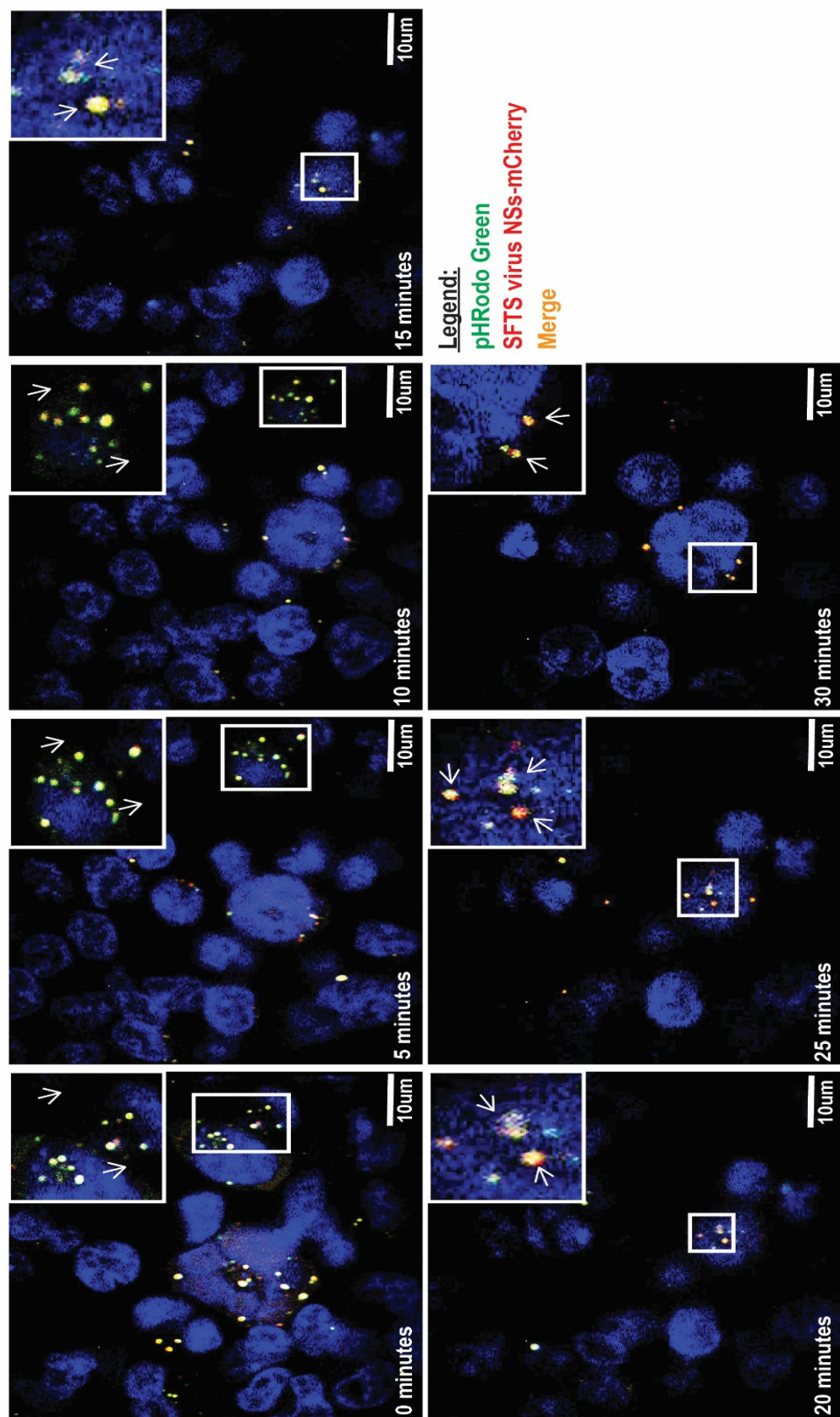


**Figure 2.5. SFTS virus NSs-mCherry positive cytoplasmic structures harbor an acidic environment.**

HeLa SFTS virus NSs-mcherry cell line was incubated in the presence of 10uM pHRedo-Green and visualized for 30 minutes with a Parairie/Technologies/Nikon multimodal live cell imaging system. Representative images were extracted in 5 minute increments.

## CHAPTER 3

# EXTRACELLULAR VESICLES MEDIATE RECEPTOR INDEPENDENT TRANSMISSION OF NOVEL TICK-BORNE BUNYAVIRUS<sup>2</sup>

### INTRODUCTION

The *Bunyaviridae* family comprises five genera, including Orthobunyavirus, Phlebovirus, Nairovirus, Hantavirus, and Tospovirus. The majority of viruses within this family (except Hantaviruses) are considered arthropod-borne viruses and are important causes of morbidity and mortality around the world. These viruses are associated with a range of clinical symptoms characterized by febrile illness, and in the most severe cases, fatal hepatitis, hemorrhagic fever or neurological manifestations requiring intensive care have been reported.

Due to advances in genomic and virus identification approaches, novel bunyaviruses have been discovered and identified as important causes of human disease during recent years [25, 45, 109]. One example is Severe Fever with Thrombocytopenia Syndrome (SFTS) virus, a new member of the family *Bunyaviridae*, genus *Phlebovirus* [25, 29]. The virus was first isolated in China in 2009 from patients presenting with a hemorrhagic fever illness [25, 43]. The initial case fatality rate reported for SFTS was 12-30%, and a recent serosurvey among persons living in rural Jiangsu Province found that 3.6% of residents had neutralizing antibodies to SFTS virus [110]. Evidence has also been obtained about the possibility of person-to-person transmission [39, 111]. Furthermore, hemorrhagic fever cases with mortality rates as high as 50% have now been recognized in Japan and Korea, further highlighting the emerging potential of this pathogen [25, 45, 54,

112, 113]. Therefore, SFTS virus is a highly pathogenic phlebovirus, and due to its recent emergence, the mechanism of disease pathogenesis is still unclear. Like other members of the family *Bunyaviridae*, SFTS virus possesses a negative sense tripartite genome consisting of the S, M and L segments. The L segment encodes for the viral RNA polymerase (L), the M segment encodes the glycoproteins (Gn/Gc), and the S segment uses an ambisense coding strategy to encode for a non-structural protein (NSs) and a nucleocapsid protein (NP) [114]. Although many bunyaviruses, including the prototype virus in the *Bunyaviridae* family Bunyamwera virus (BUNV), also encodes the nonstructural protein NSm within the M segment, some members of the *Phlebovirus* genus, including SFTS and Uukuniemi viruses (UUKV) do not encode this viral protein [25, 115]. The BUNV NSm is known to serve as a scaffold protein that associates to globular and tubular structures derived from the Golgi apparatus [116-118]. These structures have been shown to harbor the ribonucleoprotein (RNP), a complex essential for the transcription and replication of viral RNA [116]. Although SFTS virus does not encode the NSm protein, it has been recently suggested that the SFTS virus NSs may exert some of the NSm's function by serving as a scaffold protein and forming viral replication factories [66]. Co-localization of the early endosomal marker Rab5 with the viral factories induced by SFTS virus NSs suggests that these structures are of endosomal origin and not derived from the Golgi apparatus [61]. Additionally, the SFTS virus NSs protein has also been shown to play a critical role in the inhibition of host innate immunity [61, 63]. While these findings are consistent with previous studies on bunyavirus NSs proteins describing the NSs as a major virulence factor that acts as a global inhibitor of host cell transcription and antagonist of the IFN system [13, 119, 120], our previous studies have shown that, unlike any other bunyavirus NSs, the SFTS virus NSs interacts with and relocalizes TBK-1, RIG-I, and TRIM25 into endosome-like structures [61]. Thus, SFTS virus appears to use a different mechanism for virus replication and inhibition of IFN responses than those described for other bunyaviruses.

Studies aimed at characterizing early events of the phlebovirus replication cycle have shown that the prototype member, UUKV, enters the cells through a clathrin-independent mechanism. Specifically, UUKV has been shown to use Rab5a+ early endosomes and later Rab7a+ and LAMP-1+ endosomes, suggesting that after entering, the virus is directed towards the classical endosomal pathway [12]. Interestingly, our studies have also shown that the SFTS virus NSs-positive cytoplasmic structures co-localize with Rab5, but not with Rab4 [61]. Furthermore, we found that LC3, an important marker for autophagy, also co-localizes with these NSs-cytoplasmic structures; however, these structures were still observed in cells lacking Atg7, a gene essential for conventional autophagy [61, 121]. These results led us to hypothesize that these SFTS virus NSs-positive structures were not conventional autophagosomes but rather they are derived from the endosomal pathway. Due to the significant role that these structures play in viral replication and evasion of host innate immunity, we have investigated the sources and the trafficking of these structures within the cells. Surprisingly, we observed that some of the SFTS virus NSs-positive structures were secreted into the extracellular space and were taken up by neighboring cells. Furthermore, we also demonstrated that these structures possess markers associated with extracellular vesicles and, more importantly, they contain infectious virions that were efficiently transported by these secreted structures into uninfected cells and were able to sustain efficiently- replication of SFTS virus. Altogether, the data suggest that SFTS virus exploits extracellular vesicles to mediate receptor-independent transmission of the virus.

## **MATERIALS AND METHODS**

### **Cells, Plasmids, and Viruses**

HeLa and Vero76 cells were obtained from ATCC and maintained with Minimal Essential Medium Eagle (Lonza) supplemented with L-glutamine, 1% penicillin/streptomycin (Gibco), and 10% Fetal Bovine Serum. Cells used in the isolation of secreted vesicles were



grown in media containing 10% Fetal Bovine Serum depleted of endogenous vesicles by ultracentrifugation at 100,000 X g for 16 hours. Human Embryonic Kidney cells (HEK 293T) were obtained from ATCC and maintained in Dulbecco's Minimal Essential Medium (Lonza) supplemented with L-Glutamine, 1% penicillin/streptomycin, and 10% Fetal Bovine Serum. The SFTS virus NSs plasmid was constructed by PCR using overlapping deoxyoligonucleotides corresponding to the published GenBank Sequence (NC018137.1) and has been described elsewhere [60]. The SFTS virus NSs-mCherry was constructed using standard cloning techniques [60]. The mCherry and the SFTS virus NSs-mCherry genes were then cloned into a third-generation lentivirus vector and used to generate lentiviruses. HeLa cells were transduced with the lentivirus particles, and the mCherry and SFTS virus NSs-mCherry stable cell lines were generated by antibiotic selection and cloning of the mCherry fluorescent cells to select those with a high level of protein expression as determined by confocal microscopy and Western blot analyses.

The SFTS virus strain used in this study was provided by the Chinese Center for Disease Control and Prevention and passaged twice in Vero76 cells to generate viral stocks for this study. Generation of viral stocks was performed in Vero76 cells, with titers determined by plaque assay as previously described [61, 122].

### **Transfections and Immunoblotting**

All transfections were carried using 500 ng of plasmid DNA and Lipofectamine 3000 (Invitrogen) following manufacturer's established protocol. Transfected cells were lysed with NP-40 lysis buffer (150mM NaCl, 1.0% NP-40, 50nM Tris-Cl, pH 8.0) containing complete protease inhibitor cocktail (Roche) at 16-24 hours post transfection (h.p.t.). For immunoblotting, proteins were resolved by SDS-PAGE and subsequently transferred onto



a 0.2  $\mu$ m polyvinylidene difluoride (PVDF) membrane (Thermo Scientific). PVDF membranes were blocked for 1 hr with 5% non-fat dry milk or 5% bovine serum albumin (BSA) (Fisher) in Tris-Buffered Saline with 1% TWEEN-20 (TBS-T). Membranes were then incubated for 16-18 hrs at 4°C with primary antibodies. After incubation, membranes were washed three times and incubated with anti-mouse or anti-rabbit secondary antibodies conjugated with horseradish peroxidase (HRP) for 1 hour. Lastly, blots were developed by using Western Lightning ECL (Perkin Elmer) substrate following the manufacturer's protocol. The following primary antibodies were used for immunoblotting: rabbit anti-SFTS virus NSs (1:500) (GenScript), mouse anti-SFTS virus NP (1:500), rabbit anti-CD63 (1:100) (Abcam), mouse anti- $\beta$  Tubulin (1:1000) (Abcam), rabbit anti- LC3 (1:1000) (Abcam), and rabbit anti-Rab5 (1:1000)(Abcam). The secondary antibodies used were: donkey anti-rabbit IgG HRP conjugated antibody (1:5000) and sheep anti-mouse IgG HRP conjugated (1:5000) antibody from GE Healthcare. For the detection of the exosomal marker CD63, the purified extracellular vesicles were lysed and resolved under non-denaturing conditions to detect the glycosylated forms of CD63 as per the manufacturer's recommendation. For comparison purpose, both reduced and non-reduced samples were transferred onto PVDF membrane and western blot performed as indicated above.

### **Immunofluorescence**

HeLa cells were seeded onto coverslips treated with 50  $\mu$ g/ml Mouse Laminin-I (Cutler) and infected following standard procedures. Cells were then incubated overnight at 37°C in 5% CO<sub>2</sub>. Cells prepared for infection were infected with SFTS virus (MOI 0.5) for 24, 48, or 72 hrs, then fixed with 4% paraformaldehyde for 30 minutes and permeabilized with 0.1% Triton-X (Sigma) for 10 minutes. Then, the cells were washed, and a blocking

incubation step with 10% goat serum (Sigma) and 3% BSA (Thermo Scientific) was carried out. Next, cells were incubated with primary antibodies for 1 hr. Cell nuclei were visualized with Hoechst 33342 (1:1000) (Invitrogen) or with TO-PRO-3 Iodide (Invitrogen) following manufacturer's protocol. The following AlexaFluor conjugated antibodies from Invitrogen were used: AlexaFluor®488 Goat Anti-Mouse or AlexaFluor®594 Goat Anti-Rabbit. All secondary antibodies were used at a 1:1000 concentration and samples visualized with a Zeiss LSM510META laser scanning confocal microscope or Olympus Spinning Disc Confocal Microscope.

### **Live cell imaging**

HeLa cells stably expressing the SFTS virus NSs-mCherry were plated on 35mm glass bottom culture dishes (MatTek Corporation) and incubated overnight at 37°C in 5% CO<sub>2</sub>. Before live cell imaging, cell culture media was removed, cells washed with DPBS, and live cell imaging solution (Invitrogen) was added. Cells were visualized for 16 hrs using a Prairie Technologies/Nikon multimodal live cell imaging system.

### **Isolation and Purification of extracellular vesicles.**

Isolation of SFTS virus NSs-positive vesicles was first standardized in the stable cell line expressing the NSs fused to mCherry fluorescent protein. Cells were grown to 90% confluency for approximately three days, and supernatants were later collected and clarified by centrifugation. Cleared supernatant was concentrated using a 3,000 MW column (Sartorius) and voided of any cellular debris by centrifugation at 10,000 x g for 30 minutes. Vesicles were then pelleted at 100,000 x g for 90 minutes. To further purify the vesicles and remove any contaminant protein, the pellet containing the vesicles was washed

with ice-cold PBS and re-pelleted at 100,000 x g for 90 minutes. The pellets used for electron microscopy were resuspended in 100 µl of molecular grade water. For western blot analysis, pellets were resuspended in 100 µl of NP40 lysis buffer and sonicated for 1 minute. For isolation and purification of vesicles produced during SFTS virus infection, the same centrifugation procedure was employed. However, the final pellet was subjected to an immunoprecipitation step using magnetic beads coated with anti-CD63 antibody at 4°C overnight. Beads were then washed with ice-cold PBS, and re-suspension released the CD63+ vesicles in elution buffer (100mM glycine-HCL, pH 2.8). To further ensure that the CD63+ vesicles were free of SFTS virions not packaged into the vesicles, we carried an immunoprecipitation (negative selection) step using magnetic beads coated with antibodies against SFTS virus and the mix was incubated overnight. The supernatant containing the CD63+ vesicles was then removed and incubated at 4°C for 4 hrs with SFTS virus mouse hyperimmune serum at a 1:1 ratio. The virus-antibody complex was then removed, and the clarified supernatant was used to infect HeLa cells as described below to determine the capacity of the CD63+ vesicles in mediating transmission of SFTS virus. To verify that the above procedures were effective at removing SFTS virions that were not packaged within the extracellular vesicles, we employed the same methodology (immunoprecipitation and incubation with antibodies against SFTS virus) using SFTS virus stock (titer  $1 \times 10^6$  PFU/ml). The resulting preparation was then used to infect HeLa cells as described below.

#### **Infection of HeLa cells with purified extracellular vesicles.**

Adsorption of the purified vesicles was performed by overlaying the purified preparation onto cells and incubated at 37°C for 1 hr. Where indicated, HeLa cells were pre-treated

with 2 $\mu$ g/mL of mouse anti-CD63, mouse IgG1, or mouse anti-SFTS virus antibodies for 1 hour before overlaying the cells with the purified vesicles or infecting them with SFTS virus. Supernatants were collected at 0, 24, 48, and 72 hrs post-infection (hpi) and assayed by plaque assay.

### **Transmission Electron Microscopy (TEM)**

For ultrastructural analysis in ultrathin sections, infected cells were fixed for at least 1 hour in a mixture of 2.5% formaldehyde prepared from paraformaldehyde powder, and 0.1% glutaraldehyde in 0.05M cacodylate buffer pH 7.3 to which 0.03% picric acid and 0.03%  $\text{CaCl}_2$  were added. The monolayers were washed in 0.1 M cacodylate buffer; cells were scraped off and processed further as a pellet. The pellets were post-fixed in 1%  $\text{OsO}_4$  in 0.1M cacodylate buffer pH 7.3 for 1 hr, washed with distilled water and en bloc stained with 2% aqueous uranyl acetate for 20 minutes at 60°C. The pellets were dehydrated in ethanol, processed through propylene oxide and embedded in Poly/Bed 812 (Polysciences, Warrington, PA). Ultrathin sections were cut on Leica EM UC7 ultramicrotome (Leica Microsystems, Buffalo Grove, IL), stained with lead citrate and examined with a Philips 201 transmission electron microscope at 60 kV.

For immunogold labeling of thin sections, infected cells were fixed for at least 2 hrs in a mixture of 2.5% formaldehyde prepared from paraformaldehyde powder, and 0.1% glutaraldehyde in 0.05M cacodylate buffer pH 7.3 to which 0.03% picric acid and 0.03%  $\text{CaCl}_2$  were added. The monolayers were washed in 0.1 M cacodylate buffer; cells were scraped off and processed further as a pellet. The pellets were en bloc stained with 2% aqueous uranyl acetate for 20 minutes at 60°C. The pellets were dehydrated in ethanol, processed through propylene oxide and embedded in LR White (Polysciences, Warrington,

PA). Ultrathin sections were then cut on Leica EM UC7 ultramicrotome (Leica Microsystems, Buffalo Grove, IL). Sections were then labeled with incubated with mouse anti-SFTS virus NSs and rabbit anti-LC3 (1:20) or mouse anti-SFTS virus NSs and rabbit anti-Rab5 (1:20) primary antibodies for 1 hour at room temperature and overnight at 4°C. The sections were next washed three times with 1% BSA in TBS and incubated with secondary antibody goat anti-rabbit labeled with 6nm colloidal gold (1:20) and goat anti-mouse labeled with 15nm colloidal gold (1:20) for 1 hr. After washing with water, grids were fixed with glutaraldehyde for 5 minutes, washed with water and negatively stained with 2% aqueous uranyl acetate for 5 minutes. A final wash with water was performed three times followed by staining with lead citrate for 30 seconds. They were examined with a Philips CM-100 transmission electron microscope at 60 kV.

For visualization of isolated microvesicles by electron microscopy, purified vesicles were adsorbed onto Formvar-carbon-coated nickel grids for 15 minutes, washed three times with molecular grade water and negatively stained with 2% aq. Uranyl acetate. For immunogold labeling, the sample was first adsorbed onto nickel grids as previously described [62], then incubated with rabbit anti-SFTS virus NSs and mouse anti-CD63 (1:10) antibodies for 1 hr at room temperature in the wet chamber. The grids were next washed three times with 1% BSA in TBS and incubated with secondary antibody goat anti-mouse labeled with 6nm colloidal gold (1:20) and goat anti-rabbit labeled with 15nm colloidal gold (1:20) for 1 hour. After washing with water, grids were fixed with glutaraldehyde for 10 minutes, washed with water and negatively stained with 2% aqueous uranyl acetate. They were examined with a Philips CM-100 transmission electron microscope at 60 kV.

Additionally, for ultrastructural analysis in ultrathin sections, purified vesicles were fixed overnight at 4°C in a mixture of 2.5% formaldehyde prepared from paraformaldehyde powder, and 0.1% glutaraldehyde in 0.05M cacodylate buffer. The pellets were washed in cacodylate buffer followed by post-fixation in 1% OsO<sub>4</sub> for 1 hour, washed and en bloc stained with 2% aqueous uranyl acetate for 20 minutes at 60°C. The pellets were dehydrated in ethanol, processed through propylene oxide and embedded in Poly/Bed 812 (Polysciences). For conventional TEM, SFTS virus-infected cells were fixed and processed the same way. For immunoelectron microscopy on ultrathin sections post-fixation was omitted, and after dehydration, in 75% ethanol the pellets were processed and embedded in LR White resin. Ultrathin sections were cut on Leica EM UC7 ultramicrotome (Leica Microsystems), stained with lead citrate and examined with a Philips CM-100 transmission electron microscope at 60 kV. Grids were then processed as mentioned above for immunostaining.

### **Statistical analysis**

Statistical analyses were carried out using two-way ANOVA for multiple comparisons to determine statistical differences in virus titers by plaque assay. Results of the electron microscopy experiments were analyzed by performing student t-tests. All analyses were done using GraphPad Prism Version 6.05 (GraphPad Software). A value of  $p < 0.05$  was considered significant.

## **RESULTS**

**SFTS virus infection induces the formation of cytoplasmic structures reminiscent of early endosomes.**

We and others have recently reported that SFTS virus infection induces the formation of cytoplasmic structures that play a critical role during SFTS virus replication and for evasion of innate immune responses [61, 66]. Furthermore, we reported that these structures colocalized with the early endosomal marker Rab-5 and the autophagy marker LC3, but not with the endosomal marker Rab-4 [60]. It was also reported that formation of these cytoplasmic structures in SFTS virus-infected cells was dependent on lipid metabolism and that lipid droplets may play a role during SFTS virus infection [65]. Therefore, we conducted transmission electron microscopy studies to gain further insight into the sources, morphology, and composition of these cytoplasmic structures in HeLa cells stably expressing mCherry or SFTS virus NSs-mCherry. Electron microscopy studies were also conducted in SFTS virus-infected or mock-infected Vero cells. Consistent with our previous observations [60], transmission electron microscopy revealed the formation of structures reminiscent of early endosomes in cells stably expressing SFTS virus NSs as well as in virus-infected cells (**Figure 3.1A and 3.1B, respectively**). Similar structures have also been described during UUKV infection [12]. Additionally, we conducted immuno-gold electron microscopy on ultrathin sections of infected cells to substantiate that these structures were of endosomal origin. In correlation with our previous findings, we observed the colocalization of Rab5 and LC3 with the SFTS virus NSs-positive structures (**Figure 3.1C and 3.1D, respectively**).

#### **SFTS virus NSs-positive structures are released into the extracellular space.**

To gain a better understanding on how these SFTS virus NSs-positive structures traffic within the cells, we conducted live cell imaging of HeLa cells expressing SFTS virus NSs-

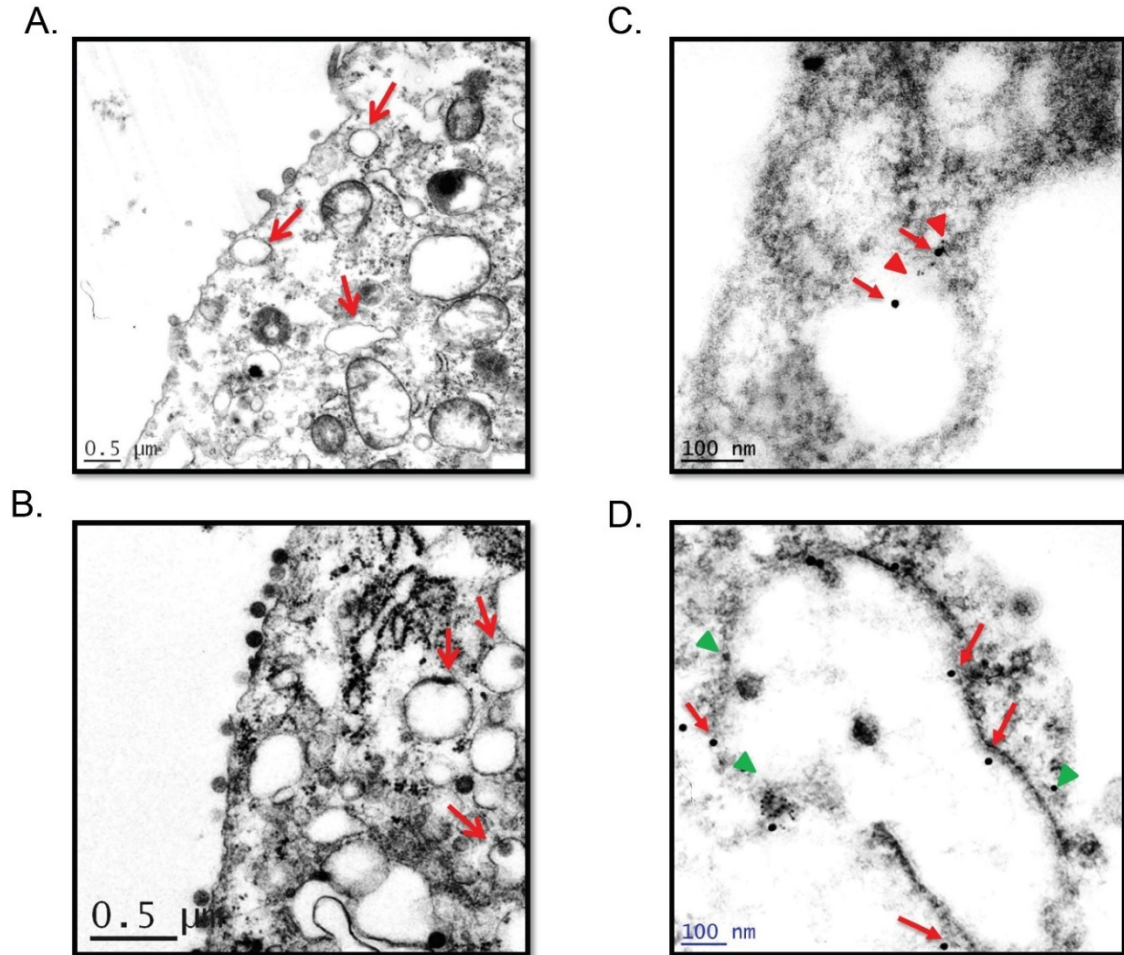


**Figure 3.1. SFTS virus NSs induces the formation of endosomal-like structures.**

Ultrastructure analyses of SFTS virus NSs-expressing cells (A) and SFTS virus-infected cells (B) showing cytoplasmic structures reminiscent of early endosomes (arrows) in ultrathin sections. Immunogold staining of distinct ultrathin sections showing cytoplasmic structures positive for SFTS virus NSs and Rab5 (C) or SFTS virus NSs and LC3B (D) are shown. Solid red arrows indicate SFTS virus NSs in panels C and D while red triangle (in panel C) and green triangle (in panel D) indicate the detection of Rab5 and LC3B, respectively. Ultrathin sections of mock-infected cells were also labeled as indicated above (not shown) to ensure specificity of the antibody. Representatives images are shown.

mCherry. This approach allows the direct observation of the SFTS virus NSs-cytoplasmic structures due to the fluorescent signal. Cells were plated and monitored for 16 hours using a Prairie Technologies/Nikon multimodal live cell imaging system. Interestingly, we



observed that a portion of the SFTS virus NSs-structures was secreted into the extracellular space and was taken up by neighboring cells (**Figure 3.2**). This data suggests that the released SFTS virus NSs-cytoplasmic structures may be extracellular vesicles. The release of extracellular vesicles has been shown to be one mechanism for intercellular communication. These vesicles are referred to as exosomes (if they originated from multivesicular endosome) or microvesicles (if they originate from the plasma membrane) [73]. In light of the results described above related to the involvement of the endosomal pathway in the formation of SFTS virus NSs-induced structures, as well as the active transfer of secreted SFTS virus NSs-positive structures into neighboring cells, we hypothesized that the cytoplasmic structures produced by SFTS virus NSs-expressing cells were exosomes. To test this hypothesis, we initially purified the extracellular vesicles produced by HeLa cells expressing mCherry and SFTS virus NSs-mCherry (**as described in Figure 3.3A**) and carried out SDS-PAGE coupled with western blotting to investigate the presence of tetraspanins such as CD63 that are known to be abundant in exosomes [123]. Consistent with our hypothesis, the presence of CD63 was confirmed in the purified extracellular vesicles produced by SFTS virus NSs-mCherry expressing cells as well as in cells expressing the mCherry protein (**Figure 3.3B**).

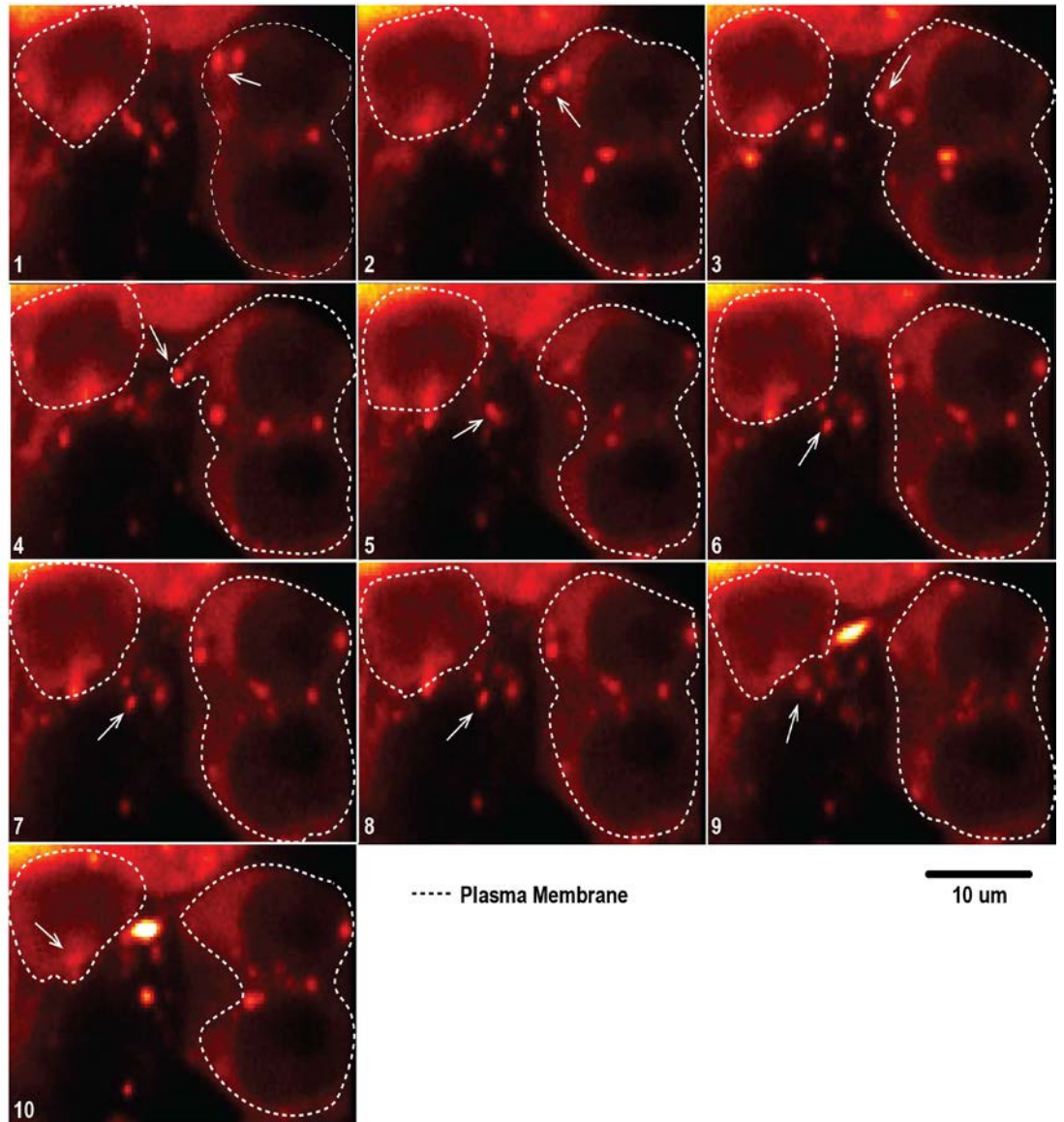


**Figure 3.2. Cytoplasmic vesicles containing SFTS virus NSs-mCherry are secreted into the extracellular space and are endocytosed by neighboring cells.**

Live cell imaging (LCI) was carried out in HeLa cell line stably expressing SFTS virus NSs-mCherry. Cells were visualized for 16 hours using a Prairie Technologies/Nikon multimodal live cell imaging system. The arrow highlights the movement of the vesicle from cell to cell.

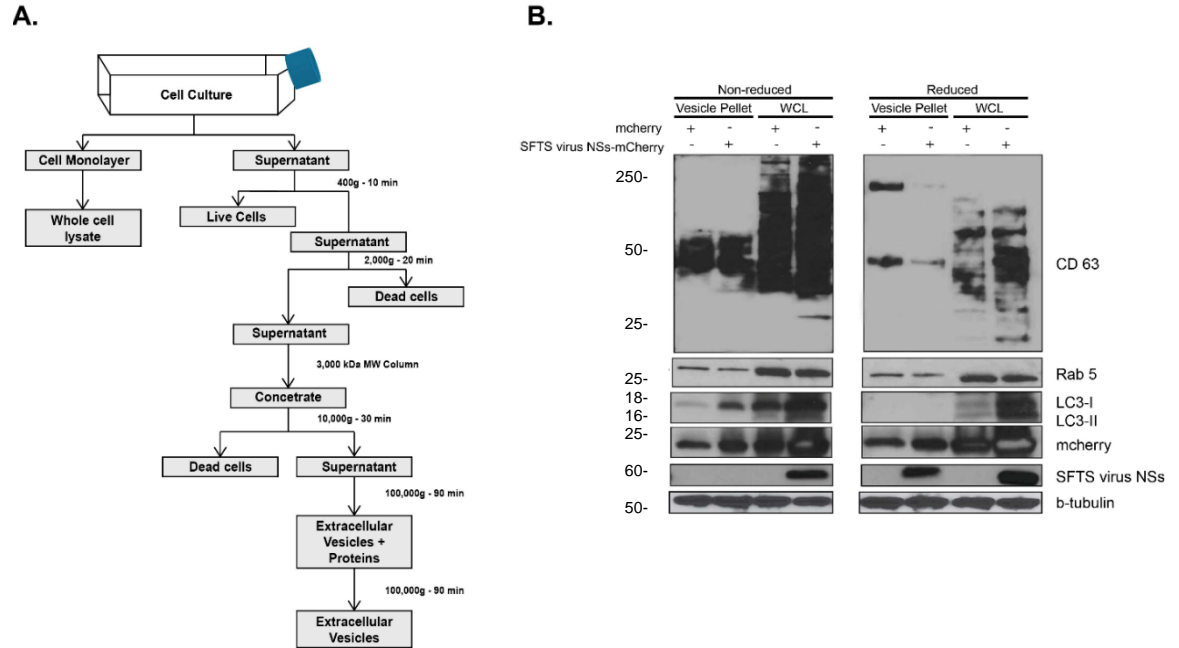


**Figure 3.3. Isolation and characterization of SFTS virus NSs-positive secreted extracellular vesicles.**

(A) Schematic representation of the protocol for the isolation of secreted extracellular vesicles by ultracentrifugation (B) Supernatant from cell lines expressing the mCherry and SFTS virus NSs-mCherry proteins were collected, and isolation of extracellular microvesicles was performed as indicated in Figure 3.3A. The final pellet was re-suspended in lysis buffer, sonicated and resolved by SDS-PAGE electrophoresis, transferred to PVDF membrane, and blotted for SFTS virus NSs, LC3B, and common markers for microvesicles such as Rab5,  $\beta$ -tubulin, and CD63 (core protein: 26kDa; glycosylated: 30-60kDa). The cell monolayer was used to generate the whole cell lysate (WCL) and assayed for the detection of proteins indicated above.

The presence of both Rab5 and LC3-I was also detected in the extracellular vesicles produced by both mCherry and SFTS virus NSs-mCherry expressing cells. However, it was evident that in the presence of SFTS virus NSs, there was an increased amount of LC3-I protein being incorporated into the extracellular vesicles but not Rab5. The increased detection of LC3-I also correlates with the increased amount of mCherry protein being

detected in SFTS virus NSs-expressing cells, which may indicate that the SFTS virus NSs induces or enhances the production of extracellular vesicles (**Figure 3.3B**).

Furthermore, the mCherry protein was also detected in the extracellular vesicles, which could indicate that the mCherry protein may be mediating the incorporation of SFTS virus NSs into these vesicles rather than the viral protein. Therefore, we proceeded to investigate whether or not extracellular vesicles are produced during SFTS virus infection and determine if the SFTS virus NSs protein was incorporated within these vesicles, similar to what was found in NSs-expressing cells. The approach for the isolation and purification of the extracellular vesicles is described in **Figure 3.4A**. Consistent with the results obtained in HeLa cells expressing the viral protein NSs, Western blot analyses revealed the presence of SFTS virus NSs, LC3-I as well as the endosomal marker Rab5 within the extracellular purified vesicles produced by SFTS virus-infected Vero cells (**Figure 3.4B**). Furthermore, the viral nucleoprotein NP was also detected (**Figure 3.4B**). These data provide evidence that SFTS virus NSs is incorporated within extracellular vesicles produced in NSs-expressing cells as well as those generated during SFTS virus infection.

#### **Ultrastructural analysis of purified SFTS virus NSs-positive extracellular vesicles.**

Extracellular vesicles are known to be secreted by most cell types [124]. Thus, we next explored the possibility that the majority of the extracellular vesicles released in SFTS virus NSs-mCherry expressing cells, and SFTS virus-infected cells harbor the NSs viral protein, which could suggest that SFTS virus directly targets the secretory multivesicular

endosomal pathway. To evaluate this possibility, extracellular vesicles produced by HeLa

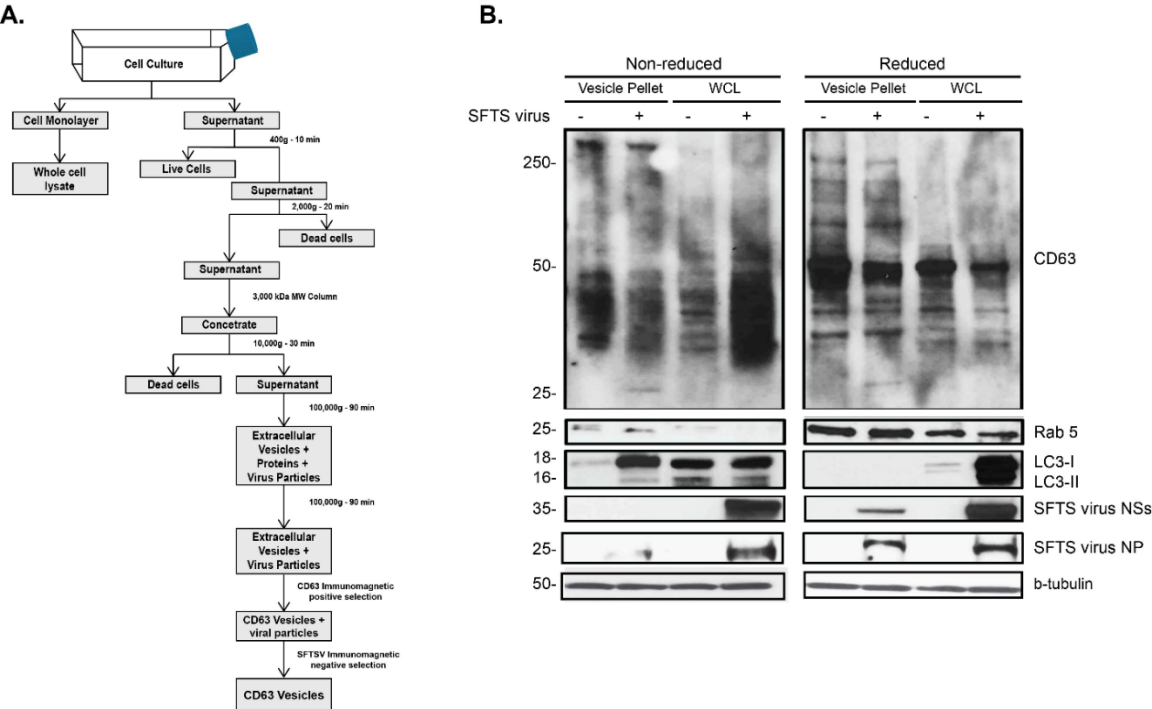


**Figure 3.4. Characterization of extracellular microvesicles secreted during SFTS virus infection.**

HeLa cells were mock infected or infected with SFTS virus for 72 hours. (A) The supernatant was collected, and isolation of extracellular microvesicles was performed as indicated. (B) The final pellet was re-suspended in lysis buffer, sonicated and resolved by SDS-PAGE electrophoresis, transferred to PVDF membrane, and blotted for SFTS virus NSs, SFTS virus NP, and LC3B, in addition to common markers for microvesicles such as Rab5, CD63, and  $\beta$ -tubulin. The cell monolayer was used to generate the WCL and assayed for the detection of proteins indicated above.

cells expressing the mCherry or SFTS virus NSs-mCherry and SFTS virus-infected or Mock-Infected HeLa cells were purified and examined by electron microscopy and immuno-gold electron microscopy using antibodies against the SFTS virus NSs and CD63. The extracellular vesicles isolated from mCherry and mock- infected cells were only

positive for the exosomal marker CD63 and were 50-100 nm in size, which is consistent with the normal 30-150 nm size range of exosomes [125, 126] (**Figure 3.5A and 3.5B, left panels**). The extracellular vesicles isolated from SFTS virus NSs-mCherry and SFTS virus-infected cells were positive for CD63 (**Figure 3.5A and 3.5B, right bottom panels**). Interestingly, the SFTS virus NSs protein (**Figure 3.5A and 3.5B, right bottom panels**) was detected in approximately 35-50% of these CD63+ vesicles produced by NSs-expressing cells and SFTS virus-infected cells (**Figure 3.5C**). No significant difference in size was observed among the extracellular vesicles whether they were positive for SFTS virus NSs or not. These results suggest that SFTS virus efficiently targets the secretory multivesicular endosomal pathway.

#### **SFTS virus NSs-positive extracellular vesicles contain SFTS virions.**

Several studies have implicated the role of extracellular vesicles in many cellular processes, including tissue injury and immune responses, and for the transport of proteins, mRNA and microRNAs (miRNAs) between cells [127]. More recently, evidence has also been obtained for the role of extracellular vesicles in the transmission of infectious agents as well as in the modulation of host immune responses to many pathogens [71, 75, 77, 128-130]. With regard to SFTS virus, a recent study suggested that the SFTS virus NSs-positive cytoplasmic structures play a role during SFTS virus replication on the basis of co-localization with viral RNPs and double-stranded RNA [66]. In light of the results described above and the role of SFTS virus NSs cytoplasmic structures during virus replication, we next investigated if the extracellular vesicles released by SFTS virus-infected cells contained infectious virions. Extracellular vesicles produced during SFTS

virus infection were purified as shown in **Figure 3.3A**. Briefly, due to the possibility that the virions and extracellular vesicles may have similar sizes and densities that our procedure would not completely devoid the extracellular vesicles from free virions [124, 131], we carried out immune-selection step using anti-CD63 beads (**Figure 3.4A**) as previously described [70], followed by a second immune-(negative) selection using magnetic beads coated with antibodies against SFTS virus (**Figure 3.4A**). As a final step and to ensure removal of contaminant SFTS virions in our sample, the purified vesicles were incubated with SFTS virus mouse hyperimmune serum at a 1:1 ratio (**Figure 3.4A**). The antibody:virus complex was then removed with magnetic beads. The resulting purified vesicles were then used for plaque assay (**Figure 3.6A**) and to infect HeLa cells. Notably, we observed that the CD63-purified extracellular vesicles that underwent only immune-negative magnetic selection and those that were incubated with anti-SFTS virus hyperimmune ascitic fluid after immune-negative selection were able to produce viral titers of  $4.5 \times 10^3$  PFU/ml and  $2.5 \times 10^3$  PFU/ml, respectively (**Figure 3.6A**). In contrast, the SFTS virus stock produced a titer of  $7.5 \times 10^5$  PFU/ml whereas the extracellular vesicles that solely underwent CD63 positive immunomagnetic selection produced a titer of  $7.5 \times 10^4$  PFU/ml. This indicates that: 1) centrifugation and CD63 positive immunoselection are not sufficient enough to void the vesicle preparation of free SFTS virions, and 2) purified extracellular vesicles produced by SFTS virus-infected cells are capable of mediating productive infection. We confirmed that our immune-negative selection step and further incubation with anti-SFTS virus antibodies was successful in removing virus particles not packaged into vesicles because our virus stock (titer  $7.5 \times 10^5$  PFU/ml) was

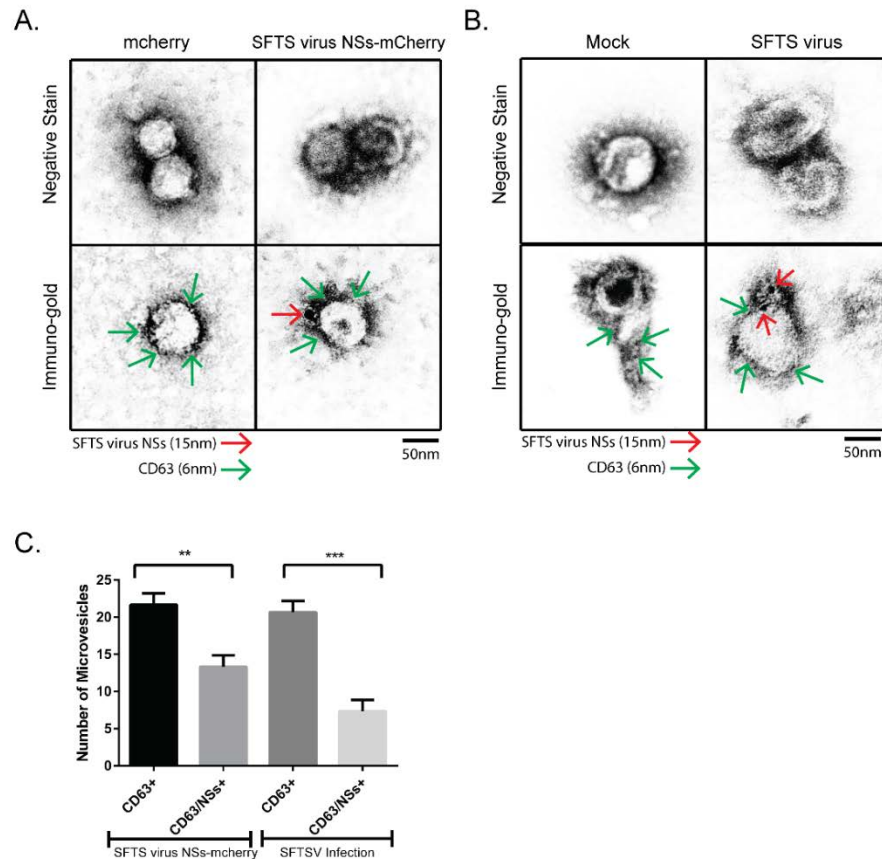


**Figure 3.5. Isolated extracellular vesicles are positive for SFTS virus NSs and the exosomal marker CD63.**

The supernatant was collected from (A) HeLa cells stably expressing mCherry or SFTS virus NSs-mCherry, and from (B) HeLa cells mock-infected or infected with SFTS virus and isolation of extracellular microvesicles was performed as depicted in Figure 3.3A. The final pellet was re-suspended in molecular grade water. The sample was adsorbed onto Ni grids and negatively stained with 2% aq. Uranyl acetate. Additional grids were incubated with primary antibodies against SFTS virus NSs (rabbit) and CD63 (mouse), then secondary goat anti-mouse IgG coupled to 6 nm colloidal gold and goat anti-rabbit IgG coupled to 15 nm colloidal gold antibodies, and negatively stained with 2% aq. Uranyl acetate. SFTS virus NSs is indicated by red arrows and CD63 by green arrows. (C) The number of CD63-positive and CD63/SFTS virus NSs-positive extracellular vesicles was quantified based on immune-gold labeling observed from 10 fields of view. A total of 22 vesicles were seen in each experiment, of which an average of 14 was positive for both SFTS virus NSs and CD63. All electron microscopy experiments were repeated three times. Results are expressed as mean + SEM. Asterisks specify statistically significant difference ( $p < 0.05$ ) between the indicated groups.



subjected to the same procedure, and subsequently assayed by plaque assay and we were unable to detect viral plaques (**Figure 3.6A**). Lastly, these data suggest that the extracellular vesicles contribute as much as 2-logs of infectious virus particles to the total

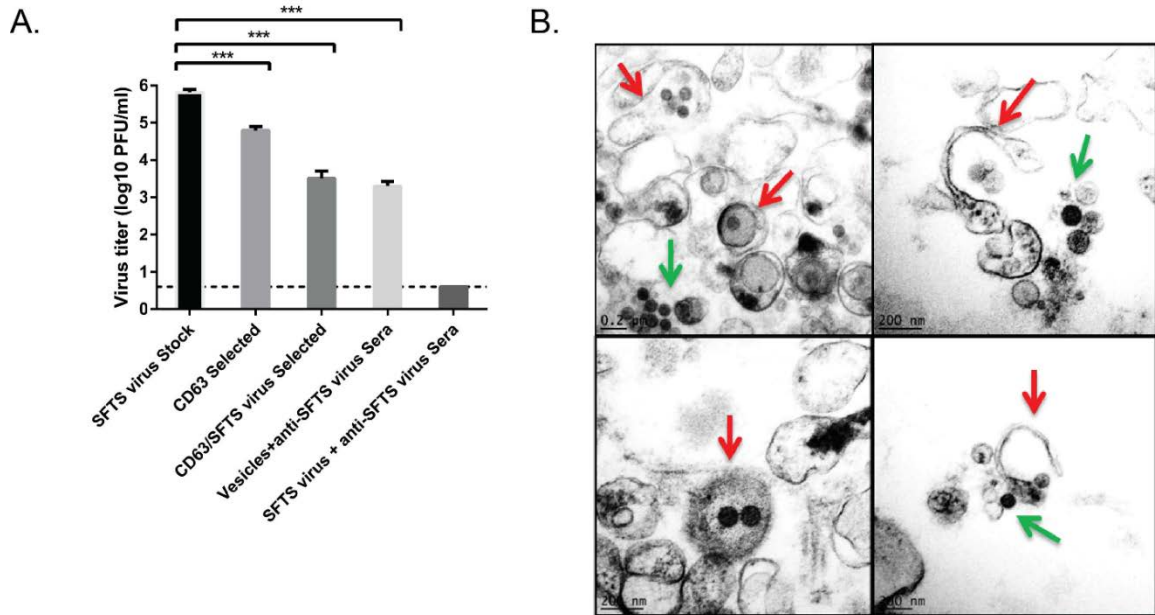


**Figure 3.6. SFTS virus NSs-positive extracellular vesicles harbor infectious SFTS virus virions.**

(A) Extracellular vesicles were isolated as indicated in Figure 3.4A and samples were collected at each step of the purification process for evaluation by plaque assay. The sample resulting from the immune selection step using anti-CD63 beads is depicted in the figure as CD63 selected whereas those resulting from the subsequent immune-(negative) selection step is shown as CD63/SFTSV selected. As a final step, the purified vesicles were incubated with SFTS virus mouse hyperimmune serum at a 1:1 ratio and the antibody:virus complex was then removed with magnetic beads. Plaque assay of the resulting purified vesicles is shown as vesicles+anti-SFTS virus sera. Plaque assay of the virus stock (infected cells from which the extracellular vesicles were derived) is shown as SFTS virus stock. As a control, the stock was also subjected to the immune-negative selection step followed by the incubation step with the SFTS virus antibody as indicated above and plaque assay was carried out (depicted as SFTS virus+anti-SFTS virus sera). Dashed line indicates the limit of detection. Results are expressed as mean + SEM. Asterisks specify statistically significant difference ( $p < 0.05$ ) between the indicated groups. (B) Electron micrograph of isolated extracellular vesicles reveals the presence of virus-like particles contained within the vesicles (red arrow). The presence of free virions from broken vesicles is also observed (green arrow).

viral titer (compare SFTS virus stock titer to CD63/SFTS virus selected vesicles). To further confirm that the extracellular vesicles contain infectious virions, vesicles were purified from SFTS virus infected cells as shown in **Figure 3.4A** and analyzed by electron microscopy. Astonishingly, electron microscopy studies revealed the presence of intact virus particles within the isolated vesicles (**Figure 3.6B**). These data indicate that SFTS virus hijacks the secretory multivesicular endosomal pathway to possibly mediate transmission of the virus.

#### **Extracellular vesicles produced during SFTS virus infection mediate receptor-independent transmission of SFTS virus.**

It has been previously shown that Hepatitis C (HCV) hijacks secreted vesicles for receptor-independent transmission of viral RNA [70, 77]. Furthermore, hepatitis A virus (HAV) is released cloaked in host membranes in a release mechanism resembling those of exosomes [72, 132]. Additionally, Coxsackievirus B3 (CVB3) has been shown to target secreted vesicles for virus dissemination [71]. We, therefore, hypothesized that extracellular vesicles produced during SFTS virus infection might mediate transmission of SFTS virus between cells. Extracellular vesicles were purified, subjected to immune selection using anti-CD63 and anti-SFTS virus antibodies, and incubated with SFTS virus mouse hyperimmune ascitic fluid as indicated above. Purified vesicles were overlaid onto uninfected HeLa cells pre-treated with 2 $\mu$ g/mL of either mouse anti-CD63 (**Figure 3.7C**), mouse IgG1 (**Figure 3.7B**), or mouse anti-SFTS virus antibodies (**Figure 3.7D**). As a control, PBS was used for the Naïve group (**Figure 3.7A**). Supernatants were collected at 0, 24, 48, and 72 hpi and virus titer assayed by plaque assay. Consistent with our hypothesis, the purified extracellular vesicles were able to mediate productive infection of SFTS virus with titers at 24 hpi of 1.5x10<sup>3</sup> PFU/ml (**Figure 3.7A**) and 1.85x10<sup>3</sup> PFU/ml (**Figure 3.7B**) in the PBS and IgG-treated HeLa cells, respectively. In contrast, we

observed a 10-fold reduction in virus titer in cells treated with an anti-CD63 antibody that were infected with the purified vesicles derived from SFTS virus infection (**Figure 3.7C**). In correlation with virus titers observed in the naïve or IgG-treated group, we observed a viral titer of  $1.7 \times 10^3$  PFU/ml in cells pre-treated with mouse anti-SFTS virus antibodies and infected with the purified vesicles (**Figure 3.7D**). These results differ from the viral titers observed in cells infected with SFTS virus due to a 100-1,000 fold difference in viral

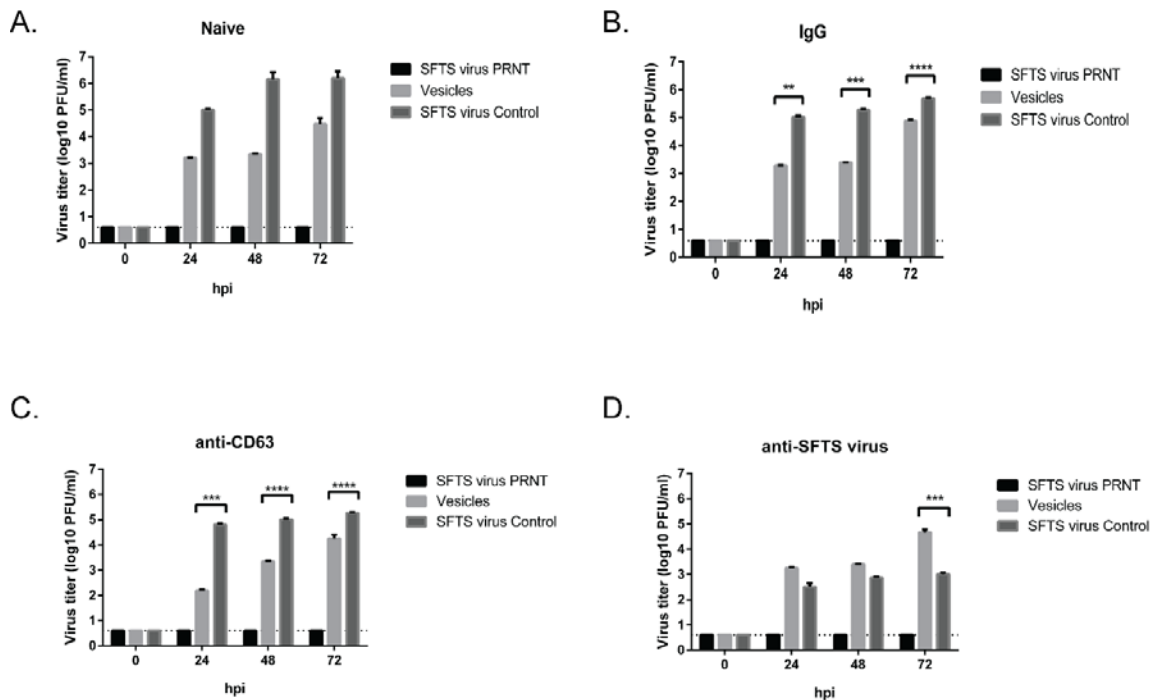


**Figure 3.7. SFTS virus NSs-positive extracellular vesicles can mediate receptor-independent transmission of SFTS virus.**

HeLa cells were pre-treated with (A) PBS, (B) IgG control, (C) anti-CD63 antibody, or (D) anti-SFTS virus antibody before infection with the purified extracellular vesicles, SFTS virus or the SFTS virus preparation subjected to the immune-negative selection and antibody incubation step described in Figure 3.4A. Supernatants were harvested at 0, 24, 48, and 72 hpi and a plaque assay performed. Dashed line indicates the limit of detection (4 PFU/ml). All experiments were repeated three times with consistent results. Results presented are expressed as mean + SEM. Asterisks specify statistically significant difference ( $p < 0.05$ ) between the indicated groups.

replication in cells treated with anti-SFTS virus antibodies (**compare Figure 3.7B and 3.7D**). This data suggests that the extracellular vesicles produced during SFTS virus infection can mediate receptor independent transmission of SFTS virus. Lastly, to further confirm that the SFTS virus particles produced as a result of the infection with the extracellular vesicles can mediate additional rounds of replication, supernatants collected from cells infected with the purified, CD63 immune-selected extracellular vesicles described in Figure 3.7A were used to infect HeLa cells. At 0, 24, 48 and 72 hours after infection, immunofluorescence was performed in the infected cells using antibodies against SFTS virus NP and NSs. As predicted, we were able to detect SFTS virus proteins 24 to 72 hours after infection (**Figure 3.8**). Altogether, our results suggest that SFTS virus hijacks the secretory multivesicular endosomal pathway to mediate receptor-independent transmission of the virus.

## **DISCUSSION**

Recent studies conducted by us and others have determined that this pathogen counteracts innate immune responses via mechanisms distinct from those described for other bunyaviruses. Unlike any other bunyavirus nonstructural protein NSs, the SFTS virus NSs interacts with and relocalizes multiple components of the IFN response into cytoplasmic structures [61, 64, 65, 91]. With regard to SFTS virus replication, it has been recently shown that these cytoplasmic structures might also play a role in virus replication because double stranded RNA and the viral proteins NP and L that are known to be involved in virus replication co-localize within these structures [66]. These structures were also found to co-localize with lipid droplets. Moreover, inhibitors affecting the synthesis of fatty acids negatively impacted the formation of these cytoplasmic structures as well as

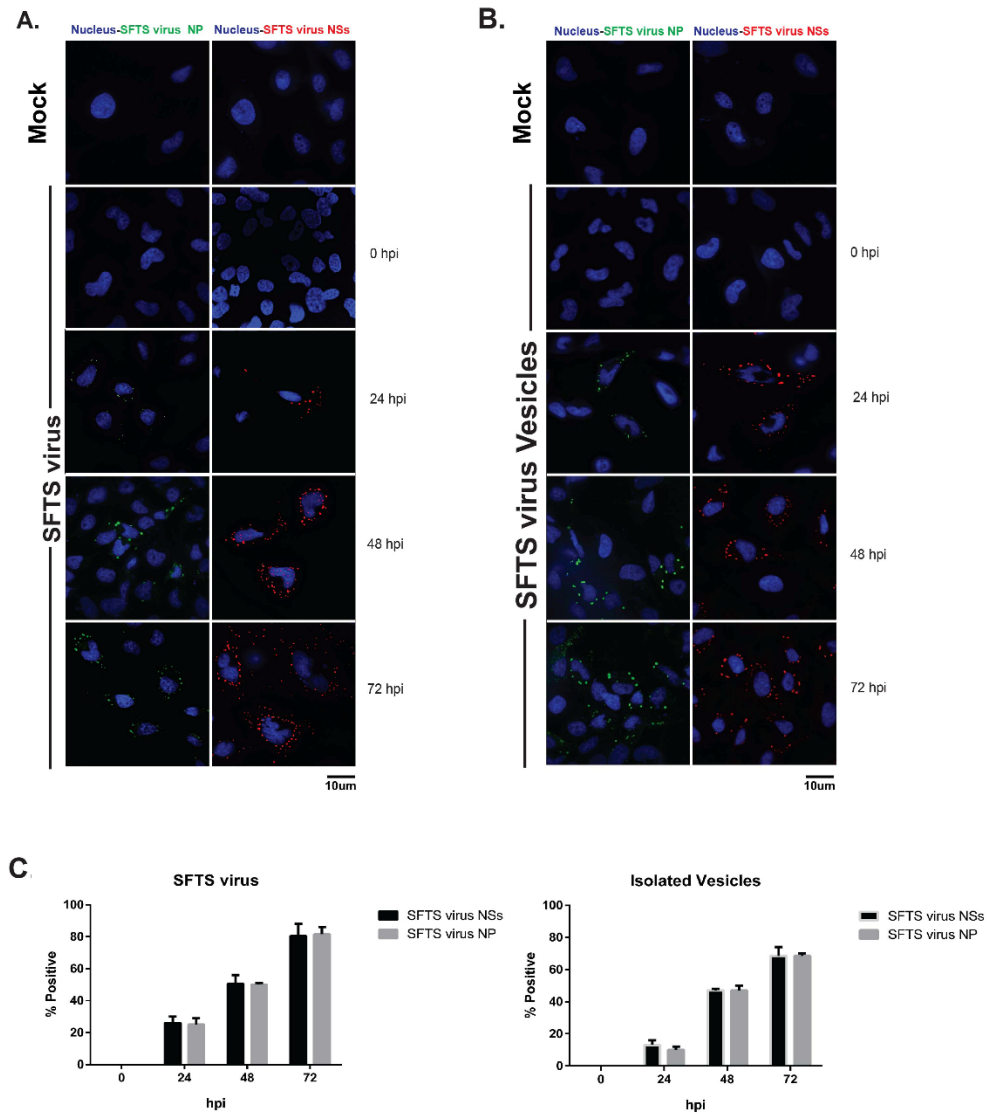


**Figure 3.8. Virions harbored within SFTS virus NSs-positive extracellular vesicles are capable of establishing a productive infection.**

HeLa cells were mock-infected (top panels), infected with SFTS virus (A) or with supernatants collected from cells infected with the purified, CD63 immune-selected extracellular vesicles described in Figure 3.4A (B). Cells were fixed at 0, 24, 48, and 72 hours post infection. Immunofluorescence was performed using primary antibodies against SFTS virus NP or NSs and AlexaFluor488 as the secondary. Nuclei were visualized with Hoechst 33342. Representative images for the mock-infected groups are shown. (C). Percent of cells positive for SFTS virus NP or NSs calculated by cell counts in 10 fields of view. A total of 150 cells were counted, the percentage was calculated by dividing total cells positive for SFTS virus NP or NSs by 150.

virus replication. In an attempt to identify the source of these structures, we found that they were most likely of endosomal oRIG-In because of the early endosomal marker Rab5, but no markers associated with the Golgi apparatus, co-localized with these cytoplasmic structures [61].

Although these initial investigations provided preliminary critical knowledge on the source of these structures, it was still unclear whether or not these structures containing viral RNA traffic within the cells to incorporate the glycoproteins to form infectious virions. Thus, in order to provide further insights into the intracellular trafficking of these structures, we initially conducted live cell imaging studies on cells expressing SFTS virus NSs fused to the mCherry protein. Surprisingly, these investigations revealed that a portion of the SFTS virus NSs-expressing cytoplasmic structures were released into the extracellular space and were taken up by neighboring cells. Subsequent studies carried out in SFTS virus-infected cells further confirmed that the SFTS virus NSs was incorporated in extracellular vesicles produced by these cells and, more importantly, they carried virions capable of sustaining transmission of the virus to neighboring cells. Furthermore, the extracellular vesicles produced from cells expressing the SFTS virus NSs were not cellular debris released from dying cells because live cell imaging studies clearly showed that these structures were released from cells that were still alive and without noticeable damage. Additionally, SFTS virus does not induce a cytopathic effect on infected cells and, more importantly, these extracellular vesicles were detected in significant amount only three days after infection.

The extracellular vesicles produced by SFTS virus NSs-expressing cells and SFTS virus-infected cells displayed markers characteristic of exosomes, such as being positive

for the tetraspanin CD63, a widely used exosome marker [133]. Interestingly, we also found that the extracellular vesicles preferentially contain LC3-I rather than LC3-II. The limited detection of LC3-II lipidated form, which is known to associate with membranes upon the induction of autophagy [134, 135], and during infection with several different viruses, including poliovirus, rhinovirus, enterovirus 71, CVB3 and foot-and-mouth disease virus among others [136-138], suggests that these structures are not derived from the autophagy pathway. Further, the shedding mechanism is distinct from the previously described autophagosome-mediated exit without lysis (AWOL) model for poliovirus release and also differs from a similar model described recently for CVB3 [71, 139]. Since the non-lipidated form of LC3 is preferentially incorporated into the extracellular vesicles secreted by SFTS virus-infected cells, it is likely that this represents another example of a role for LC3 that is unrelated to autophagy. It has been previously reported that the non-lipidated form of LC3, referred as LC3-I, is also associated with membranes of the ER-associated degradation (ERAD) tuning vesicles (or EDEMosomes) and recent studies have suggested that these structures may serve as a scaffold for positive-strand RNA virus replication complexes [140, 141]. In our attempts to determine the source of the cytoplasmic structures induced by SFTS virus, we previously explored the possibility that they might be derived from the ERAD tuning pathway; however, we did not find any evidence supporting this possibility [61]. In contrast, our data suggest that these structures are derived from the multivesicular endosomal pathway and might be classified as exosomes. Thus, our studies indicate that the non-lipidated form of LC3 is incorporated into extracellular vesicles of endosomal RIG-In and may facilitate replication of negative strand RNA viruses (such as SFTS virus) as well.

It has been recently shown that hepatitis C virus (HCV) hijacks exosomes to incorporate infectious RNA into these structures that are then capable of mediating receptor-independent transmission of the virus [70, 77]. Here, we describe another model for subversion of exosome-like structures to mediate receptor-independent transmission

involving the novel bunyavirus SFTS virus. Similar to the CVB3, but in contrast to HCV, we were able to detect one to five virions harbored within the exosome-like structures that were capable of establishing productive infection of cells that received them. These findings are quite remarkable because there have not been prior reports describing the localization of bunyavirus or any other arthropod-borne viruses within extracellular vesicles to mediate receptor-independent transmission of the virus. Thus, our findings highlight an elegant strategy by which the recently recognized SFTS virus subverts exosome-like structures for virus dissemination. Our data also suggest that this mechanism of infection is likely beneficial for SFTS virus because it provides a degree of protection against neutralizing antibodies and therefore contributes to the immune evasion properties of the virus. Future studies are needed to define the role of these “infectious exosome-like structures” in expanding the tropism of the virus and their contribution to viral pathogenesis. Additional studies are also needed to define exactly how these structures deliver the virus and viral RNA into the cells and the fusion mechanisms that probably occur between the viral and cellular vesicles membranes for infection to occur. Furthermore, studies are needed to determine whether the infectious extracellular vesicles are also produced during infection of the arthropod host and whether they play a significant role during the transmission cycle involving host and vector.



## **CHAPTER 4**

# **SUBVERSION OF THE UBIQUITIN-PROTEASOMAL PATHWAY BY SFTS VIRUS FOR INHIBITION OF INNATE IMMUNE RESPONSES**

### **INTRODUCTION**

Pattern recognition receptors (PRRs) are used to detect or recognize pathogen-associated molecular patterns (PAMPs), such as nucleic acids, carbohydrates, or proteins of viruses or other invading microorganisms. PRRs such as the Toll-like receptors (TLRs) and the C-type lectin receptors (CLRs) recognize viral DNA or RNA in the endosomal compartment, while the RNA helicases retinoic acid-inducible gene 1 (RIG-I) like receptors such as RIG-I or melanoma differentiation-associated protein 5 (MDA5) recognize 5'-triphosphate dsRNA or long higher order structure dsRNA, respectively [142-145]. RIG-I is comprised of a C-terminal domain, a central helicase domain, and two N-terminal caspase recruitment domains (CARDs). The inactive form of RIG-I is maintained through interactions between the helicase and CARD domains; however, binding of the viral dsRNA by both the helicase and C-terminal domains results in a conformational change that exposes the CARDs, and subsequent K63 ubiquitination by TRIM25 occurs [146]. Activation of RIG-I leads to the subsequent activation of kinases belonging to the inhibitor of nuclear factor Kappa-B Kinase (IKK) family. IKK kinases can be divided into the canonical (IKK $\alpha$ /IKK $\beta$ ) or the non-canonical IKK $\epsilon$ /TANK-binding kinase-1 (TBK-1)

[147]. Here, we will focus on the non-canonical kinase group IKK $\epsilon$ /TBK-1 which activate the interferon (IFN) regulatory factors (IRF) 3 and 7.

Regulation of PRR activation is critical in order to prevent overproduction of cytokines that can result in tissue damage, chronic inflammation, or even autoimmune disorders. Cells regulate PRR activation by reversible post-translation modifications (PTMs) such as ubiquitination and/or phosphorylation. Ubiquitin is a small molecule that can be attached to lysine (K) residues on proteins in order to modulate or alter their function. This attachment or conjugation process is mediated by a stepwise system that involves 3 different types of proteins, E1 (activates ubiquitin), E2 (ubiquitin acceptor/conjugator), and E3 (ubiquitin ligase) [148-150]. Through elegant interactions, these 3 proteins carry out protein ubiquitination. E3 ligases are responsible for substrate specificity and can be divided into 4 families, the really interesting new gene (RING), homologous to E6-associated protein C-terminus (HECT), UFD2 homology (U-box), and RING-in-between-RING (RBR) [151, 152].

Conjugation of ubiquitin at specific lysine residues determines the functional role of the ubiquitinated protein. Typically, proteins can be mono-, di-, or polyubiquitinated. To date, 7 different ubiquitin lysine residues have been identified. The K-48 and K63 ubiquitin linkages have been well characterized and play a major role in the activation and regulation of the innate immune response [153]. K-48 ubiquitination leads to degradation of proteins by the proteasome; while K63 ubiquitination leads to signal transduction/activation [153]. In regard to the RIG-I signaling cascade, it is well known that K63 linked ubiquitination of the RIG-I 2CARD domains is mediated by members of the tripartite motif (TRIM) protein family, specifically TRIM25, at lysine residues in the

second CARD of RIG-I (K99, K169, K172, K181, K190, and K193) [154, 155]. Even though TRIM25 is known to mediate K63 ubiquitination of RIG-I, two additional E3 ligases, MEX3C and RIPLET, have also been implicated as mediators of K63 ubiquitination of RIG-I [156-160].

Viral pathogens have evolved intricate mechanisms to counteract the innate immune response. In this regard, members of the *Bunyaviridae*, encode proteins that facilitate the inhibition of host cell immune responses. More specifically, the small non-structural protein, NSs encoded by bunyaviruses such as RVFV, or LACV has been implicated as the main inhibitor of innate immune responses. For example, RVFV NSs shuts down host cell transcription and promotes degradation of PKR, while LACV NSs promotes proteasomal degradation of mammalian RNA polymerase II subunit RPB1 [13, 14, 104]. SFTS virus has a 3-segmented genome that is composed of the L segment, M segment, and the S segment. The latter segment encodes the nucleocapsid protein and the small non-structural protein NSs via an ambisense coding strategy. The SFTS virus NSs has been shown to be major virulence factor during infection. Initial studies demonstrated that the SFTS virus NSs is a potent inhibitor of IFN- $\beta$  and localizes to cytoplasmic structures derived from the early endosomal pathway [61, 65, 66, 91]. Further studies have revealed that inhibition of the IFN response correlates with sequestration of RIG-I, TRIM25, TBK-1, STAT1/2, and IRF-3 into the SFTS virus NSs positive structures [61, 65, 66, 91, 107]. Additionally, our studies have determined that ubiquitin also colocalizes with the SFTS virus NSs positive structures and spectrometry analysis of these structures detected the presence of components of the 26S proteasome. In this chapter, we focus on the fate of RIG-I and its signaling molecules during SFTS virus infection. Infection of

SFTS virus leads to a decrease in cytoplasmic protein expression of TBK-1 and a 50% reduction in the active form of RIG-I; however, inhibition of the Ubiquitin-Proteasomal Pathway restores the cytoplasmic concentration of these proteins. Additionally, we report that mutation of K63 ubiquitination of RIG-I at K172 obligates interaction and co-localization with SFTS virus NSs. TBK-1 can be activated by K63 ubiquitination at K30 and K401 along with phosphorylation at serine 172; however, mutation of K30 and K401 to alanine impairs K63 mediated activation [161-164]. Furthermore, studies have shown that a phosphorylation-deficient TBK-1 can still undergo K63 ubiquitination [163]. The cellular balance of TBK-1 is maintained through K48 mediated degradation [161] Lastly, we observed a 30% decrease in colocalization between K63 and K48 TBK-1 mutants, indicating that ubiquitination in part plays a role in TBK-1/NSs colocalization. Interestingly, we only observed a 4% localization between NSs and a kinase-deficient TBK-1 mutant. Altogether, these data suggest that both ubiquitination and phosphorylation play a major role in interaction and co-localization of SFTS virus NSs with RIG-I and TBK-1.

## **MATERIALS AND METHODS**

### **Cells, Plasmids, Reagents**

Human embryonic kidney (HEK293T) cells were obtained from ATCC and maintained in Dulbecco's minimal essential medium (Lonza) supplemented with L-glutamine, sodium pyruvate, and 10% fetal bovine serum (Atlanta Biologicals). HeLa and Vero76 cells were obtained from ATCC and maintained with Eagle minimal essential medium (Lonza) supplemented with L-glutamine, penicillin-streptomycin, and 10% fetal bovine serum. The plasmid carrying SFTSV NSs was constructed as previously described [61]. Plasmids

carrying RIG-I and TBK-1 were previously described [165, 166] or constructed following standard cloning procedures. SFTS virus strain YL-1 was provided by the Chinese Center for Disease Control and Prevention and passaged twice in Vero E6 cells to generate viral stocks for this study. The SFTS virus titers were determined by plaque assays as previously described [122].

### **Transfection, immunoblotting, and immunoprecipitation.**

Unless otherwise stated, all transfections were carried out by using 1  $\mu$ g of plasmid DNA and the Lipofectamine 3000 reagent (Invitrogen) following the manufacturer's recommendations. At 16 to 24 hr posttransfection, the cells were harvested and lysed with NP-40 lysis buffer containing 1% Halt protease inhibitor cocktail (Thermo Scientific). For separation of insoluble and soluble fractions, cells lysed in NP-lysis buffer on ice for 10 minutes and centrifuged for 5 minutes at 3,000 X g. The clarified supernatant was considered soluble and the pellet insoluble. For immunoblotting, proteins were separated by SDS-PAGE and subsequently transferred to a 0.2- $\mu$ m-pore-size polyvinylidene difluoride (PVDF) membrane (Millipore). The PVDF membranes were blocked for 45 min with 5% nonfat dry milk in Tris-buffered saline with 1% Tween 20 (TBST). Membranes were incubated with primary antibodies for 16 to 18 h at 4°C. The membranes were washed in TBST and incubated with secondary horseradish peroxidase (HRP)-conjugated antibodies for 1 h. Blots were developed by using Western Lightning ECL substrate (PerkinElmer) according to the manufacturer's recommendations. For protein immunoprecipitation, lysates were incubated in the presence of anti-hemagglutinin (anti-HA) agarose (Pierce). Eluted proteins and the corresponding lysates were separated by SDS-PAGE, followed by immunoblotting as described above. The following primary

antibodies were utilized for immunoblotting procedures: rabbit anti-FLAG (1:1,000; Sigma), rabbit anti-HA (1:1,000; Sigma), rabbit anti- $\beta$ -tubulin (1:10,000; Abcam), mouse anti-RIG-I NT (1:1000; EMD Millipore), anti-RIG-I (1:1000; Thermo Scientific), and anti-TBK-1 (1:1000; Thermo Scientific). The secondary antibodies utilized were donkey anti-rabbit IgG HRP-conjugated antibody (1:5,000) and sheep anti-mouse IgG HRP-conjugated antibody (1:5,000) (GE Healthcare).

### **Immunofluorescence and confocal microscopy**

HeLa cells were seeded on mouse Laminin I-treated coverslips and transfected following standard procedures. Cells were incubated overnight at 37°C in 5% CO<sub>2</sub>. Following this incubation, cells were either fixed with 1:1 Acetone:Methanol mix or infected with SFTSV (multiplicity of infection [MOI] = 1.0) for 24 h and then fixed and permeabilized with a solution of phosphate-buffered saline (PBS) containing 0.1% Triton X-100 (Sigma). Following permeabilization, the cells were washed and blocked with 10% goat serum and 3% bovine serum albumin (BSA; Thermo Scientific) in PBS (Lonza). If required by the experiment, cells were stained overnight with primary antibodies. Cell nuclei were stained with Hoechst 33342 (1:1,000; Invitrogen), and the coverslips were mounted onto glass slides by using ProLong Gold antifade reagent (Invitrogen). The following primary antibodies were used in immunofluorescence experiments: polyclonal rabbit anti-SFTSV NSs generated by GenScript (Piscataway, NJ) (1:500), rabbit anti-FLAG (1:1000; Sigma), rabbit anti-TBK-1 (ThermoFisher), rabbit anti-RIG-I NT (1:100, EMD Millipore). The following antibodies were used as secondary antibodies for immunofluorescence experiments: Alexa Fluor 488-conjugated goat anti-rabbit (1:1,000; Molecular Probes) and Alexa Fluor 594-conjugated goat anti-rabbit (1:2,000; Molecular

Probes) antibodies. All samples were visualized in a Zeiss LSM510META laser scanning confocal microscope or an Olympus spinning disc confocal microscope.

## RESULTS

**SFTS virus NSs localizes with components of the RIG-I signaling cascade.** We and others have shown that the SFTS virus NSs localizes with elements of the RIG-I signaling cascade RIG-I, TBK-1 [61, 66, 91], and TRIM25; however the mechanism by which NSs localizes with these components remains to be understood. To this end, HeLa cells were seeded on glass coverslips and mock infected or infected with SFTS virus (MOI=1). At 24 hpi, cells were fixed and stained using antibodies against human TBK-1, RIG-I, and ubiquitin, and the SFTS virus NSs. We observed colocalization of the SFTS virus NSs with TBK-1 and ubiquitin (**Figure 4.1, A-B**). Interestingly, we were not able to detect the presence of the active form of RIG-I (RIG-I NT) in cells infected with SFTS virus. However, we observed RIG-I staining in non-infected neighboring cells (**Figure 4.1 C**).

**SFTS virus infection leads to a decrease in RIG-I NT and TBK-1 expression.** Our confocal data led us to investigate the fate of the proteins sequestered into SFTS virus NSs-positive structures. To this end, HeLa cells were mock infected or infected with SFTS virus NSs and cell lysates and RNA collected at 0, 12, and 24 hpi and resolved by SDS-PAGE, transferred onto PVDF membrane and blotted for human RIG-I NT (N-terminus, recognizes the active form of RIG-I), RIG-I CT (C-terminus, recognizes the helicase domain of RIG-I), TBK-1, SFTS virus NSs, and  $\beta$ -tubulin (**Figure 4.2 A**). Interestingly, the expression levels of TBK-1 during SFTS virus infection began to decrease, and by 72 hpi it was not detected (**Figure 4.2B**). We observed no decrease in RIG-I CT levels but observed a 50% decrease in RIG-I NT by 12 and 24 hpi (**Figure 4.2 A, C**). It is well known

that the Rift Valley Fever virus NSs is a potent inhibitor of global cell transcription [56, 59, 105, 106]; however, SFTS virus NSs does not have a similar function. Due to our previous observation regarding the decrease expression of the active form of RIG-I and the inhibition of TBK-1 expression, we nevertheless explored the possibility that SFTS virus was affecting RIG-I and TBK-1 transcription. To this end, RNA collected at 0, 8, 12, 24, and 48 hpi was used to perform SYBR Green qPCR using primers directed against TBK-1 or RIG-I, which revealed that SFTS virus NSs does not affect host cell transcription of these genes (**Figure 4.3**). These data suggest that SFTS virus infection target components of the RIG-I signaling cascade at the protein level, specifically the active form of RIG-I and TBK-1.

**Proteasome inhibition leads to recovery of RIG-I signaling cascade.** Mass Spectrometry analysis of purified SFTS virus NSs-cytoplasmic structures from infected HeLa cells identified ubiquitin, components of the 26S proteasome, and Rab GTPases within these structures (data not shown). Our previous observation that levels of RIG-I and TBK-1 decrease during SFTS virus infection and the detection of the 26S proteasome and ubiquitin within these cytoplasmic structures lead us to investigate whether RIG-I and TBK-1 were being targeted for degradation via the Ubiquitin-Proteasomal Pathway (UPP). To test this possibility, HeLa cells were pre-treated with PBS, DMSO (vehicle), or 10uM of MG-132 (a potent inhibitor of the proteasome) and mock infected or infected with SFTS virus (MOI=1). Soluble and insoluble fractions were collected at 0, 12, and 24 hours post infection. Fractions were then resolved by SDS-PAGE, transferred onto PVDF membrane and blotted for SFTS virus NSs, b-tubulin, TBK-1, RIG-I NT, and RIG-I CT. Interestingly,



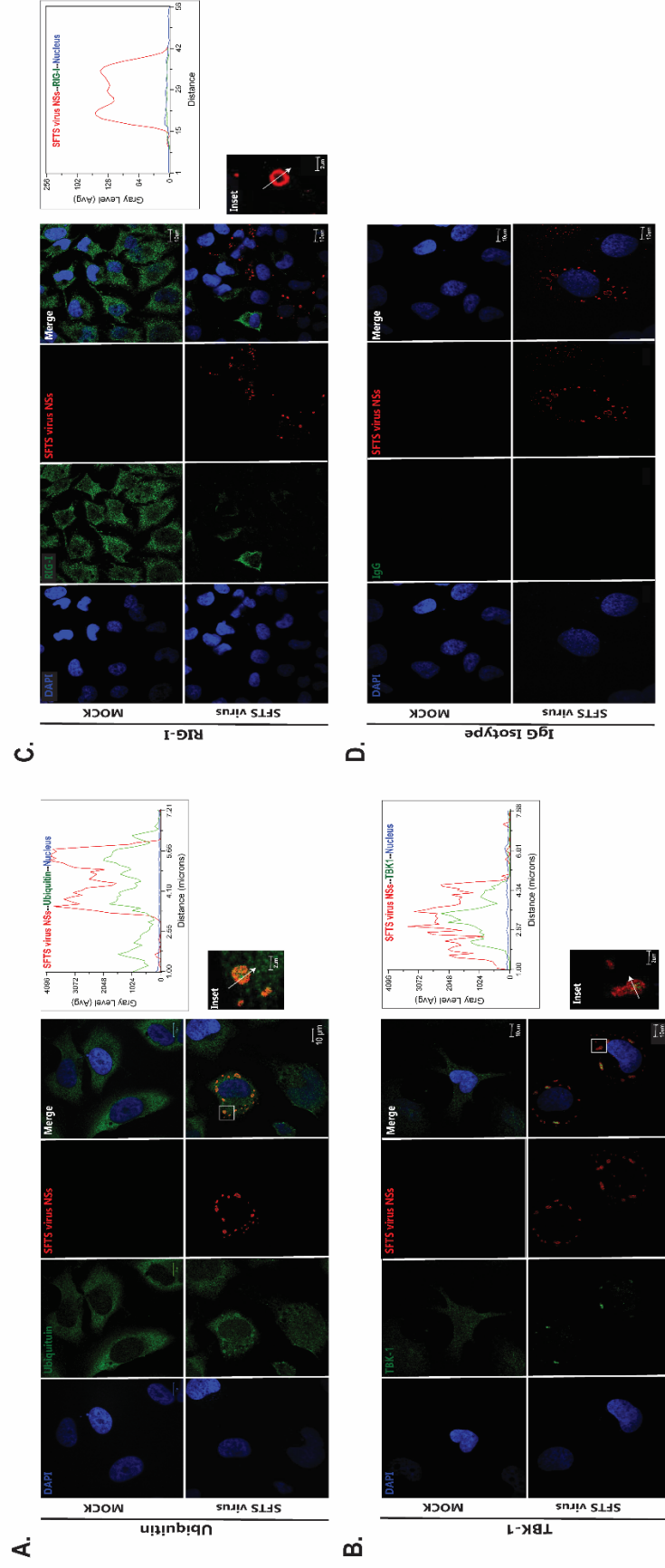
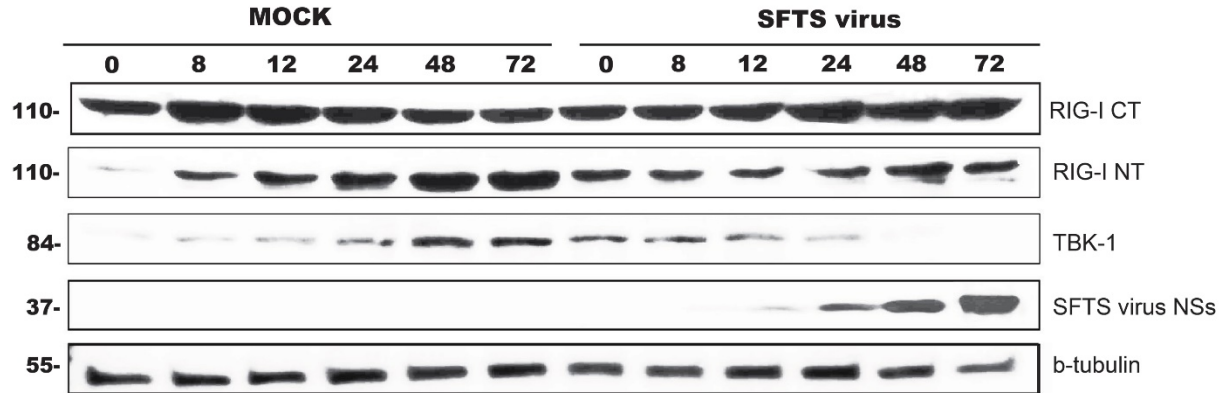


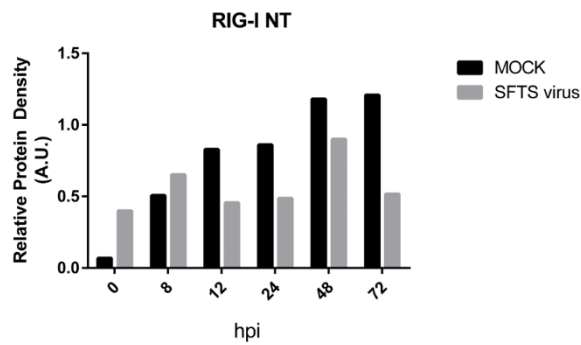
**Figure 4.1. SFTS virus NSs localizes with endogenous TBK-1 and ubiquitin.**

HeLa cells were seeded on glass coverslips and mock infected or infected with SFTS virus (MOI=1). At 24 hpi, cells were fixed and permeabilized. Immunofluorescence was performed using primary antibodies against RIG-I, TBK-1, ubiquitin, and SFTS virus NSs. AlexaFluor594 was used as the secondary antibody for SFTS virus NSs and AlexaFluor488 for all endogenous proteins. An IgG isotype was used in order to show the specificity of the endogenous protein staining. Line scan analysis using LSM510 was performed to determine co-localization of SFTS virus NSs with RIG-I, TBK-1, and ubiquitin.

**A.**



**B.**



**C.**

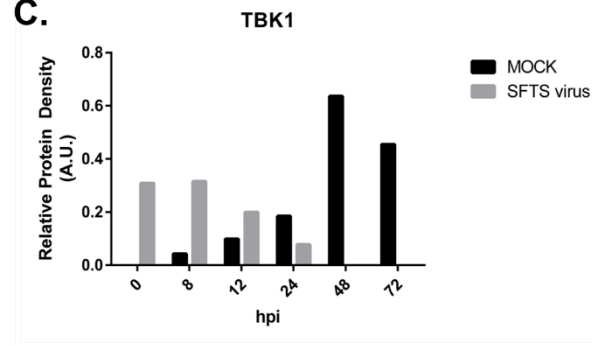


**Figure 4.2. SFTS virus infection decreases levels of TBK-1 and RIG-I NT.**

HeLa cells were mock infected or infected with SFTS virus (MOI=1) and lysates collected using Ambion® PARIS system at 0, 8, 12, 24, 48, and 72 hpi. (A) 60 ug of lysates per well was resolved by SDS-PAGE, transferred onto PDVF membrane and blotted for RIG-I CT, RIG-I NT, TBK-1, SFTS virus NSs and b-tubulin. Densitometry analysis was performed to determine the expression of (B) RIG-I and (C) TBK-1.

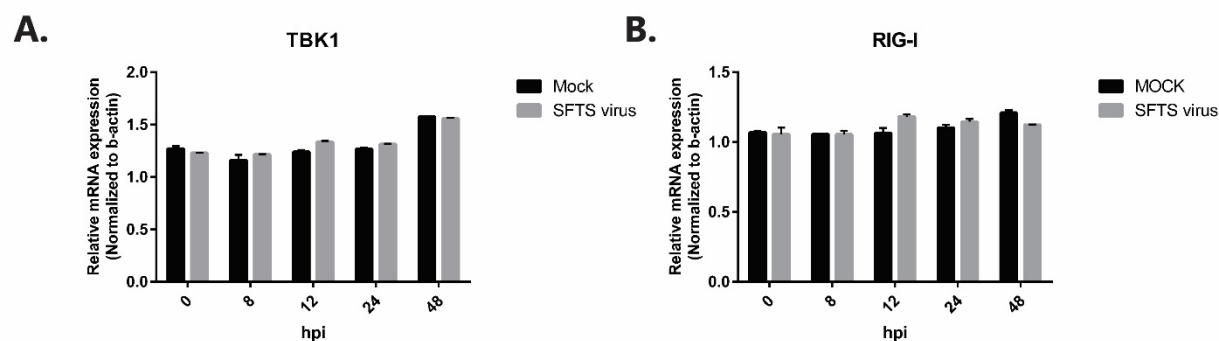


**Figure 4.3. SFTS virus infection does not affect RIG-I and TBK-1 mRNA levels.**

HeLa cells were mock infected or infected with SFTS virus (MOI=1) and total RNA collected using Ambion® PARIS system at 0, 8, 12, 24, 48, and 72 hpi. mRNA levels of (A) RIG-I and (B) TBK-1 were quantified by qPCR using total RNA. qPCR was performed in triplicates by SYBR qPCR assay using b-tubulin as the reference gene. The experiment was carried out in triplicates with consistent results.

we observed that inhibition of the proteasome during SFTS virus infection resulted in a shift of TBK-1 from the insoluble to soluble fraction (**Figure 4.4**). Additionally, we observed a 50% increase in RIG-I NT levels in the soluble fraction of SFTS virus-infected cells treated with MG-132 compared to the PBS-infected control, while no change in the RIG-I CT was evident. Furthermore, RIG-I CT nor RIG-NT were detected in the soluble pellet as TBK-1 was. These data suggests that inhibition of the UPP pathway disrupts the sequestration of TBK-1 and that SFTS virus NSs might be acting on the active form of RIG-I.

**Ubiquitination in part mediates interaction/colocalization between SFTS virus NSs and RIG-I or TBK-1.** It is well known that TRIM25 along with MEX3C and RIPLET mediate K63 ubiquitination of RIG-I [156-160]. In particular, the ubiquitination of the 2CARD domain at K172 of RIG-I by TRIM25 has been shown to be essential in initiating the RIG-I signaling cascade for induction of IFN [154]. We have previously shown that SFTS virus NSs interacts and co-localizes with TRIM25 [61], additionally, we have observed that ubiquitin also localizes to NSs-positive cytoplasmic structures. This along with the above-mentioned data regarding that inhibition of the

UPP restores TBK-1 and RIG-I NT levels, led us to investigate whether the interaction of TBK-1 or RIG-I with SFTS virus NSs was mediated through ubiquitination. Studies have shown that K63 ubiquitination of TBK-1 occurs at K30 and K401, and that mutation of both of these residues obligates K63 ubiquitination, while K48 ubiquitination of TBK-1 occurs at K670. Since our observations suggest that SFTS NSs acts on the active form of RIG-I, we also investigated whether SFTS virus NSs would interact with a kinase-deficient TBK-1. To this end, HEK 293T cells were transfected with plasmids encoding FLAG-tagged RIG-I WT, RIG-I K172R, TBK-1 WT, TBK-1 K401A, TBK-1 K30A, TBK-1 K63 (K30/K401A), TBK-1 K48 (K670A), or TBK-1 K38M alone or in the presence of SFTS virus NSs-HA. Mutation of TBK-1 at K38M inhibits the kinase activity of TBK-1. At 18 hours post transfection, whole cell lysates (WCL) were harvested and

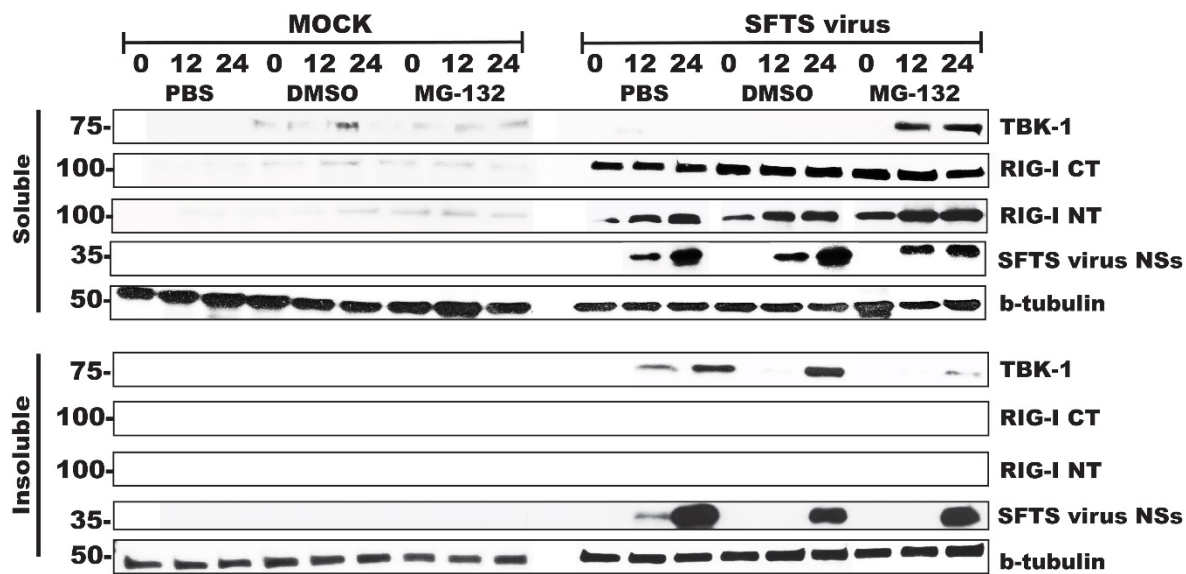


**Figure 4.4. Inhibition of the Ubiquitin-Proteasomal Pathway restores TBK-1 and RIG-I NT levels.**

HeLa cells were mock infected or infected with SFTS virus (MOI=1) 1 hour after treatment with PBS, DMSO, or 10  $\mu$ M MG-132. Soluble and insoluble fractions were collected at 0, 12, and 24 hpi. 30 $\mu$ g of each fraction per well was resolved by SDS-PAGE, transferred onto PDVF membrane and blotted for RIG-I NT, RIG-I CT, TBK-1, SFTS virus NSs and b-tubulin.

subjected to immunoprecipitation (IP) with anti-HA agarose beads. After 4 hours, beads were washed, and proteins eluted, resolved by SDS-PAGE, transferred onto PDVF membrane and blotted for FLAG or HA tags. Interestingly, mutation of RIG-I at K172 prevented the interaction with SFTS virus NSs (**Figure 4.5, compare lanes 16 and 17 top panel**). In contrast, mutation of TBK-1 at K48 or K63 ubiquitination sites did not impede the relocation of TBK-1 to the pellet fraction in the presence of SFTS virus NSs (**Figure 4.5, compare lanes 10 with 13 and 14 bottom panel**). Additionally, mutation (K38M) of the kinase activity of TBK-1 did not prevent the relocation of TBK-1 into the pellet in the presence of SFTS virus NSs either. Eventhough most of the WT and mutant forms of TBK-1 were shuttled into the pellet in the presence of SFTS virus NSs, we observed a minute amount of mutant TBK-1 in the soluble (input) (**Figure 4.5, compare lane 10 with lanes 11-15, third and fifth panels**).

Concurrently, we performed confocal microscopy to determine if our immunoprecipitation

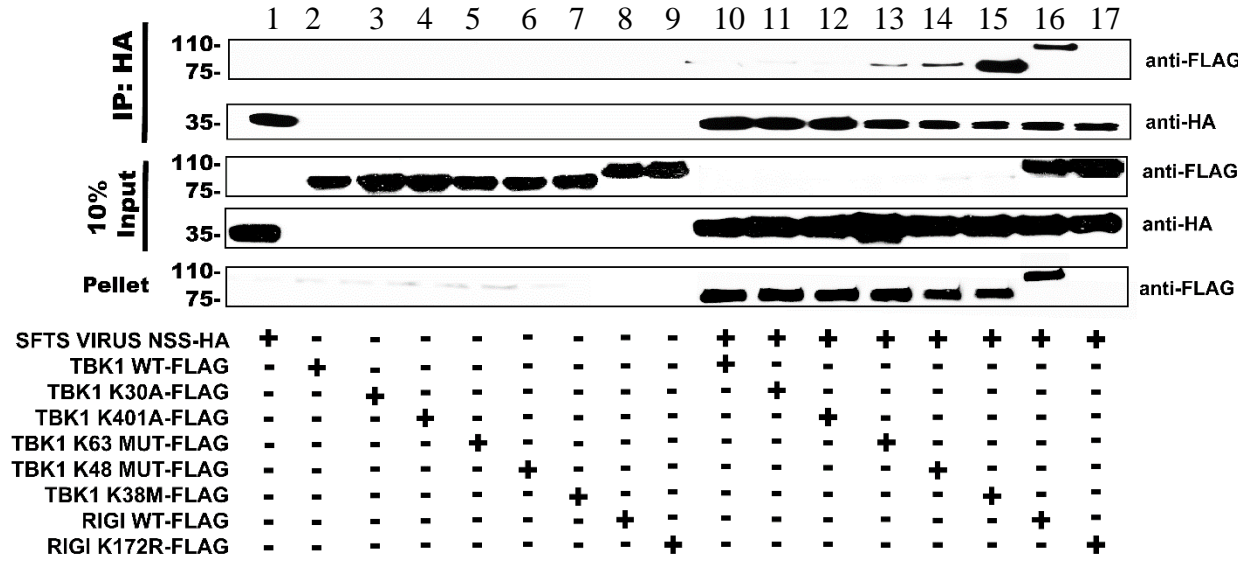


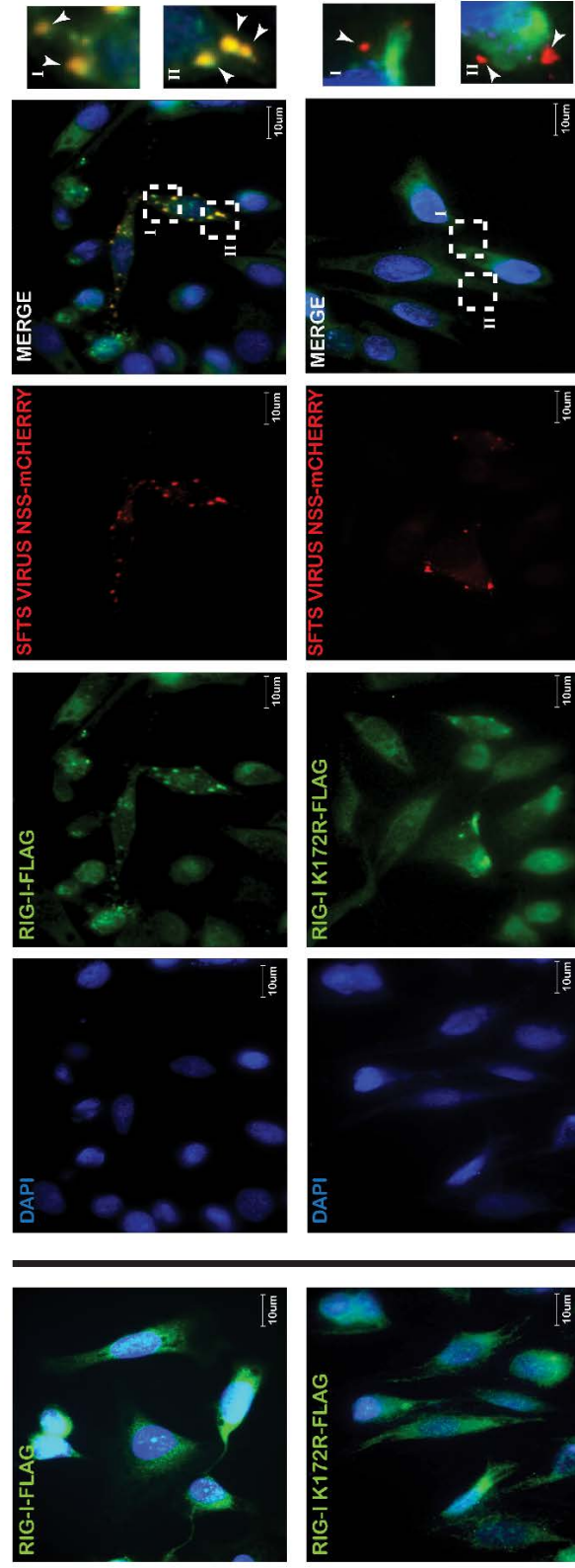
**Figure 4.5. Ubiquitination in part mediates interaction between SFTS virus NSs and RIG-I or TBK-1.**

HEK 293TN cells were transfected with expression plasmids encoding FLAG-tagged RIG-I WT, RIG-I K172R, TBK-1 WT, TBK-1 K30A, TBK-1 K401A, TBK-1 K63, TBK-1 K48, or TBK-1 K38M in the with or without HA-tagged SFTS virus NSs. At 18 hours post transfection, cell lysate

was subject to immunoprecipitation using anti-HA agarose. Protein elutes, 10% input, and insoluble fraction were resolved by SDS-PAGE, transferred onto PDVF membrane and blotted for FLAG and HA tags.

data correlated with co-localization of TBK-1 or RIG-I with SFTS virus NSs. HeLa cells were transfected as stated above and immunofluorescence performed. In regard to RIG-I, we did not observe any co-localization of RIG-I K172R with SFTS virus NSs (**Figure 4.6B**), which correlates with our IP data (**Figure 4.5**). For TBK-1 and its respective ubiquitin mutants, we observed a 30% decrease in colocalization events (**Figure 4.7A**). In contrast, only 4% of TBK-1 K38M and SFTS virus NSs localization events were observed (**Figure 4.7B**). This data suggests that SFTS virus NSs acts upon the active form of RIG-I. However, the mechanism for the interaction with TBK-1 still needs to be deciphered.

**A.**



**B.**

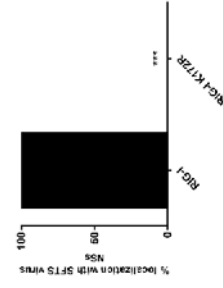


**Figure 4.6. Ubiquitination in part mediates colocalization between SFTS virus NSs and RIG-I.**

HeLa cells were transfected with plasmids encoding FLAG-tagged (A) RIG-I WT, RIG-I K172R, with or without mCherry tagged SFTS virus NSs. At 18 hours post transfection, cells were fixed, permeabilized, blocked, and incubated with anti-FLAG antibody overnight. AlexaFluor488 was used as the secondary antibody, nuclei visualized with DAPI. (B) Experiment was repeated twice and a total of 250 cells were counted per experiment to determine percentage of co-localization events.



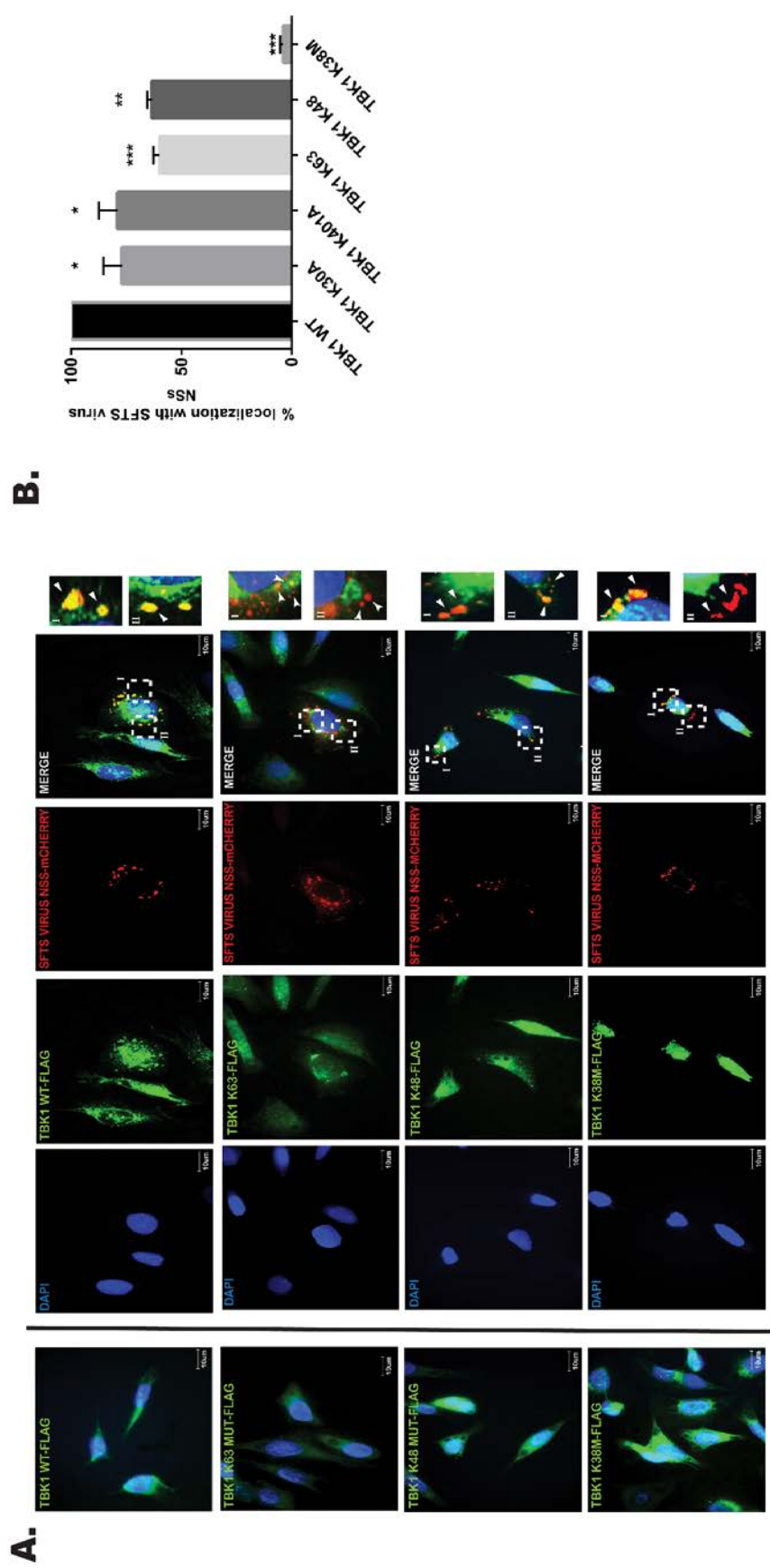


**Figure 4.7 Ubiquitination in part mediates colocalization between SFTS virus NSs and TBK-1.**

HeLa cells were transfected with plasmids encoding FLAG-tagged (A) TBK-1, TBK-1 K48, TBK-1 K63, or TBK-1 K38M with or without mCherry tagged SFTS virus NSs. At 18 hours post transfection, cells were fixed, permeabilized, blocked, and incubated with anti-FLAG antibody overnight. AlexaFluor488 was used as the secondary antibody, nuclei visualized with DAPI. (B) Experiment was repeated twice and a total of 250 cells were counted per experiment to determine percentage of co-localization events.



## DISCUSSION

The innate immune response is the first line of defense against invading pathogens. Activation of the innate immune response begins by recognition of pathogen-associated molecular patterns (PAMPS), by cytosolic pattern recognition receptors, PRRs [147, 167-170]. PRRs such as the RNA helicases retinoic acid-inducible gene 1 (RIG-I) or melanoma differentiation-associated protein 5 (MDA5) recognize 5'-triphosphate dsRNA or long higher order structure dsRNA, respectively [142-145]. RIG-I is comprised of a C-terminal domain, a central helicase domain, and two N-terminal caspase recruitment domains (CARDS). Interactions between the helicase and CARD domains of RIG-I maintain RIG-I in its inactive form; however, binding of the viral dsRNA by both the helicase and C-terminal domains results in a conformational change that exposes the CARDS [146]. This, in turn, allows K63 ubiquitination by TRIM25 at K172 of the RIG-I N-terminus (NT), which results in a signaling cascade to induce activation of IFN related genes [154, 166, 167, 171, 172].

Ubiquitin is one of the most significant post-translation modifications (PTMs) that determines the fate of the modified protein, activation or degradation. It has been shown that K63 ubiquitination mainly results in activation, while K48 leads to proteasomal degradation [152, 153, 170, 173]. As previously mentioned, TRIM25 mediates K63 ubiquitination of RIG-I at K172; however, RIPILET and MEX3C can also ubiquitinate RIG-I at other lysine residues [156-158, 160]. In contrast, TBK-1 undergoes both K63 (at residues K30 and K401) and K48 (at K670 residue) ubiquitination [162]. Furthermore, TBK-1 also possesses kinase activity, and studies have shown that mutation at K38 inactivates kinase activity of TBK-1 but does not prevent autophosphorylation in trans at serine 172.

In this study, we aimed to determine the mechanism by which the SFTS virus NSs targeted RIG-I and TBK-1 into cytoplasmic structures, which correlates with inhibition of immune responses. As previously stated, TRIM25 and ubiquitin play a major role in the activation of the innate immune response [154]. This in addition to both TRIM25 and ubiquitin also targeted into SFTS virus NSs-

positive cytoplasmic structures suggest that NSs inhibits the RIG-I signaling cascade through the use of ubiquitin. We have shown that during SFTS virus infection, TBK-1 is removed from the cytoplasm and shuttled into the insoluble cellular fraction—most likely this is the TBK-1 that is sequestered into the cytoplasmic structures. In contrast, when using antibodies directed against the active N-terminus of RIG-I, we were unable to observe RIG-I in the insoluble fraction by western blot nor in infected cells by indirect immunofluorescence. However, in overexpression experiments, we have noted that FLAG-tagged RIG-I levels decrease by 50% in the presence of SFTS virus NSs and is detected in the insoluble fraction. Interestingly, when detecting RIG-I with an antibody directed at the C-terminus, we see no change in protein expression—this could further indicate that SFTS virus NSs targets only the active form of RIG-I. To further elucidate the role that these NSs-positive structures play in inhibition of the RIG-I signaling cascade, Mass Spectrometry Analysis was performed on purified NSs-positive cytoplasmic structures from infected HeLa cells. This analysis revealed that components of the 26S proteasome were harbored within these structures, suggesting that these structures could function as sites of protein degradation.

In light of our findings, we inhibited the Ubiquitin-Proteasomal Pathway with MG132 during SFTS virus infection and were to recover levels of the active form of RIG-I and surprisingly observed a shift of TBK-1 from the insoluble to soluble fraction. These results lead us to investigate the linkage-specific ubiquitination of RIG-I and TBK-1 by overexpressing ubiquitin mutant forms of each signaling protein. We identified that in regard to RIG-I, abolishing the K63 site at K172 completely prevented interaction and co-localization of RIG-I with NSs. This further suggests that the active form is targeted by NSs. Removal of TBK-1 ubiquitination sites and kinase activity, however, had minimal, ~30%, reduction in interaction and co-localization with SFTS virus NSs, suggesting that the mechanism of TBK-1/SFTS virus NSs interaction is much more complex, and may require a linker protein that mediates the interaction between NSs and TBK-1. Since the activation of TBK-1

can be carried out through ubiquitination and or phosphorylation, a detailed study looking into each activator of TBK-1 would be required in order to grasp a better understanding of how NSs is targeting TBK-1.

This study has given insight into the use of ubiquitination as means to target components of the RIG-I signaling cascade into cytoplasmic structures by the SFTS virus NSs. Our data suggests that NSs targets the activated RIG-I for degradation via the UPP, however, in regard to TBK-1, further studies using an entirely inactive mutant (both ubiquitin and kinase-deficient) of TBK-1 are required to decipher the mechanism by which TBK-1 is targeted by SFTS virus NSs.

## SUMMARY

In this study, we have gained insights into the molecular pathogenesis of the emerging tick-borne phlebovirus SFTS virus. We have observed that the cytoplasmic structures induced by SFTS virus NSs traffic within and out the cell, suggesting that these structures may play different roles during infection. Further characterization of the intracellular structures identified that they localize with compartments associated with endosomal recycling or degradation and that they contain an acidic environment with a pH below 5. One of the most significant findings of this study is that the SFTS virus NSs-positive secreted structures harbor infectious virus-like particles that are able to maintain SFTS virus infection in the presence of neutralizing antibodies. This novel mechanism for receptor-independent transmission of SFTS virus challenges the current dogma of bunyavirus dissemination. Furthermore, we have gained insight into the innate immune antagonistic activity of SFTS virus NSs. We have shown that SFTS virus NSs may utilize ubiquitin as means to remove RIG-I and other signaling molecules such as TBK-1 from the RIG-I signaling cascade—preventing the induction of interferon beta related genes. Lastly, we have observed that by inhibiting the Ubiquitin-Proteasomal Pathway, we are able to recover RIG-I and TBK-1 protein levels, suggesting that these molecules are targeted for degradation. Altogether our data suggests novel and complex mechanisms employed by SFTS virus to circumvent host innate immune responses and aid in replication and dissemination.

## REFERENCES

1. Boushab, B.M., et al., *Severe Human Illness Caused by Rift Valley Fever Virus in Mauritania, 2015*. Open Forum Infect Dis, 2016. **3**(4): p. ofw200.
2. Boussini, H., et al., *Prevalence of Rift Valley fever in domestic ruminants in the central and northern regions of Burkina Faso*. Rev Sci Tech, 2014. **33**(3): p. 893-901.
3. Ikegami, T., *Rift Valley fever vaccines: an overview of the safety and efficacy of the live-attenuated MP-12 vaccine candidate*. Expert Rev Vaccines, 2017. **16**(6): p. 601-611.
4. Muga, G.O., et al., *Sociocultural and economic dimensions of Rift Valley fever*. Am J Trop Med Hyg, 2015. **92**(4): p. 730-8.
5. Pepin, M. and C.R.-M.e.l.I.d.V.S. avec la participation de la, *[Rift Valley fever]*. Med Mal Infect, 2011. **41**(6): p. 322-9.
6. Copps, S.C. and A.C. Elston, *California virus (La Crosse strain) encephalitis*. Wis Med J, 1969. **68**(11): p. 329-31.
7. Golnar, A.J., R.C. Kading, and G.L. Hamer, *Quantifying the potential pathways and locations of Rift Valley fever virus entry into the United States*. Transbound Emerg Dis, 2017.
8. Wichgers Schreur, P.J., et al., *Four-segmented Rift Valley fever virus-based vaccines can be applied safely in ewes during pregnancy*. Vaccine, 2017. **35**(23): p. 3123-3128.
9. Jin, M., et al., *Hantaan virus enters cells by clathrin-dependent receptor-mediated endocytosis*. Virology, 2002. **294**(1): p. 60-9.
10. Wang, H., et al., *Old World hantaviruses do not produce detectable amounts of dsRNA in infected cells and the 5[prime] termini of their genomic RNAs are monophosphorylated*. J. Gen. Virol., 2011. **92**: p. 1199-1204.
11. Santos, R.I., et al., *Oropouche virus entry into HeLa cells involves clathrin and requires endosomal acidification*. Virus Res, 2008. **138**(1-2): p. 139-43.
12. Lozach, P.Y., et al., *Entry of bunyaviruses into mammalian cells*. Cell Host Microbe, 2010. **7**(6): p. 488-99.
13. Blakqori, G., et al., *La Crosse bunyavirus nonstructural protein NSs serves to suppress the type I interferon system of mammalian hosts*. J Virol, 2007. **81**(10): p. 4991-9.
14. Verbruggen, P., et al., *Interferon antagonist NSs of La Crosse virus triggers a DNA damage response-like degradation of transcribing RNA polymerase II*. J Biol Chem, 2011. **286**(5): p. 3681-92.
15. Gauld, L.W., et al., *Observations on a natural cycle of La Crosse virus (California group) in Southwestern Wisconsin*. Am J Trop Med Hyg, 1974. **23**(5): p. 983-92.
16. Al-Abri, S.S., et al., *Current status of Crimean-Congo haemorrhagic fever in the World Health Organization Eastern Mediterranean Region: issues, challenges, and future directions*. Int J Infect Dis, 2017. **58**: p. 82-89.
17. Brackney, D.E. and P.M. Armstrong, *Transmission and evolution of tick-borne viruses*. Curr Opin Virol, 2016. **21**: p. 67-74.
18. Simon, M., C. Johansson, and A. Mirazimi, *Crimean-Congo hemorrhagic fever virus entry and replication is clathrin-, pH- and cholesterol-dependent*. J Gen Virol, 2009. **90**(Pt 1): p. 210-5.
19. Ciancaglini, M., et al., *Hantavirus pulmonary syndrome in Tucuman province associated to an unexpected viral genotype*. Medicina (B Aires), 2017. **77**(2): p. 81-84.

20. Jiang, H., et al., *Hantavirus infection: a global zoonotic challenge*. Virol Sin, 2017. **32**(1): p. 32-43.
21. Mustonen, J., et al., *Kidney disease in Puumala hantavirus infection*. Infect Dis (Lond), 2017. **49**(5): p. 321-332.
22. de St Maurice, A., et al., *Exposure Characteristics of Hantavirus Pulmonary Syndrome Patients, United States, 1993-2015*. Emerg Infect Dis, 2017. **23**(5): p. 733-739.
23. Christova, I., et al., *Clinical aspects of hantavirus infections in Bulgaria*. Wien Klin Wochenschr, 2017.
24. Tesikova, J., et al., *Hantavirus Strains in East Africa Related to Western African Hantaviruses*. Vector Borne Zoonotic Dis, 2017. **17**(4): p. 278-280.
25. Yu, X.J., et al., *Fever with thrombocytopenia associated with a novel bunyavirus in China*. N Engl J Med, 2011. **364**(16): p. 1523-32.
26. Jiao, Y., et al., *Experimental and Natural Infections of Goats with Severe Fever with Thrombocytopenia Syndrome Virus: Evidence for Ticks as Viral Vector*. PLoS Negl Trop Dis, 2015. **9**(10): p. e0004092.
27. Wang, S., et al., *SFTS virus in ticks in an endemic area of China*. Am J Trop Med Hyg, 2015. **92**(4): p. 684-9.
28. Zhang, Y.Z., et al., *The ecology, genetic diversity and phylogeny of Huaiyangshan virus in China*. J Virol, 2011.
29. Yun, S.M., et al., *Severe fever with thrombocytopenia syndrome virus in ticks collected from humans, South Korea, 2013*. Emerg Infect Dis, 2014. **20**(8): p. 1358-61.
30. Niu, G., et al., *Severe fever with thrombocytopenia syndrome virus among domesticated animals, China*. Emerg Infect Dis, 2013. **19**(5): p. 756-63.
31. Li, Z., et al., *Seroprevalence of antibodies against SFTS virus infection in farmers and animals, Jiangsu, China*. J Clin Virol, 2014. **60**(3): p. 185-9.
32. Zhao, L., et al., *Severe fever with thrombocytopenia syndrome virus, Shandong Province, China*. Emerg Infect Dis, 2012. **18**(6): p. 963-5.
33. Hwang, J., et al., *Molecular detection of severe fever with thrombocytopenia syndrome virus (SFTSV) in feral cats from Seoul, Korea*. Ticks Tick Borne Dis, 2016.
34. Hayasaka, D., et al., *Seroepidemiological evidence of severe fever with thrombocytopenia syndrome virus infections in wild boars in Nagasaki, Japan*. Trop Med Health, 2016. **44**: p. 6.
35. Tabara, K., et al., *Investigation of Severe Fever with Thrombocytopenia Syndrome Virus Antibody among Domestic Bovines Transported to Slaughterhouse in Shimane Prefecture, Japan*. Jpn J Infect Dis, 2016. **69**(5): p. 445-7.
36. Park, S.W., et al., *Prevalence of severe fever with thrombocytopenia syndrome virus in Haemaphysalis longicornis ticks in South Korea*. Ticks Tick Borne Dis, 2014. **5**(6): p. 975-7.
37. Zhang, Y.Z. and J. Xu, *The emergence and cross species transmission of newly discovered tick-borne Bunyavirus in China*. Curr Opin Virol, 2016. **16**: p. 126-31.
38. Liu, Y., et al., *Person-to-person transmission of severe fever with thrombocytopenia syndrome virus*. Vector Borne Zoonotic Dis, 2012. **12**(2): p. 156-60.
39. Bao, C.J., et al., *A family cluster of infections by a newly recognized bunyavirus in eastern China, 2007: further evidence of person-to-person transmission*. Clin Infect Dis, 2011. **53**(12): p. 1208-14.
40. Jiang, X.L., et al., *A cluster of person-to-person transmission cases caused by SFTS virus in Penglai, China*. Clin Microbiol Infect, 2015. **21**(3): p. 274-9.

41. Xing, X., et al., *Natural Transmission Model for Severe Fever With Thrombocytopenia Syndrome Bunyavirus in Villages of Hubei Province, China*. Medicine (Baltimore), 2016. **95**(4): p. e2533.
42. Yoo, J.R., et al., *Family Cluster Analysis of Severe Fever with Thrombocytopenia Syndrome Virus Infection in Korea*. Am J Trop Med Hyg, 2016. **95**(6): p. 1351-1357.
43. Ding, F., et al., *Epidemiologic features of severe fever with thrombocytopenia syndrome in China, 2011-2012*. Clin Infect Dis, 2013. **56**(11): p. 1682-3.
44. Yu, X.J., et al., *Fever with thrombocytopenia associated with a novel bunyavirus in China*. N Engl J Med, 2011. **364**(16): p. 1523-32.
45. Liu, Q., et al., *Severe fever with thrombocytopenia syndrome, an emerging tick-borne zoonosis*. Lancet Infect Dis, 2014. **14**(8): p. 763-72.
46. Park, S.W., et al., *Severe fever with thrombocytopenia syndrome virus, South Korea, 2013*. Emerg Infect Dis, 2014. **20**(11): p. 1880-2.
47. Hiraki, T., et al., *Two autopsy cases of severe fever with thrombocytopenia syndrome (SFTS) in Japan: a pathognomonic histological feature and unique complication of SFTS*. Pathol Int, 2014. **64**(11): p. 569-75.
48. Liu, K., et al., *Epidemiologic features and environmental risk factors of severe fever with thrombocytopenia syndrome, Xinyang, China*. PLoS Negl Trop Dis, 2014. **8**(5): p. e2820.
49. Liu, K., et al., *A national assessment of the epidemiology of severe fever with thrombocytopenia syndrome, China*. Sci Rep, 2015. **5**: p. 9679.
50. Cui, F., et al., *Clinical and epidemiological study on severe fever with thrombocytopenia syndrome in Yiyuan County, Shandong Province, China*. Am J Trop Med Hyg, 2013. **88**(3): p. 510-2.
51. Huang, Y.T., et al., *Neutralizing Antibodies to Severe Fever with Thrombocytopenia Syndrome Virus 4 Years after Hospitalization, China*. Emerg Infect Dis, 2016. **22**(11): p. 1985-1987.
52. Zeng, P., et al., *A study of seroprevalence and rates of asymptomatic viremia of severe fever with thrombocytopenia syndrome virus among Chinese blood donors*. Transfusion, 2015. **55**(5): p. 965-71.
53. Takahashi, T., et al., *The First Identification and Retrospective Study of Severe Fever With Thrombocytopenia Syndrome in Japan*. J Infect Dis, 2013.
54. Kim, K.H., et al., *Severe fever with thrombocytopenia syndrome, South Korea, 2012*. Emerg Infect Dis, 2013. **19**(11): p. 1892-4.
55. Ikegami, T., et al., *Dual functions of Rift Valley fever virus NSs protein: inhibition of host mRNA transcription and post-transcriptional downregulation of protein kinase PKR*. Ann N Y Acad Sci, 2009. **1171 Suppl 1**: p. E75-85.
56. Kalveram, B., et al., *Rift Valley fever virus NSs inhibits host transcription independently of the degradation of dsRNA-dependent protein kinase PKR*. Virology, 2013. **435**(2): p. 415-24.
57. Leonard, V.H., et al., *Interaction of Bunyamwera Orthobunyavirus NSs protein with mediator protein MED8: a mechanism for inhibiting the interferon response*. J Virol, 2006. **80**(19): p. 9667-75.
58. van Knippenberg, I., C. Carlton-Smith, and R.M. Elliott, *The N-terminus of Bunyamwera orthobunyavirus NSs protein is essential for interferon antagonism*. J Gen Virol, 2010. **91**(Pt 8): p. 2002-6.
59. Billecocq, A., et al., *NSs protein of Rift Valley fever virus blocks interferon production by inhibiting host gene transcription*. J Virol, 2004. **78**(18): p. 9798-806.

60. Bouloy, M., et al., *Genetic evidence for an interferon-antagonistic function of rift valley fever virus nonstructural protein NSs*. J Virol, 2001. **75**(3): p. 1371-7.
61. Santiago, F.W., *Hijacking of RIG-I signaling proteins into virus-induced cytoplasmic structures correlates with the inhibition of type I interferon responses*. J. Virol., 2014. **88**: p. 4572-4585.
62. Qu, B., et al., *Suppression of the interferon and NF- $\kappa$ B responses by severe fever with thrombocytopenia syndrome virus*. J Virol, 2012. **86**(16): p. 8388-401.
63. Ning, Y.J., et al., *Viral suppression of innate immunity via spatial isolation of TBK1/IKK $\epsilon$  from mitochondrial antiviral platform*. J Mol Cell Biol, 2014. **6**(4): p. 324-37.
64. Ning, Y.J., et al., *Disruption of type I interferon signaling by the nonstructural protein of severe fever with thrombocytopenia syndrome virus via the hijacking of STAT2 and STAT1 into inclusion bodies*. J Virol, 2015. **89**(8): p. 4227-36.
65. Ning, Y.J., et al., *Viral suppression of innate immunity via spatial isolation of TBK1/IKK{epsilon} from mitochondrial antiviral platform*. J Mol Cell Biol, 2014.
66. Wu, X., et al., *Roles of viroplasm-like structures formed by nonstructural protein NSs in infection with severe fever with thrombocytopenia syndrome virus*. FASEB J, 2014. **28**(6): p. 2504-2516.
67. Sun, Y., et al., *Host cytokine storm is associated with disease severity of severe Fever with thrombocytopenia syndrome*. J Infect Dis, 2012. **206**(7): p. 1085-94.
68. Jin, C., et al., *Pathogenesis of emerging severe fever with thrombocytopenia syndrome virus in C57/BL6 mouse model*. Proc Natl Acad Sci U S A, 2012. **109**(25): p. 10053-8.
69. Sun, L., et al., *Detection and evaluation of immunofunction of patients with severe fever with thrombocytopenia syndrome*. Clin Exp Med, 2014. **14**(4): p. 389-95.
70. Bukong, T.N., et al., *Exosomes from hepatitis C infected patients transmit HCV infection and contain replication competent viral RNA in complex with Ago2-miR122-HSP90*. PLoS Pathog, 2014. **10**(10): p. e1004424.
71. Robinson, S.M., et al., *Coxsackievirus B exits the host cell in shed microvesicles displaying autophagosomal markers*. PLoS Pathog, 2014. **10**(4): p. e1004045.
72. Colombo, M., G. Raposo, and C. Thery, *Biogenesis, secretion, and intercellular interactions of exosomes and other extracellular vesicles*. Annu Rev Cell Dev Biol, 2014. **30**: p. 255-89.
73. Raposo, G. and W. Stoorvogel, *Extracellular vesicles: exosomes, microvesicles, and friends*. J Cell Biol, 2013. **200**(4): p. 373-83.
74. Canitano, A., et al., *Exosomes released in vitro from Epstein-Barr virus (EBV)-infected cells contain EBV-encoded latent phase mRNAs*. Cancer Lett, 2013. **337**(2): p. 193-9.
75. Kalamvoki, M., T. Du, and B. Roizman, *Cells infected with herpes simplex virus 1 export to uninfected cells exosomes containing STING, viral mRNAs, and microRNAs*. Proc Natl Acad Sci U S A, 2014. **111**(46): p. E4991-6.
76. Nour, A.M. and Y. Modis, *Endosomal vesicles as vehicles for viral genomes*. Trends Cell Biol, 2014. **24**(8): p. 449-54.
77. Ramakrishnaiah, V., et al., *Exosome-mediated transmission of hepatitis C virus between human hepatoma Huh7.5 cells*. Proc Natl Acad Sci U S A, 2013. **110**(32): p. 13109-13.
78. Conner, S.D. and S.L. Schmid, *Regulated portals of entry into the cell*. Nature, 2003. **422**(6927): p. 37-44.
79. Steinman, R.M., et al., *Endocytosis and the recycling of plasma membrane*. J Cell Biol, 1983. **96**(1): p. 1-27.
80. Doherty, G.J. and H.T. McMahon, *Mechanisms of endocytosis*. Annu Rev Biochem, 2009. **78**: p. 857-902.



81. Nabi, I.R. and P.U. Le, *Caveolae/raft-dependent endocytosis*. J Cell Biol, 2003. **161**(4): p. 673-7.
82. Lakadamyali, M., M.J. Rust, and X. Zhuang, *Ligands for clathrin-mediated endocytosis are differentially sorted into distinct populations of early endosomes*. Cell, 2006. **124**(5): p. 997-1009.
83. Leonard, D., et al., *Sorting of EGF and transferrin at the plasma membrane and by cargo-specific signaling to EEA1-enriched endosomes*. J Cell Sci, 2008. **121**(Pt 20): p. 3445-58.
84. Ghosh, R.N., D.L. Gelman, and F.R. Maxfield, *Quantification of low density lipoprotein and transferrin endocytic sorting HEP2 cells using confocal microscopy*. J Cell Sci, 1994. **107** ( Pt 8): p. 2177-89.
85. Matsui, T. and M. Fukuda, *Methods of analysis of the membrane trafficking pathway from recycling endosomes to lysosomes*. Methods Enzymol, 2014. **534**: p. 195-206.
86. Mayle, K.M., A.M. Le, and D.T. Kamei, *The intracellular trafficking pathway of transferrin*. Biochim Biophys Acta, 2012. **1820**(3): p. 264-81.
87. Chua, C.E. and B.L. Tang, *Engagement of the small GTPase Rab31 protein and its effector, early endosome antigen 1, is important for trafficking of the ligand-bound epidermal growth factor receptor from the early to the late endosome*. J Biol Chem, 2014. **289**(18): p. 12375-89.
88. Duan, L., et al., *Cbl-mediated ubiquitinylation is required for lysosomal sorting of epidermal growth factor receptor but is dispensable for endocytosis*. J Biol Chem, 2003. **278**(31): p. 28950-60.
89. Longva, K.E., et al., *Ubiquitination and proteasomal activity is required for transport of the EGF receptor to inner membranes of multivesicular bodies*. J Cell Biol, 2002. **156**(5): p. 843-54.
90. Roepstorff, K., et al., *Differential effects of EGFR ligands on endocytic sorting of the receptor*. Traffic, 2009. **10**(8): p. 1115-27.
91. Wu, X., et al., *Evasion of antiviral immunity through sequestering of TBK1/IKKepsilon/IRF3 into viral inclusion bodies*. J Virol, 2014. **88**(6): p. 3067-76.
92. Gruenberg, J. and H. Stenmark, *The biogenesis of multivesicular endosomes*. Nat Rev Mol Cell Biol, 2004. **5**(4): p. 317-23.
93. Roepstorff, K., et al., *Endocytic downregulation of ErbB receptors: mechanisms and relevance in cancer*. Histochem Cell Biol, 2008. **129**(5): p. 563-78.
94. Raiborg, C., T.E. Rusten, and H. Stenmark, *Protein sorting into multivesicular endosomes*. Curr Opin Cell Biol, 2003. **15**(4): p. 446-55.
95. Hollidge, B.S., et al., *Orthobunyavirus entry into neurons and other mammalian cells occurs via clathrin-mediated endocytosis and requires trafficking into early endosomes*. J Virol, 2012. **86**(15): p. 7988-8001.
96. Hofmann, H., et al., *Severe fever with thrombocytopenia virus glycoproteins are targeted by neutralizing antibodies and can use DC-SIGN as a receptor for pH-dependent entry into human and animal cell lines*. J Virol, 2013. **87**(8): p. 4384-94.
97. Yuan, F. and A. Zheng, *Entry of severe fever with thrombocytopenia syndrome virus*. Virol Sin, 2017. **32**(1): p. 44-50.
98. Drake, M.J., et al., *A role for glycolipid biosynthesis in severe fever with thrombocytopenia syndrome virus entry*. PLoS Pathog, 2017. **13**(4): p. e1006316.
99. Gorvel, J.P., et al., *rab5 controls early endosome fusion in vitro*. Cell, 1991. **64**(5): p. 915-25.
100. McLauchlan, H., et al., *A novel role for Rab5-GDI in ligand sequestration into clathrin-coated pits*. Curr Biol, 1998. **8**(1): p. 34-45.

101. Pereira-Leal, J.B. and M.C. Seabra, *Evolution of the Rab family of small GTP-binding proteins*. J Mol Biol, 2001. **313**(4): p. 889-901.
102. Maxfield, F.R. and T.E. McGraw, *Endocytic recycling*. Nat Rev Mol Cell Biol, 2004. **5**(2): p. 121-32.
103. Roland, J.T., et al., *Myosin Vb interacts with Rab8a on a tubular network containing EHD1 and EHD3*. Mol Biol Cell, 2007. **18**(8): p. 2828-37.
104. Habjan, M., et al., *NSs protein of rift valley fever virus induces the specific degradation of the double-stranded RNA-dependent protein kinase*. J Virol, 2009. **83**(9): p. 4365-75.
105. Ikegami, T., et al., *Rift Valley fever virus NSs protein promotes post-transcriptional downregulation of protein kinase PKR and inhibits eIF2alpha phosphorylation*. PLoS Pathog, 2009. **5**(2): p. e1000287.
106. Kalveram, B., O. Lihoradova, and T. Ikegami, *NSs protein of rift valley fever virus promotes posttranslational downregulation of the TFIIH subunit p62*. J Virol, 2011. **85**(13): p. 6234-43.
107. Chaudhary, V., et al., *Suppression of type I and type III IFN signalling by NSs protein of severe fever with thrombocytopenia syndrome virus through inhibition of STAT1 phosphorylation and activation*. J Gen Virol, 2015. **96**(11): p. 3204-11.
108. Hu, Y.B., et al., *The endosomal-lysosomal system: from acidification and cargo sorting to neurodegeneration*. Transl Neurodegener, 2015. **4**: p. 18.
109. Muehlenbachs, A., et al., *Heartland virus-associated death in tennessee*. Clin Infect Dis, 2014. **59**(6): p. 845-50.
110. Jiao, Y., et al., *Preparation and evaluation of recombinant severe fever with thrombocytopenia syndrome virus nucleocapsid protein for detection of total antibodies in human and animal sera by double-antigen sandwich enzyme-linked immunosorbent assay*. J Clin Microbiol, 2012. **50**(2): p. 372-7.
111. Liu, Y., et al., *Person-to-person transmission of severe fever with thrombocytopenia syndrome virus*. Vector Borne Zoonotic Dis, 2012. **12**(2): p. 156-60.
112. Zhang, Y.Z., et al., *Hemorrhagic fever caused by a novel tick-borne Bunyavirus in Huaiyangshan, China*. Zhonghua Liu Xing Bing Xue Za Zhi, 2011. **32**(3): p. 209-20.
113. Chang, M.S. and J.H. Woo, *Severe fever with thrombocytopenia syndrome: tick-mediated viral disease*. J Korean Med Sci, 2013. **28**(6): p. 795-6.
114. Guu, T.S., W. Zheng, and Y.J. Tao, *Bunyavirus: structure and replication*. Adv Exp Med Biol, 2012. **726**: p. 245-66.
115. Palacios, G., et al., *Characterization of the Uukuniemi virus group (Phlebovirus: Bunyaviridae): evidence for seven distinct species*. J Virol, 2013. **87**(6): p. 3187-95.
116. Fontana, J., et al., *The unique architecture of Bunyamwera virus factories around the Golgi complex*. Cell Microbiol, 2008. **10**(10): p. 2012-28.
117. Novoa, R.R., et al., *Key Golgi factors for structural and functional maturation of bunyamwera virus*. J Virol, 2005. **79**(17): p. 10852-63.
118. Salanueva, I.J., et al., *Polymorphism and structural maturation of bunyamwera virus in Golgi and post-Golgi compartments*. J Virol, 2003. **77**(2): p. 1368-81.
119. Bridgen, A., et al., *Bunyamwera bunyavirus nonstructural protein NSs is a nonessential gene product that contributes to viral pathogenesis*. Proc Natl Acad Sci U S A, 2001. **98**(2): p. 664-9.
120. Elliott, R.M. and F. Weber, *Bunyaviruses and the type I interferon system*. Viruses, 2009. **1**(3): p. 1003-21.
121. Komatsu, M., et al., *Impairment of starvation-induced and constitutive autophagy in Atg7-deficient mice*. J Cell Biol, 2005. **169**(3): p. 425-34.

122. Brennan, B., et al., *Reverse genetics system for severe fever with thrombocytopenia syndrome virus*. J Virol, 2015. **89**(6): p. 3026-37.
123. Escola, J.M., et al., *Selective enrichment of tetraspan proteins on the internal vesicles of multivesicular endosomes and on exosomes secreted by human B-lymphocytes*. J Biol Chem, 1998. **273**(32): p. 20121-7.
124. Lai, F.W., B.D. Lichty, and D.M. Bowdish, *Microvesicles: ubiquitous contributors to infection and immunity*. J Leukoc Biol, 2015. **97**(2): p. 237-45.
125. Harding, C., J. Heuser, and P. Stahl, *Endocytosis and intracellular processing of transferrin and colloidal gold-transferrin in rat reticulocytes: demonstration of a pathway for receptor shedding*. Eur J Cell Biol, 1984. **35**(2): p. 256-63.
126. Pan, B.T., et al., *Electron microscopic evidence for externalization of the transferrin receptor in vesicular form in sheep reticulocytes*. J Cell Biol, 1985. **101**(3): p. 942-8.
127. Valadi, H., et al., *Exosome-mediated transfer of mRNAs and microRNAs is a novel mechanism of genetic exchange between cells*. Nat Cell Biol, 2007. **9**(6): p. 654-9.
128. Pegtel, D.M., et al., *Functional delivery of viral miRNAs via exosomes*. Proc Natl Acad Sci U S A, 2010. **107**(14): p. 6328-33.
129. Mack, M., et al., *Transfer of the chemokine receptor CCR5 between cells by membrane-derived microparticles: a mechanism for cellular human immunodeficiency virus 1 infection*. Nat Med, 2000. **6**(7): p. 769-75.
130. Raposo, G., et al., *B lymphocytes secrete antigen-presenting vesicles*. J Exp Med, 1996. **183**(3): p. 1161-72.
131. Zhang, X., et al., *An emerging hemorrhagic fever in China caused by a novel bunyavirus SFTSV*. Sci China Life Sci, 2013. **56**(8): p. 697-700.
132. Feng, Z., et al., *A pathogenic picornavirus acquires an envelope by hijacking cellular membranes*. Nature, 2013. **496**(7445): p. 367-71.
133. Natasha, G., et al., *Exosomes as immunotheranostic nanoparticles*. Clin Ther, 2014. **36**(6): p. 820-9.
134. Kabeya, Y., et al., *LC3, a mammalian homologue of yeast Apg8p, is localized in autophagosome membranes after processing*. EMBO J, 2000. **19**(21): p. 5720-8.
135. Ichimura, Y., et al., *A ubiquitin-like system mediates protein lipidation*. Nature, 2000. **408**(6811): p. 488-92.
136. Huang, S.C., et al., *Enterovirus 71-induced autophagy detected in vitro and in vivo promotes viral replication*. J Med Virol, 2009. **81**(7): p. 1241-52.
137. Klein, K.A. and W.T. Jackson, *Human rhinovirus 2 induces the autophagic pathway and replicates more efficiently in autophagic cells*. J Virol, 2011. **85**(18): p. 9651-4.
138. O'Donnell, V., et al., *Foot-and-mouth disease virus utilizes an autophagic pathway during viral replication*. Virology, 2011. **410**(1): p. 142-50.
139. Bird, S.W., et al., *Nonlytic viral spread enhanced by autophagy components*. Proc Natl Acad Sci U S A, 2014. **111**(36): p. 13081-6.
140. Reggiori, F., C.A. de Haan, and M. Molinari, *Unconventional use of LC3 by coronaviruses through the alleged subversion of the ERAD tuning pathway*. Viruses, 2011. **3**(9): p. 1610-23.
141. Reggiori, F., et al., *Coronaviruses Hijack the LC3-I-positive EDEMosomes, ER-derived vesicles exporting short-lived ERAD regulators, for replication*. Cell Host Microbe, 2010. **7**(6): p. 500-8.
142. Goubau, D., *Antiviral immunity via RIG-I-mediated recognition of RNA bearing 5[prime]-diphosphates*. Nature, 2014. **514**: p. 372-375.

143. Goubau, D., S. Deddouche, and C. Reis e Sousa, *Cytosolic sensing of viruses*. Immunity, 2013. **38**: p. 855-869.
144. Marq, J.B., et al., *Short double-stranded RNAs with an overhanging 5[prime]-ppp-nucleotide, as found in arenavirus genomes, act as RIG-I decoys*. J. Biol. Chem., 2011. **286**: p. 6108-6116.
145. Marq, J.B., D. Kolakofsky, and D. Garcin, *Unpaired 5[prime]-ppp-nucleotides, as found in arenavirus double-stranded RNA panhandles, are not recognized by RIG-I*. J. Biol. Chem., 2010. **285**: p. 18208-18216.
146. Saito, T., et al., *Innate immunity induced by composition-dependent RIG-I recognition of hepatitis C virus RNA*. Nature, 2008. **454**: p. 523-527.
147. Loo, Y.M., *Distinct RIG-I and MDA5 signaling by RNA viruses in innate immunity*. J. Virol., 2008. **82**: p. 335-345.
148. Pickart, C.M. and M.J. Eddins, *Ubiquitin: structures, functions, mechanisms*. Biochim Biophys Acta, 2004. **1695**(1-3): p. 55-72.
149. Pickart, C.M. and D. Fushman, *Polyubiquitin chains: polymeric protein signals*. Curr Opin Chem Biol, 2004. **8**(6): p. 610-6.
150. Thrower, J.S., et al., *Recognition of the polyubiquitin proteolytic signal*. EMBO J, 2000. **19**(1): p. 94-102.
151. Berndsen, C.E. and C. Wolberger, *New insights into ubiquitin E3 ligase mechanism*. Nat Struct Mol Biol, 2014. **21**(4): p. 301-7.
152. Mattioli, F. and T.K. Sixma, *Lysine-targeting specificity in ubiquitin and ubiquitin-like modification pathways*. Nat Struct Mol Biol, 2014. **21**(4): p. 308-16.
153. Ikeda, F., N. Crosetto, and I. Dikic, *What determines the specificity and outcomes of ubiquitin signaling?* Cell, 2010. **143**(5): p. 677-81.
154. Gack, M.U., *TRIM25 RING-finger E3 ubiquitin ligase is essential for RIG-I-mediated antiviral activity*. Nature, 2007. **446**: p. 916-920.
155. Pauli, E.K., *The ubiquitin-specific protease USP15 promotes RIG-I-mediated antiviral signaling by deubiquitinating TRIM25*. Sci. Signal., 2014. **7**: p. ra3.
156. Oshiumi, H., et al., *Riplet/RNF135, a RING finger protein, ubiquitinates RIG-I to promote interferon-beta induction during the early phase of viral infection*. J Biol Chem, 2009. **284**(2): p. 807-17.
157. Oshiumi, H., et al., *The ubiquitin ligase Riplet is essential for RIG-I-dependent innate immune responses to RNA virus infection*. Cell Host Microbe, 2010. **8**(6): p. 496-509.
158. Oshiumi, H., et al., *A distinct role of Riplet-mediated K63-linked polyubiquitination of the RIG-I repressor domain in human antiviral innate immune responses*. PLoS Pathog., 2013. **9**: p. e1003533.
159. Gao, D., et al., *REUL is a novel E3 ubiquitin ligase and stimulator of retinoic-acid-inducible gene-I*. PLoS One, 2009. **4**(6): p. e5760.
160. Han, C., et al., *Mex3c mutation reduces adiposity partially through increasing physical activity*. J Endocrinol, 2014. **221**(3): p. 457-68.
161. Hacker, H. and M. Karin, *Regulation and function of IKK and IKK-related kinases*. Sci STKE, 2006. **2006**(357): p. re13.
162. Ikeda, F., et al., *Involvement of the ubiquitin-like domain of TBK1/IKK-i kinases in regulation of IFN-inducible genes*. EMBO J, 2007. **26**(14): p. 3451-62.
163. Ma, X., et al., *Molecular basis of Tank-binding kinase 1 activation by transautophosphorylation*. Proc Natl Acad Sci U S A, 2012. **109**(24): p. 9378-83.
164. Tu, D., et al., *Structure and ubiquitination-dependent activation of TANK-binding kinase 1*. Cell Rep, 2013. **3**(3): p. 747-58.

- 165. Gack, M.U., et al., *Influenza A virus NS1 targets the ubiquitin ligase TRIM25 to evade recognition by the host viral RNA sensor RIG-I*. Cell Host Microbe, 2009. **5**(5): p. 439-49.
- 166. Gack, M.U., et al., *Roles of RIG-I N-terminal tandem CARD and splice variant in TRIM25-mediated antiviral signal transduction*. Proc Natl Acad Sci U S A, 2008. **105**(43): p. 16743-8.
- 167. Bruns, A.M. and C.M. Horvath, *Activation of RIG-I-like receptor signal transduction*. Crit Rev Biochem Mol Biol, 2012. **47**(2): p. 194-206.
- 168. Goubau, D., S. Deddouche, and C. Reis e Sousa, *Cytosolic sensing of viruses*. Immunity, 2013. **38**(5): p. 855-69.
- 169. Kowalinski, E., *Structural basis for the activation of innate immune pattern-recognition receptor RIG-I by viral RNA*. Cell, 2011. **147**: p. 423-435.
- 170. O'Neill, L.A. and A.G. Bowie, *Sensing and signaling in antiviral innate immunity*. Curr Biol, 2010. **20**(7): p. R328-33.
- 171. Chiang, J.J., M.E. Davis, and M.U. Gack, *Regulation of RIG-I-like receptor signaling by host and viral proteins*. Cytokine Growth Factor Rev., 2014. **25**: p. 491-505.
- 172. Gack, M.U., et al., *TRIM25 RING-finger E3 ubiquitin ligase is essential for RIG-I-mediated antiviral activity*. Nature, 2007. **446**(7138): p. 916-920.
- 173. Chernorudskiy, A.L. and M.R. Gainullin, *Ubiquitin system: direct effects join the signaling*. Sci Signal, 2013. **6**(280): p. pe22.

## Vita

Jesus A. Silvas was born in Fort Stockton, TX on August 21, 1986, to Alberto and Maria Del Carmen Silvas of Santa Elena, Chihuahua. His education through the end of high school occurred in West Texas. He attended Sul Ross State University in Alpine Texas where he graduated with a B.A. in Biology and minored in Chemistry. After graduating from Sul Ross, he attended Texas A&M in Kingsville Texas where he received an M.S. in Microbiology. Through a collaboration between Texas A&M and the University of Texas, he was awarded an NIH Fellowship (Masters to Ph.D. Program) where he was able to directly enter the University of Texas Medical Branch Graduate School of Biomedical Sciences in 2011. He began working on molecular mechanisms of innate immune evasion by emerging pathogens and since then has been active in collaborations with local and international investigators. In 2016 he was awarded The Ruth L. Kirschstein National Research Service Awards for Individual Predoctoral Fellowships to Promote Diversity in Health-Related Research (F31-Diversity). Professional and teaching experience, publications, funding, awards, and mentorship obligations are summarized below:

### **Grant Support** (total direct cost are shown)

#### **Current**

2016-2018	NIH 1F31AI124662 Ruth L. Kirschstein National Research Service Award (NRSA) Individual Predoctoral Fellowship to Promote Diversity in Health-Related Research ( <b>Priority score=23</b> ) \$63,286 over two years
-----------	--

#### **Past**

2011	NIH/UTMB “Bridges to the Doctorate” (PI: David Neisel, Ph.D.) \$15,000 per year
------	---

### **HIGH BIOCONTAINMENT RESEARCH/TRAINING EXPERIENCES**

2012-present

Certified for Biosafety level III (BSL3) cell culture work at UTMB. Also trained several researchers including one post-doctoral fellow, one research scientist, and two research technicians.

## **TEACHING RESPONSIBILITIES:**

### **A. TEACHING RESPONSIBILITIES AT UTMB**

#### **a. Students/Mentees/Advisees/Trainees**

##### **i. Post-doctoral fellows:**

- 2012 Felix Santiago-Maldonado, Ph.D.. Scientist I, Luminex Corporation, Austin, Texas. Training on immunofluorescence assays, protein:protein interaction assays, western blotting, and BSL3 cell culture.
- 2015 Evandro Winkleman, Ph.D.. University of Texas Medical Branch, Galveston, Texas. Training on immunofluorescence assays for detection of flavivirus RNA and labeling of cellular compartments.
- 2015 Brenna McGruder-Rawson, Ph.D.. University of Texas Medical Branch, Galveston, Texas. Training on isolation of microvesicles and exosomes, and electron microscopy techniques.
- 2017 Ian Patterson, Ph.D. University of Texas Medical Branch, Galveston, Texas. Training in immunofluorescence and confocal microscopy.

##### **ii. Research Associates**

- 2013 Alamelu Vankachalam. Training on immunofluorescence assays, protein:protein interaction assays, western blotting, and BSL3 cell culture.
- 2014 Patricia Barrera. Training on immunofluorescence assays, protein:protein interaction assays, and western blotting.
- 2015 Dionna Scharton. University of Texas Medical Branch, Galveston, Texas. Training on immunofluorescence assays, protein:protein interaction assays, western blotting, and BSL3 cell culture.

##### **iii. Visiting Scientists**

- 2014 Dr. Natalia Kuzmina, Research Scientist, University of Texas Medical Branch, Galveston, Texas. Training on BSL3 tissue culture work and techniques.
- 2015 Dr. Juan Rodas, Associate Professor, University of Antioquia , Colombia. Training on serological assays for alphaviruses.

2017 Dr. Francisco Diaz, Associate Professor, University of Antioquia , Colombia. Training on serological assays for alphaviruses and BSL3.

#### **iv. Student Mentor**

June 2015–August 2015	Christopher Roundy, University of Texas Medical Branch, Galveston, Texas. Training in antibody standardization for detection of arboviruses by western blotting.
-----------------------	--

### **B. TEACHING RESPONSIBILITIES AT TEXAS A&M**

#### **a. Students/Mentees/Advisees/Trainees**

##### **i. Undergraduate students**

2009-2011	Allyson Bryce
2010-2012	Juan Celedon
2010-2012	Antonio Lopez

##### **ii. Post-baccalaureate students**

August 2015-May 2016	Antonio Muruato
----------------------	-----------------

### **MEMBERSHIP IN SCIENTIFIC SOCIETIES/PROFESSIONAL ORGANIZATIONS**

American Society for Tropical Medicine and Hygiene  
American Society for Microbiology

### **HONORS:**

2003	Southwest Texas Municipal Gas Corp Early Graduate Award
2003	Alpine High School Early Graduate Award
2004-2005	Joint Admission Medical Program (JAMP) Scholarship. Sul Ross State University, Alpine, Texas
2005	Department of Biology Scholarship, Sul Ross State University, Alpine, Texas
2009-2010	Department of Biology Scholarship, Texas A&M University, Kingsville, Texas
2010	Texas A&M 1 <sup>st</sup> Annual Research Symposium, Best Oral Presentation Award, Texas A&M University , Kingsville, Texas
2014	The Edward S. Reynolds Award for Pathology Research, University of Texas Medical Branch, Galveston, Texas



2014	IHII/McLaughlin Colloquium on Infection and Immunity Travel Award, University of Texas Medical Branch, Galveston, Texas
2015	The Edward S. Reynolds Award for Pathology Research, University of Texas Medical Branch, Galveston, Texas
2015	IHII/McLaughlin Colloquium on Infection and Immunity Travel Award, University of Texas Medical Branch, Galveston, Texas
2016	IHII/McLaughlin Colloquium on Infection and Immunity Travel Award, University of Texas Medical Branch, Galveston, Texas
2017	IHII/McLaughlin Colloquium on Infection and Immunity Travel Award, University of Texas Medical Branch, Galveston, Texas
2017	The Edward S. Reynolds Award for Pathology Research, University of Texas Medical Branch, Galveston, Texas

## PUBLISHED

### A. ARTICLES IN PEER-REVIEWED JOURNALS:

1. Santiago FW, Covalada LM, Sanchez-Aparicio MT, **Silvas JA**, Diaz-Vizarreta AC, Patel JR, Popov V, Yu X, García-Sastre A, Aguilar PV. Hijacking of RIG-I signaling proteins into virus-induced cytoplasmic structures correlates with the inhibition of Type I interferon responses. *J Virol*. 2014 Apr;88(8):4572-85. doi: 10.1128/JVI.03021-13. Epub 2014 Jan 29. PMID: 24478431  
**Impact Factor: 4.648**
2. Hontz RD, Guevara C, Halsey ES, **Silvas JA**, Santiago FW, Widen SG, Wood TG, Casanova W, Vasilakis N, Watts DM, Kochel TJ, Ebihara H, Aguilar PV. Itaya virus, a Novel Orthobunyavirus Associated with Human Febrile Illness, Peru. *Emerg Infect Dis*. 2015 May;21(5):781-8. doi: 10.3201/eid2105.141368. PMID: 25898901  
**Impact Factor: 7.327**
3. Santiago FW, Halsey ES, Siles C, Vilcarromero S, Guevara C, **Silvas JA**, Ramal C, Ampuero JS, Aguilar PV. Long-Term Arthralgia after Mayaro Virus Infection Correlates with Sustained Pro-inflammatory Cytokine Response. *PLoS Negl Trop Dis*. 2015 Oct 23;9(10):e0004104. doi: 10.1371/journal.pntd.0004104. eCollection 2015 Oct.  
**Impact Factor: 4.489**
4. **Silvas JA**, Popov VL, Paulucci-Holthauzen A, Aguilar PV. 2016. Extracellular Vesicles Mediate Receptor-Independent Transmission of Novel Tick-Borne Bunyavirus. *J Virol* 90:873-886.  
**\*\*Selected by the editors of the Journal of Virology for inclusion in "Spotlight", a feature in the Journal that highlights research articles of significant interest from the current issue.**  
**Impact Factor: 4.648**
5. **Silvas JA** and PV Aguilar. Emergence of Severe Fever with Thrombocytopenia Syndrome Virus. *ASTMH. In Press*.

### B. PUBLISHED ABSTRACTS

1. Santiago-Maldonado FW, Covalada L, Sanchez MT, Diaz-Vizarreta A, **Silvas JA**, Patel JR, Yu XJ, Garcia-Sastre A, Aguilar PV. Hijacking of RIG-I signaling proteins into virus-induced cytoplasmic structures inhibits Type I interferon responses. Innate Immunity to Viral Infections Keystone Symposia Conference. January 2014. Keystone Resort, Keystone, Colorado.
2. Guevara C., **Silvas JA.**, Hontz R., Casanova W., Vasilakis N., Watts D., Kochel T., Ampuero J.S., Ebihara H., Aguilar PV. Itaya virus: a novel Orthobunyavirus associated with human febrile illness in Peru. American Society for Tropical Medicine and Hygiene meeting. November 2014. New Orleans, Louisiana.
3. **Silvas J.A.**, Barrera P., Paulucci-Holthauzen A., Popov V., Aguilar PV. Extracellular microvesicles mediate receptor-independent transmission of novel tick-borne bunyavirus. American Society for Tropical Medicine and Hygiene meeting. October 2015. Philadelphia, Pennsylvania.
4. **Silvas J.A. and P.V. Aguilar.** Subversion of cellular pathways by emerging tick-borne Phlebovirus for inhibition of interferon responses. Hemorrhagic Fever Viruses. December 2016. Hilton Santa Fe Historic Plaza Hotel. Santa Fe, NM.

Permanent address: 205 S Jackson St. Alpine, TX 79830

This dissertation was typed by Jesus A. Silvas.